

## Improved emission of Yb(III) ions in triazacyclononane-based macrocyclic ligands compared to cyclen-based ones

Salauat Kiraev,<sup>†</sup> Emilie Mathieu,<sup>†</sup> Daniel Kovacs,<sup>†</sup> Jordann A. L. Wells,<sup>†</sup> Monika Tomar,<sup>†</sup> Julien Andres,<sup>\*,§</sup> K. Eszter Borbas<sup>\*,†</sup>

<sup>†</sup> Department of Chemistry, Ångström Laboratory, Uppsala University, Box 523, 75120, Uppsala, Sweden, [eszter.borbas@kemi.uu.se](mailto:eszter.borbas@kemi.uu.se)

<sup>§</sup> Chemical and Chemical Engineering Section, Ecole Polytechnique Fédérale de Lausanne, BCH 3311, CH-1015, Lausanne, Switzerland

Materials and methods	S2
General procedures	S2
Chromatography	S2
Spectroscopy	S2
Near-infrared spectra	S4
Paramagnetic <sup>1</sup> H NMR	S5
Crystallography	S5
Electrochemistry	S5
Syntheses	S6
Synthesis schemes	S6
Synthetic procedures and characterisation data	S6
<sup>1</sup> H NMR spectra of Yb(III) complexes	S11
X-ray crystallography	S14
Electrochemical characterisation	S17
Photophysical characterisation	S20
77 K measurements	S27
Fluorescence decay fits and residuals	S28
Photostability experiments	S30
Driving force for photoinduced electron transfer	S32
Calculations of Franck-Condon factors	S33
<sup>1</sup> H, <sup>13</sup> C, and <sup>19</sup> F NMR spectra	S34
LC-MS traces	S51
FT-IR spectra of <b>YbL</b>	S53
References	S55

## **MATERIALS AND METHODS**

**General Procedures.**  $^1\text{H}$  NMR (400 MHz),  $^{13}\text{C}$  NMR (101 MHz) and  $^{19}\text{F}$  NMR (376 MHz) spectra were recorded on a JEOL 400 MHz instrument. Chemical shifts were referenced to residual solvent peaks and are given as follows: chemical shift ( $\delta$ , ppm), multiplicity (s, singlet; br, broad; d, doublet, t, triplet; q, quartet; m, multiplet), coupling constant (Hz), integration. LC-MS analysis was carried out using an analytical Dionex UltiMate 3000 HPLC instrument coupled to a Thermo Finnigan LCQ DECA XP MAX mass spectrometer. FT-IR spectra were recorded at r.t. on a Spectrum One FT-IR Spectrometer using KBr for making pellets in 1:100 ratio (complex : KBr). HR-ESI-MS analyses were performed at the Organisch Chemisches Institut WWU Münster, Germany. All compounds displayed the expected isotope distribution pattern. Anhydrous  $\text{CH}_2\text{Cl}_2$  was obtained by distillation from  $\text{CaH}_2$  under an Ar atmosphere.

Compounds  $\text{S1}^{\text{X}}$  ( $\text{X} = \text{H}, \text{OMe}, \text{Cl}, \text{CF}_3$ )<sup>1</sup> and  $\text{L}^{\text{X}}$ ,<sup>1</sup> were synthesised following literature methods. All other chemicals were from commercial sources and used as received.

**Chromatography.** Preparative chromatography was carried out on silica gel [Normasil 60 chromatographic silica media (40–63 micron)] and Al oxide [activated, neutral, Brockmann Activity I, Sigma-Aldrich]. Thin layer chromatography was performed on silica-coated (60G F254) aluminium plates from Merck and Al oxide coated with 254 nm fluorescent indicator Al plates from Sigma-Aldrich. Samples were visualised by UV-light (254 and 365 nm) or permanganate stain.

HPLC-analysis was performed on a Dionex UltiMate 3000 system using a Phenomenex Gemini® C18 TMS end-capped 150 mm×4.6 mm HPLC column with water (0.05% formic acid):  $\text{CH}_3\text{CN}$  (0.05% formic acid) eluent system using the methods: (a) 0–10 min: 10%→90%  $\text{CH}_3\text{CN}$ , 0.5 mL/min; (b) 0–12 min: 10%→50%  $\text{CH}_3\text{CN}$  & 12–14 min: 50%→90%, 0.5 mL/min; (c) 0–8 min: 10%→20% & 8–12 min: 20% iso  $\text{CH}_3\text{CN}$ , 0.5 mL/min; (d) 0–6 min: 10% iso  $\text{CH}_3\text{CN}$  & 6–12 min: 10%→50%, 0.25 mL/min. UV (UltiMate 3000 Photodiode Array Detector) and ESI-MS detections (LCQ DECA XP MAX) were used.

**Spectroscopy.** All measurements were performed in PIPES-buffered distilled water at pH 6.5. Complex concentration was nominally 10  $\mu\text{M}$ , however, small quantities of Ln salts may diminish this. Quartz cells with 1 cm optical pathlengths were used for the r.t. measurements. The absorbance spectra were measured by a Varian Cary 100 Bio UV-Visible or Cary 5000 UV-Visible spectrophotometer. The emission and excitation spectra, lifetimes, time-resolved spectra and quantum yields were recorded on a Horiba FluoroMax-4P. All emissions were corrected by the wavelength sensitivity (correction function) of the spectrometer. All measurements were performed at r.t. unless stated otherwise. All measurements in the presence of potassium fluoride (KF) were performed with appropriate amounts of powder KF samples dissolved in the buffer solutions to achieve 0.1 M. The resulting solutions were used to prepare stocks and cuvette solutions of the complexes.

Quantum yields were measured at r.t., using quinine sulfate (QS) in  $\text{H}_2\text{SO}_4$  0.05 M ( $\Phi_{\text{ref}} = 0.59$ ) as reference,<sup>1</sup> in Equation (1). Quantum yields were calculated according to (1), with  $\Phi_{\text{s}}$  the quantum yield of the sample,  $\Phi_{\text{ref}}$  the quantum yield of the reference,  $I$  the integrated corrected emission intensity of the sample (s) and of the reference (ref),  $f_{\text{A}}$  the absorption factor of the sample (s) and of the reference (ref) at the excitation wavelength and  $n$  the refractive indexes of the sample (s) and of the reference (ref). The concentration of the complexes was adjusted to obtain an absorbance around the maxima of the antennae matching that of the QS fluorescence standard ( $A = 0.10$ ). The excitation wavelength where the absorption factors of the samples and of the reference were the same was

chosen (i.e. where the absorptions are identical). The corrected emission spectra of the sample and reference standard were then measured under the same conditions over the 320–800 nm spectral range as well as blank samples containing only the solvent (i.e. water or PIPES buffered aqueous solutions). The appropriate blanks were subtracted from their respective spectra. The quantum yields were then calculated according to Equation (1). The given relative error on the quantum yields ( $\delta\Phi = \Delta\Phi/\Phi$ , where  $\Delta\Phi$  is the absolute error) take into account the accuracy of the spectrometer and of the integration procedure [ $\delta(I_s/I_{ref}) < 2\%$ ], an error of  $0.59 \pm 0.01$  on the quantum yield of the reference QS [ $\delta(\Phi_{ref}) < 2\%$ ], an error on the ratio of the absorption factors [ $\delta(f_{Aref}/f_{As}) < 5\%$ , relative to the fixed absorption factor of the reference QS] and an error on the ratio of the squared refractive indexes [ $\delta(n_s^2/n_{ref}^2) < 1\%$ ,  $< 0.25\%$  around 1.333 on each individual refractive index], which sums to a total estimated relative error that should be  $\delta\Phi_s < 10\%$ . A limit value of 10% is thus chosen.

$$\Phi_s = \frac{I_s}{I_{ref}} \cdot \frac{f_{Aref}}{f_{As}} \cdot \frac{(n_s)^2}{(n_{ref})^2} \cdot \Phi_{ref} \quad (1)$$

Low temperature measurements were done in quartz capillaries (0.2 cm optical pathlength) at 77 K by immersion in a liquid N<sub>2</sub>-filled quartz Dewar and with addition of glycerol (1 drop) to the solutions (9 drops) measured at r.t. Glycerol used for low temperature experiments was of 99.9+% purity.

The fluorescence lifetime decays in the nanosecond range were measured on Spectrofluorometer FS5 system from Edinburgh Instruments. The system was equipped with picosecond pulsed light emitting diode EPLED-340 with excitation wavelength at 341.5 nm. The data were acquired in the 50 ns measurement range with peak preset at 10<sup>4</sup> counts in 1024 channels. The repetition rate of the excitation source was 10 MHz, and the synchronisation delay was 80 ns. The scatter light profile (prompt signal, black in the decay figures) was recorded for each experiment individually in the same quartz cuvette using diluted Ludox solution in HPLC water at 341.5 nm emission wavelength with similar parameters as were used for the measured sample (red in the decay figures). All measurements were done at r.t. with such concentration of the sample that  $A = 0.10$  at 341.5 nm, and with 10 nm slits width of the emission detector and maximum optical power of the excitation source. All Yb(III) complexes were measured at 377 nm emission wavelength, and the solvent was PIPES buffered HPLC water (pH ~ 6.5). The control experiment was performed with Rose Bengal in MeOH at  $\lambda_{ex} = 577$  nm as a lifetime standard.<sup>2</sup> The obtained data were fitted in the Fluoracle software (green trace in the decay figures) using single exponential reconvolution fit model in Equation (2), where  $\tau_1$  is the sample lifetime,  $t$  is time represented in ns,  $B_1$  is the population (100% in all cases) (Figures S24–S25).

$$R(t) = B_1 * \exp(-t/\tau_1) \quad (2)$$

Photostability experiments were performed with **YbLc1** and **YbL<sup>X</sup>** on Horiba FluoroMax-4P at r.t. at  $\lambda_{ex} = 331$  nm,  $A = 0.10$  in 10 mM PIPES buffered aqueous solutions at pH 6.5. Each sample was prepared in a 1 cm quartz cuvette (3 mL) and was continuously irradiated for 2 hours with emission spectrum recorded every 15 minutes. The front slit was 3 nm, the exit slit was 2.5 nm. Each sample evolution upon light irradiation was tested via absorbance spectroscopy and LCMS before and after being irradiated. No major differences either in absorbance or LCMS were noticed for all samples. The signal of the solvent recorded in the same conditions was subtracted from the recorded emission spectra (Figure S26), which were then integrated (346–647 nm). The resulting integrated intensity values were divided by that at  $t_0$  and multiplied by 100% (Figure S27).

**Near-infrared spectra.** UV-Vis measurements were carried out by a Perkin-Elmer lambda 750 and a Perkin Elmer lambda 365 spectrophotometer. Luminescence spectra were recorded on a Horiba Fluorolog FL-3-22 equipped with CW 450W Xenon source. Data were collected by using a water-cooled UV-Vis R2658P PMT from Hamamatsu (range 220-1010 nm), a thermoelectrically-cooled

H10330-75 NIR-PMT from Hamamatsu (range 950-1700 nm) and a UV-enhanced photodiode for monitoring the intensity of the excitation light. The signals were corrected for instrument correction factors. The correction factor for the range between 930–950 nm on the NIR detector was calculated by measuring indocyanine green in DMSO ( $2.8 \cdot 10^{-5}$  M) with both PMTs, normalising the background subtracted corrected spectra at 960 nm where both detectors had a known correction function, combining the two spectra, rescaling the stitched spectrum to the initial NIR PMT CPS level and dividing the stitched corrected spectrum by the background subtracted uncorrected signal to obtain a multiplicative correction factors that can be used on background subtracted uncorrected spectra. Values below 930 nm were found to be unusable due to excessive noise generated by the strong correction (i.e. low sensitivity) of the NIR detector in this range. This procedure ensured that the Yb(III) signal could be fully measured with the NIR detector that has a much better sensitivity than the UV-Vis PMT. The Yb(III) signal could not be well-resolved on the UV-Vis PMT. Excitation spectra were calculated by dividing the dark offset subtracted intensities at the chosen emission wavelength as a function of excitation wavelength by the intensities of the excitation light at each excitation wavelength.

The measured excitation and emission spectra were compared by normalising at the peak intensity of the antenna's lowest energy band and highest energy band respectively, namely 326 nm, 339 nm and 329 nm for the excitation spectra of complexes bearing the Me-, CF<sub>3</sub>- and MOM-carbostyryl antennae, and respectively 364 nm, 388 nm and 374 nm for the emission spectra. The Yb(III) excitation spectra were recorded at emission wavelength of 997 nm.

Relative quantum yields were determined via the Equation (3) on the sample solution the absorbances of which were set at  $A = 0.10$ . The relative quantum yields were calculated by subtracting the average background signal between 1125–1150 nm ( $S_{\text{bkg}}$ ) to the uncorrected raw spectra ( $S_{\text{Yb}}$ ), applying the correction function ( $CF$ ), dividing the background subtracted corrected emission spectra by the intensity of the excitation light at each scanned wavelengths as recorded by the photodiode detector ( $R_{\text{Yb}}$ ), integrating the spectra between 932–1125 nm ( $I_{\text{Yb}}$ ), dividing the integration value by the integration value of a reference compound ( $I_{\text{Yb,ref}}$ ) and multiplying by an absorption correction factor. The absorption correction factor was calculated by dividing the absorbance ( $1-T_{\text{ref}}$ ) of the reference compound at the excitation wavelength by the absorbance ( $1-T$ ) of the complex at that same wavelength.

$$\varphi_{\text{Yb}} = \frac{\Phi_{\text{Yb}}}{\Phi_{\text{Yb,ref}}} = \frac{I_{\text{Yb}} \cdot (1-T_{\text{ref}})}{I_{\text{Yb,ref}} \cdot (1-T)} = \frac{\int_{\lambda_{\text{min}}}^{\lambda_{\text{max}}} \frac{[S_{\text{Yb}}(\lambda) - S_{\text{bkg}}(\lambda)] \cdot CF(\lambda)}{R_{\text{Yb}}(\lambda)} d\lambda}{\int_{\lambda_{\text{min}}}^{\lambda_{\text{max}}} \frac{[S_{\text{Yb,ref}}(\lambda) - S_{\text{bkg,ref}}(\lambda)] \cdot CF(\lambda)}{R_{\text{Yb,ref}}(\lambda)} d\lambda} \cdot \frac{(1-T_{\text{ref}})}{(1-T)} \quad (3)$$

The spectra used in this procedure were recorded under identical conditions by exciting at 323 nm with 1 nm increments, an integration time of 1 s and slits open at 14.7 nm and 5 nm to ensure that the collected signal has a decent intensity and therefore that the signal to noise ratio is higher. The precision of the relative quantum yields was estimated by considering the relative errors on the absorbances and the relative error on the integrated spectra. The relative error on the integrated spectra was estimated by calculating the standard deviation of the background signal and multiplying it by the number of wavelengths over which the emission was integrated. The total relative error was then calculated by taking the square root of the sum of the squared relative errors.

**Paramagnetic <sup>1</sup>H NMR.** <sup>1</sup>H NMR spectra (400 MHz) of Yb complexes at r.t. were recorded using general parameters: 1 ms relaxation delay, 1024 number of scans, 32768 number of points and –40 to 60 ppm range.

**Crystallography.** Measurements were performed using graphite-monochromatised Mo  $K_{\alpha}$  radiation at 170 K using a Bruker D8 APEX-II equipped with a CCD camera. The structures were solved by direct methods (SHELXS-2014) and refined by full-matrix least-squares techniques against  $F^2$  (SHELXL-2018). The non-hydrogen atoms were refined with anisotropic displacement parameters. The H atoms of the  $\text{CH}_2$  / CH groups were refined with common isotropic displacement parameters for the H atoms of the same group and idealised geometry. The H atoms of the methyl groups were refined with common isotropic displacement parameters for the H atoms of the same group and idealised staggered geometry; one methyl group is modelled as a disordered staggered configuration.

Specific for **YbL<sup>CF3</sup>-F**: Lattice  $\text{H}_2\text{O}$  protons were located on the difference map. Those which could not be located on the difference map were omitted.

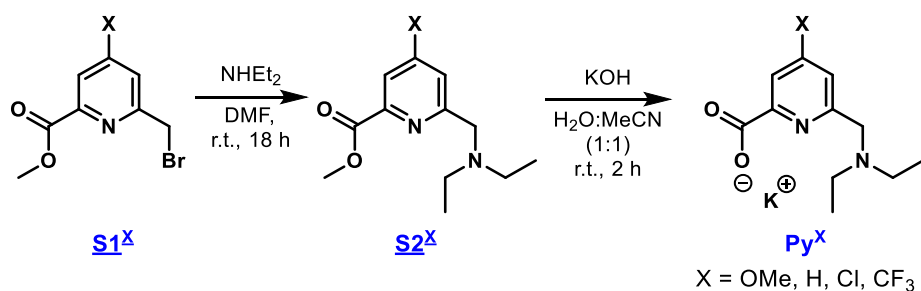
Specific for **YbL<sup>H</sup>**: The lattice  $\text{H}_2\text{O}$  protons could not be found on the difference map and were omitted. Solvent accessible voids were treated using the Olex2 solvent mask accounting for 374.5 electrons in a  $1002 \text{ \AA}^3$  large void (equivalent to approximately 37.5  $\text{H}_2\text{O}$  molecules per unit cell, or 18.75 per asymmetric unit). The final output of solvent mask is appended to the cif file.

**Electrochemistry.** Cyclic voltammograms were measured in a glovebox (Ar) at r.t. ( $\sim 20 \text{ }^\circ\text{C}$ ) using an AUTOLAB PGSTAT100 potentiostat equipped with a 3 mm glassy carbon electrode, a platinum wire auxiliary electrode, and a silver reference electrode ( $\text{Ag}/\text{AgNO}_3$  10 mM in MeCN). Measurements were performed in anhydrous DMF with  $\text{NBu}_4\text{ClO}_4$  (0.1 M) as the supporting electrolyte. The solvent was degassed prior to bringing it into the glovebox, by doing three freeze-pump-thaw cycles. The electrolyte solution was prepared in the glovebox. The voltammograms were recorded by scanning first toward more negative potential values (reduction).

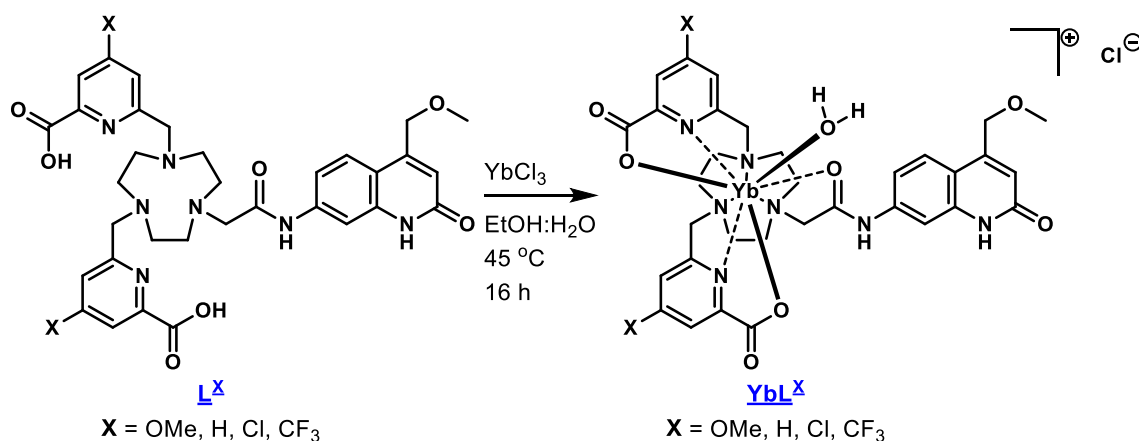
A solution of  $\text{NBu}_4\text{ClO}_4$  (0.1 M) in DMF (5 mL) was added to the electrochemical cell. The working electrode was polished with  $0.05 \text{ }\mu\text{m}$  alumina on a polishing pad, washed with water and ethanol, and dried with air before bringing into the glovebox. This was repeated before each new sample. The three electrodes (GC working electrode, platinum wire auxiliary electrode, and silver reference electrode) were inserted into the cell setup and a background scan was recorded with a scan rate of  $100 \text{ mV/s}$ , and four sweeps. The ytterbium complex was added in the solution (0.5 mM). Scans were recorded at various scan rates (50 to  $1000 \text{ mV/s}$ ) with four sweeps for each measurement. Ferrocene was used as an internal reference. At the end of the experiment, ferrocene was added to the solution, and cyclic voltammograms were recorded again at various scan rates (50 to  $1000 \text{ mV/s}$ ) with one sweep for each measurement.

## SYNTHESES

### Synthetic schemes



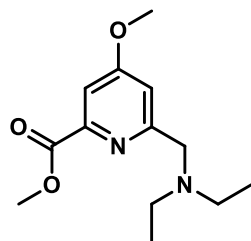
### Scheme S1. Synthesis of Py<sup>X</sup>.



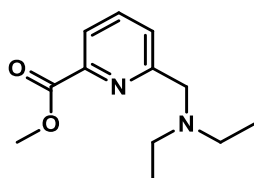
### Scheme S2. Complexation reactions for the synthesis of YbL<sup>X</sup>.

### Synthetic procedures and characterisation data

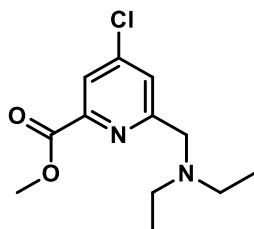
**General procedure for the synthesis of S2<sup>X</sup> (X = OMe, H, Cl, CF<sub>3</sub>).** A sample of the corresponding methyl 6-(bromomethyl)picolinate derivative (**S1<sup>X</sup>**, 1.0 equiv., 100 mg) was dissolved in DMF (0.075 M). A three-fold excess of diethylamine (3.0 equiv.) was added to the reaction mixture, which was then stirred overnight at r.t. The resulting solution of amber colour was loaded on a neutral alumina column (Heptane:Ethyl Acetate, 97:3 → 85:15). The purification yielded dark honey-coloured products of high viscosity that retained their oily appearance even after drying in vacuo.



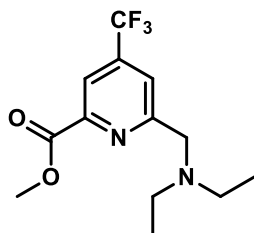
**S2<sup>OMe</sup>.** 108 mg (quant.). <sup>1</sup>H NMR (400 MHz, CD<sub>3</sub>OD) δ ppm 7.55 (d, *J* = 2.5 Hz, 1H, CH<sub>ArPy</sub>), 7.35 (d, *J* = 2.5 Hz, 1H, CH<sub>ArPy</sub>), 3.96 (s, 3H, CO<sub>2</sub>(CH<sub>3</sub>)), 3.94 (s, 3H, CO(CH<sub>3</sub>)), 3.76 (s, 2H, C<sub>ArPy</sub>CH<sub>2</sub>N), 2.61 (q, *J* = 7.0 Hz, 4H, N(CH<sub>2</sub>)<sub>2</sub>), 1.08 (t, *J* = 7.0 Hz, 6H, (CH<sub>3</sub>)<sub>2</sub>); RP-HPLC *t*<sub>R</sub> = 1.77 min (method(a)); ESI-MS obsd 253.22, calcd 253.16 (M + H)<sup>+</sup>; HR-ESI-MS obsd 275.13650, calcd 275.13661 [(M + Na)<sup>+</sup>, M = C<sub>13</sub>H<sub>20</sub>N<sub>2</sub>O<sub>3</sub>].



**S2<sup>H</sup>**. 102 mg (quant.). <sup>1</sup>H NMR (400 MHz, CD<sub>3</sub>OD) δ ppm 8.02 (d, *J* = 7.5 Hz, 1H, CH<sub>ArPy</sub>), 7.95 (t, *J* = 7.5 Hz, 1H, CH<sub>ArPy</sub>), 7.79 (d, *J* = 7.5 Hz, 1H, CH<sub>ArPy</sub>), 3.97 (s, 3H, CO<sub>2</sub>(CH<sub>3</sub>)), 3.82 (s, 2H, C<sub>ArPy</sub>CH<sub>2</sub>N), 2.61 (q, *J* = 7.0 Hz, 4H, N(CH<sub>2</sub>)<sub>2</sub>), 1.08 (t, *J* = 7.0 Hz, 6H, (CH<sub>3</sub>)<sub>2</sub>); RP-HPLC t<sub>R</sub> = 1.73 min (method(a)); ESI-MS obsd 223.61, calcd 223.15 (M + H)<sup>+</sup>; HR-ESI-MS obsd 245.12588, calcd 245.12605 [(M + Na)<sup>+</sup>, M = C<sub>12</sub>H<sub>18</sub>N<sub>2</sub>O<sub>2</sub>].

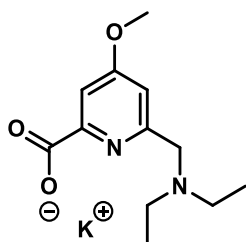


**S2<sup>Cl</sup>**. 97 mg (quant.). <sup>1</sup>H NMR (400 MHz, CD<sub>3</sub>OD) δ ppm 8.01 (dd, *J*<sub>1</sub> = 5.0 Hz, *J*<sub>2</sub> = 2.0 Hz, 1H, CH<sub>ArPy</sub>), 7.84 (s, 1H, CH<sub>ArPy</sub>), 3.98 (s, 2H, C<sub>ArPy</sub>CH<sub>2</sub>N), 3.80 (s, 3H, CO<sub>2</sub>(CH<sub>3</sub>)), 2.61 (q, *J* = 7.0 Hz, 4H, N(CH<sub>2</sub>)<sub>2</sub>), 1.07 (t, *J* = 7.0 Hz, 6H, (CH<sub>3</sub>)<sub>2</sub>); RP-HPLC t<sub>R</sub> = 1.73 min (method(a)); ESI-MS obsd 257.82, calcd 257.11 (M + H)<sup>+</sup>; HR-ESI-MS obsd 279.08742, calcd 279.08708 [(M + Na)<sup>+</sup>, M = C<sub>12</sub>H<sub>17</sub>N<sub>2</sub>O<sub>2</sub>Cl].

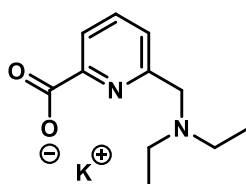


**S2<sup>CF<sub>3</sub></sup>**. 97 mg (98%). <sup>1</sup>H NMR (400 MHz, CD<sub>3</sub>OD) δ ppm 8.20 (d, *J* = 7.0 Hz, 1H, CH<sub>ArPy</sub>), 8.07 (s, 1H, CH<sub>ArPy</sub>), 4.01 (s, 2H, C<sub>ArPy</sub>CH<sub>2</sub>N), 3.91 (s, 3H, CO<sub>2</sub>(CH<sub>3</sub>)), 2.63 (q, *J* = 7.0 Hz, 4H, N(CH<sub>2</sub>)<sub>2</sub>), 1.08 (t, *J* = 7.0 Hz, 6H, (CH<sub>3</sub>)<sub>2</sub>); RP-HPLC t<sub>R</sub> = 1.73 min (method(a)); ESI-MS obsd 291.20, calcd 291.13 (M + H)<sup>+</sup>; HR-ESI-MS obsd 313.11347, calcd 313.11343 [(M + Na)<sup>+</sup>, M = C<sub>13</sub>H<sub>17</sub>N<sub>2</sub>O<sub>2</sub>F<sub>3</sub>].

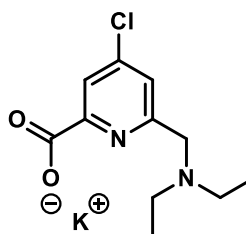
**General procedure for the synthesis of model pyridine derivatives Py<sup>X</sup> (X = OMe, H, Cl, CF<sub>3</sub>).** A sample of corresponding **S2<sup>X</sup>** (1.0 equiv., 50 mg) was suspended in an equal mixture of MeCN and H<sub>2</sub>O (0.07 M). An aqueous solution of potassium hydroxide (1.5 equiv., 1 M) was added dropwise to the suspension. The complete hydrolysis of the methyl ester was achieved after 4 h of stirring the reaction mixture at r.t. Upon conversion, the white suspension turned into a transparent beige solution, which was loaded on an alumina column conditioned with pure MeCN. Elution with MeCN:H<sub>2</sub>O, 19:1 → 9:1 under low gradient resulted in off-white sticky solids that were dried under vacuum.



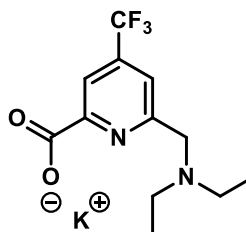
**Py<sup>OMe</sup>.** 71 mg (quant.). <sup>1</sup>H NMR (400 MHz, D<sub>2</sub>O) δ ppm 7.50 (d, *J* = 2.5 Hz, 1H, CH<sub>Ar</sub>), 7.14 (d, *J* = 2.5 Hz, 1H, CH<sub>Ar</sub>), 4.43 (s, 2H, C<sub>ArPy</sub>CH<sub>2</sub>N), 3.94 (s, 3H, CO(CH<sub>3</sub>)), 3.28 (q, *J* = 7.5 Hz, 4H, N(CH<sub>2</sub>)<sub>2</sub>), 1.31 (t, *J* = 7.5 Hz, 6H, (CH<sub>3</sub>)<sub>2</sub>); <sup>13</sup>C NMR (101 MHz, D<sub>2</sub>O) δ ppm 172.1 (CO<sub>2</sub><sup>-</sup>), 167.9 (C<sub>ArPy</sub>O(CH<sub>3</sub>)), 154.9 (C<sub>ArPy</sub>), 151.2 (C<sub>ArPy</sub>), 111.4 (CH<sub>ArPy</sub>), 110.1 (CH<sub>ArPy</sub>), 56.2 (C<sub>ArPy</sub>CH<sub>2</sub>N), 55.9 (C<sub>ArPy</sub>O(CH<sub>3</sub>)), 48.2 (N(CH<sub>2</sub>)<sub>2</sub>), 8.2 ((CH<sub>3</sub>)<sub>2</sub>); RP-HPLC t<sub>R</sub> = 1.67 min (method(a)); ESI-MS obsd 477.47, calcd 477.27 (2M + 3H)<sup>+</sup>; HR-ESI-MS obsd 261.12078, calcd 261.12096 [(M + Na + H)<sup>+</sup>, M = C<sub>12</sub>H<sub>17</sub>N<sub>2</sub>O<sub>3</sub><sup>-</sup>].



**Py<sup>H</sup>.** 86 mg (quant.). <sup>1</sup>H NMR (400 MHz, D<sub>2</sub>O) δ ppm 8.05–7.92 (m, 2H, CH<sub>ArPy</sub>), 7.58 (d, *J* = 7.0 Hz, 1H, CH<sub>ArPy</sub>), 4.52 (s, 2H, C<sub>ArPy</sub>CH<sub>2</sub>N), 3.29 (q, *J* = 7.5 Hz, 4H, N(CH<sub>2</sub>)<sub>2</sub>), 1.31 (t, *J* = 7.5 Hz, 6H, (CH<sub>3</sub>)<sub>2</sub>); <sup>13</sup>C NMR (101 MHz, D<sub>2</sub>O) δ ppm 172.4 (CO<sub>2</sub><sup>-</sup>), 152.9 (C<sub>ArPy</sub>), 149.6 (C<sub>ArPy</sub>), 139.4 (CH<sub>ArPy</sub>), 125.5 (CH<sub>ArPy</sub>), 124.0 (CH<sub>ArPy</sub>), 56.2 (C<sub>ArPy</sub>CH<sub>2</sub>N), 48.2 (N(CH<sub>2</sub>)<sub>2</sub>), 8.3 ((CH<sub>3</sub>)<sub>2</sub>); RP-HPLC t<sub>R</sub> = 1.67 min (method(a)); ESI-MS obsd 417.38, calcd 417.25 (2M + 3H)<sup>+</sup>; HR-ESI-MS obsd 231.11020, calcd 231.11040 [(M + Na + H)<sup>+</sup>, M = C<sub>11</sub>H<sub>15</sub>N<sub>2</sub>O<sub>2</sub><sup>-</sup>].



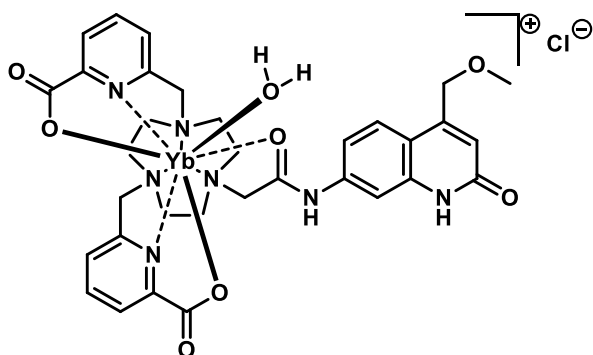
**Py<sup>Cl</sup>.** 61 mg (quant.). <sup>1</sup>H NMR (400 MHz, D<sub>2</sub>O) δ ppm 7.95 (d, *J* = 1.5 Hz, 1H, CH<sub>Ar</sub>), 7.63 (d, *J* = 1.5 Hz, 1H, CH<sub>Ar</sub>), 4.49 (s, 2H, C<sub>ArPy</sub>CH<sub>2</sub>N), 3.27 (q, *J* = 7.5 Hz, 4H, N(CH<sub>2</sub>)<sub>2</sub>), 1.29 (t, *J* = 7.5 Hz, 6H, (CH<sub>3</sub>)<sub>2</sub>); <sup>13</sup>C NMR (101 MHz, D<sub>2</sub>O) δ ppm 170.9 (CO<sub>2</sub><sup>-</sup>), 154.3 (C<sub>ArPy</sub>Cl), 151.2 (C<sub>ArPy</sub>), 146.6 (C<sub>ArPy</sub>), 125.4 (CH<sub>ArPy</sub>), 124.3 (CH<sub>ArPy</sub>), 55.7 (C<sub>ArPy</sub>CH<sub>2</sub>N), 48.3 (N(CH<sub>2</sub>)<sub>2</sub>), 8.3 ((CH<sub>3</sub>)<sub>2</sub>); RP-HPLC t<sub>R</sub> = 1.67 min (method(a)); ESI-MS obsd 485.96, calcd 485.17 (2M + 3H)<sup>+</sup>; HR-ESI-MS obsd 265.07137, calcd 265.07143 [(M + Na + H)<sup>+</sup>, M = C<sub>11</sub>H<sub>14</sub>N<sub>2</sub>O<sub>2</sub>Cl<sup>-</sup>].



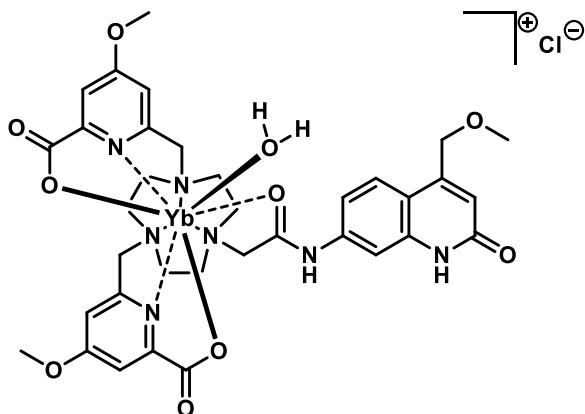
**Py<sup>CF3</sup>.** 53 mg (98%). <sup>1</sup>H NMR (400 MHz, D<sub>2</sub>O) δ ppm 8.23 (s, 1H, CH<sub>Ar</sub>), 7.90 (s, 1H, CH<sub>Ar</sub>), 4.62 (s, 2H, C<sub>ArPy</sub>CH<sub>2</sub>N), 3.30 (q, *J* = 7.5 Hz, 4H, N(CH<sub>2</sub>)<sub>2</sub>), 1.31 (t, *J* = 7.5 Hz, 6H, (CH<sub>3</sub>)<sub>2</sub>); <sup>13</sup>C NMR (101

MHz, D<sub>2</sub>O)  $\delta$  ppm 170.7 (CO<sub>2</sub><sup>-</sup>), 154.5 (C<sub>ArPy</sub>), 151.6 (C<sub>ArPy</sub>), 140.5 (q,  $J = 34.5$  Hz, C<sub>ArPy</sub>(CF<sub>3</sub>)), 122.4 (q,  $J = 273$  Hz, CF<sub>3</sub>), 121.2 (d,  $J = 4$  Hz, (CH<sub>ArPy</sub>)), 119.9 (d,  $J = 4$  Hz, (CH<sub>ArPy</sub>)), 55.9 (C<sub>ArPy</sub>CH<sub>2</sub>N), 48.4 (N(CH<sub>2</sub>)<sub>2</sub>), 8.3 ((CH<sub>3</sub>)<sub>2</sub>); <sup>19</sup>F NMR (376 MHz, D<sub>2</sub>O)  $\delta$  ppm -64.7; RP-HPLC  $t_R = 4.08$  min (method(b)); ESI-MS obsd 552.73, calcd 552.22 (2M + 2H)<sup>+</sup>; HR-ESI-MS obsd 299.09769, calcd 299.09778 [(M + Na + H)<sup>2+</sup>, M = C<sub>12</sub>H<sub>14</sub>N<sub>2</sub>O<sub>2</sub>F<sub>3</sub><sup>-</sup>].

**General procedure for the synthesis of YbL<sup>X</sup> (X = OMe, H, Cl, CF<sub>3</sub>).** Samples of the corresponding L<sup>X</sup> (1 equiv.) and anhydrous YbCl<sub>3</sub> (2.4 equiv.) were dissolved in H<sub>2</sub>O:EtOH equal mixture (0.05 M). The reaction solutions were stirred at 45 °C for 16 h. The next day the completion of the complexation was confirmed via LC-MS and TLC analysis. The reaction mixtures were purified from the excess of lanthanide(III) salt via column chromatography on neutral alumina (Isopropanol:H<sub>2</sub>O, 9:1→6:4; Isopropanol:EtOH:H<sub>2</sub>O, 4:2:4→2:4:4) yielding colourless complexes. The isolated compounds contained traces of YbCl<sub>3</sub>. For CV measurements Yb(OTf)<sub>3</sub> was used instead of the chloride for the synthesis of the analogous complexes with different counterions.

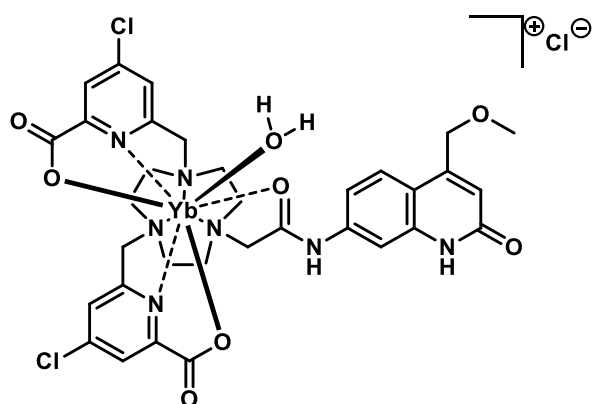


**YbL<sup>H</sup>.** 62 mg (quant.). RP-HPLC  $t_R = 3.72, 4.60$  min (method(d)); <sup>1</sup>H NMR (400 MHz, CD<sub>3</sub>OD)  $\delta$  ppm -27.86, -27.59, -19.15, -18.68, -16.70, -11.25, -9.81, -4.29, -1.33, 0.90, 1.31, 1.93, 2.04, 2.16, 5.34, 5.53, 7.22, 8.55, 8.96, 9.71, 11.55, 12.35, 13.72, 15.71, 18.88, 22.02, 24.07, 24.80, 25.82, 27.10, 33.44, 38.66, 45.43; ESI-MS obsd 815.53, calcd 815.20 (M)<sup>+</sup>; HR-ESI-MS obsd 815.19885, calcd 815.19865 [(M)<sup>+</sup>, M = C<sub>33</sub>H<sub>35</sub>N<sub>7</sub>O<sub>7</sub>Yb]; FT-IR (cm<sup>-1</sup>, KBr pellet): 3405, 1637, 1596, 1395, 1260, 1166;  $\lambda_{em} = 376$  nm ( $\lambda_{ex} = 329$  nm); 979, 1006 nm ( $\lambda_{ex} = 323$  nm).

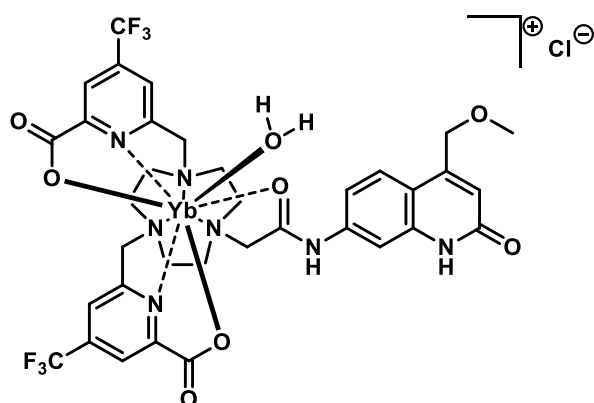


**YbL<sup>OMe</sup>.** 65 mg (quant.). RP-HPLC  $t_R = 3.73$  min (method(d)); <sup>1</sup>H NMR (400 MHz, CD<sub>3</sub>OD)  $\delta$  ppm -26.30, -22.24, -20.91, -16.20, -13.83, -13.37, -5.06, -3.80, 0.20, 0.9, 1.29, 1.60, 2.03, 2.16, 2.55,

4.61, 5.34, 6.85, 7.07, 7.37, 8.79, 10.69, 12.62, 13.95, 19.96, 21.28, 23.52, 23.95, 26.81, 31.04, 35.73, 56.77; ESI-MS obsd 875.70, calcd 875.22 (M)<sup>+</sup>; HR-ESI-MS obsd 875.22005, calcd 875.21983 [(M)<sup>+</sup>, M = C<sub>35</sub>H<sub>39</sub>N<sub>7</sub>O<sub>9</sub>Yb]; FT-IR (cm<sup>-1</sup>, KBr pellet): 3409, 1610, 1415, 1254, 1172, 1034; λ<sub>em</sub> = 375 nm (λ<sub>ex</sub> = 329 nm); 979, 1006 nm (λ<sub>ex</sub> = 323 nm).



**YbL<sup>Cl</sup>**. 43 mg (quant.). RP-HPLC *t<sub>R</sub>* = 3.58 min (method(d)); <sup>1</sup>H NMR (400 MHz, CD<sub>3</sub>OD) δ ppm -27.88, -27.50, -18.91, -16.70, -11.35, -9.68, -4.30, -1.48, 0.10, 0.90, 1.29, 1.33, 1.60, 2.03, 2.16, 4.60, 7.24, 8.45, 8.70, 8.95, 9.72, 11.55, 12.33, 13.70, 15.72, 18.87, 21.90, 24.07, 25.77, 27.14, 33.39, 38.60, 45.39; ESI-MS obsd 883.75, calcd 883.12 (M)<sup>+</sup>; HR-ESI-MS obsd 883.11937, calcd 883.11903 [(M)<sup>+</sup>, M = C<sub>33</sub>H<sub>33</sub>N<sub>7</sub>O<sub>7</sub>Cl<sub>2</sub>Yb]; FT-IR (cm<sup>-1</sup>, KBr pellet): 3408, 1654, 1589, 1375, 1255, 1161, 1032; λ<sub>em</sub> = 376 nm (λ<sub>ex</sub> = 329 nm); 979, 1006 nm (λ<sub>ex</sub> = 323 nm).



**YbL<sup>CF<sub>3</sub></sup>**. 32 mg (78%). RP-HPLC *t<sub>R</sub>* = 7.50 min (method(c)); <sup>1</sup>H NMR (400 MHz, CD<sub>3</sub>OD) δ ppm -34.82, -33.87, -21.17, -20.68, -16.77, -13.33, -9.00, -7.80, -6.23, -5.68, -1.40, 0.10, 0.90, 1.29, 1.60, 1.85, 2.16, 4.21, 4.50, 4.61, 5.34, 8.27, 10.72, 11.90, 12.12, 16.07, 16.66, 17.02, 17.24, 21.10, 23.20, 24.19, 26.36, 28.44, 33.43, 54.81; ESI-MS obsd 951.77, calcd 951.17 (M)<sup>+</sup>; HR-ESI-MS obsd 951.17407, calcd 951.17346 [(M)<sup>+</sup>, M = C<sub>33</sub>H<sub>33</sub>N<sub>7</sub>O<sub>7</sub>Cl<sub>2</sub>Yb]; FT-IR (cm<sup>-1</sup>, KBr pellet): 3544, 3406, 1651, 1456, 1325, 1258, 1171, 1033; λ<sub>em</sub> = 376 nm (λ<sub>ex</sub> = 329 nm); 979, 1006 nm (λ<sub>ex</sub> = 323 nm).

## $^1\text{H}$ NMR SPECTRA OF Yb(III) COMPLEXES

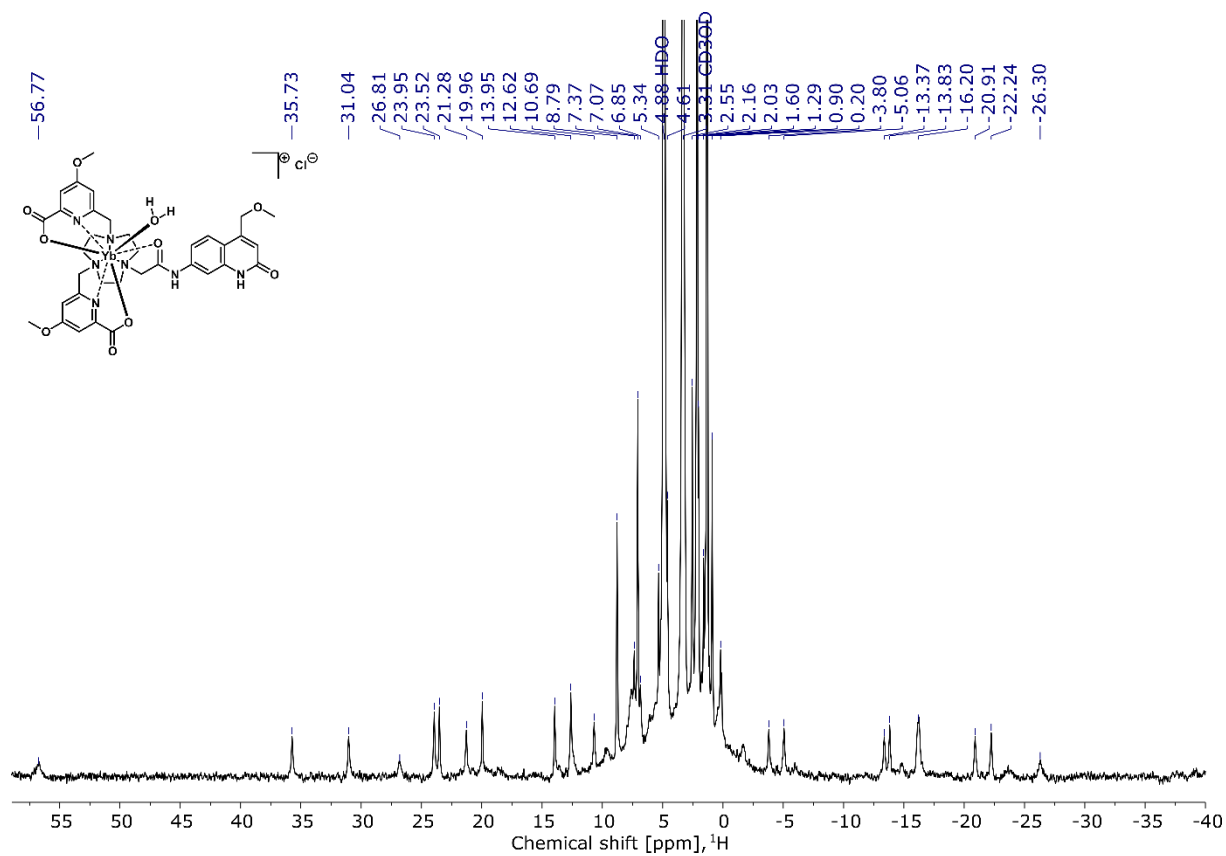


**Figure S1.**  $^1\text{H}$  NMR spectrum (400 MHz) of YbL<sup>OMe</sup> measured in CD<sub>3</sub>OD at 298 K.

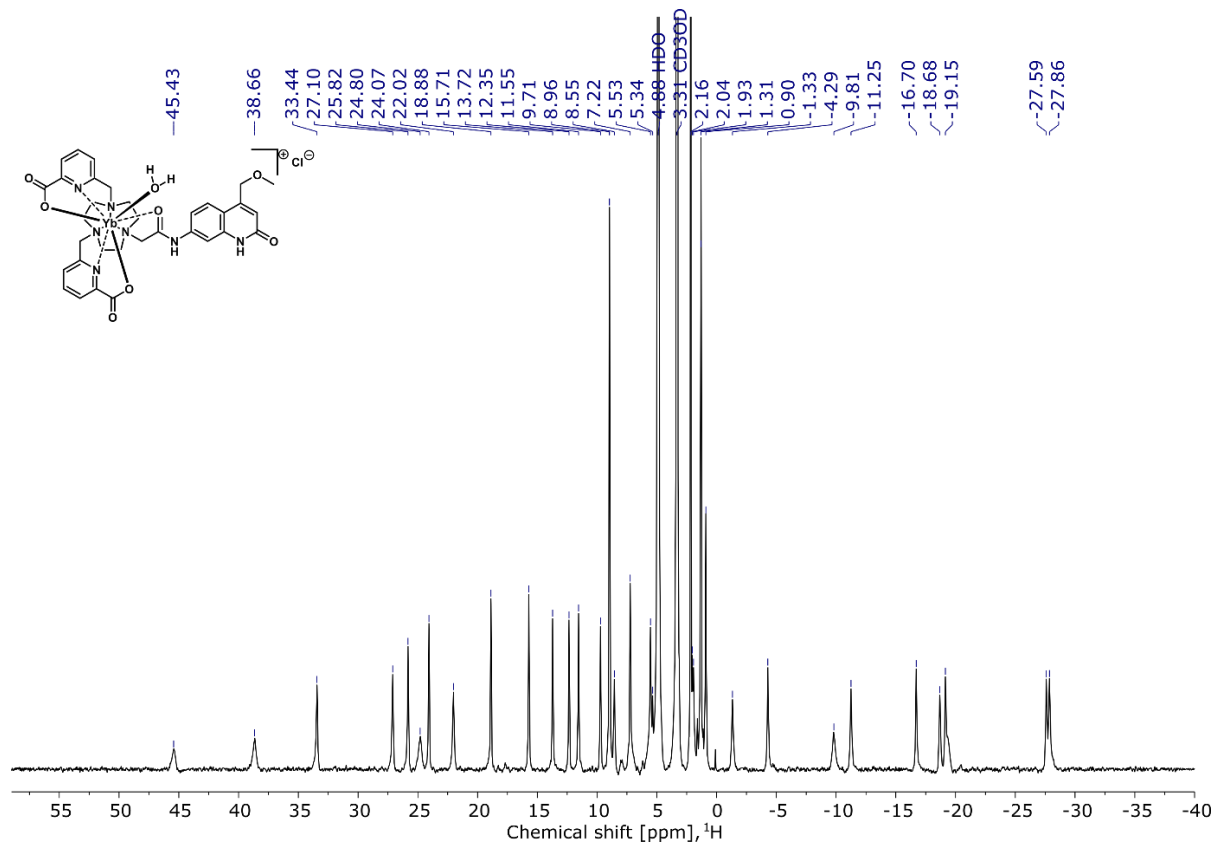


**Figure S2.**  $^1\text{H}$  NMR spectrum (400 MHz) of YbL<sup>H</sup> measured in CD<sub>3</sub>OD at 298 K.

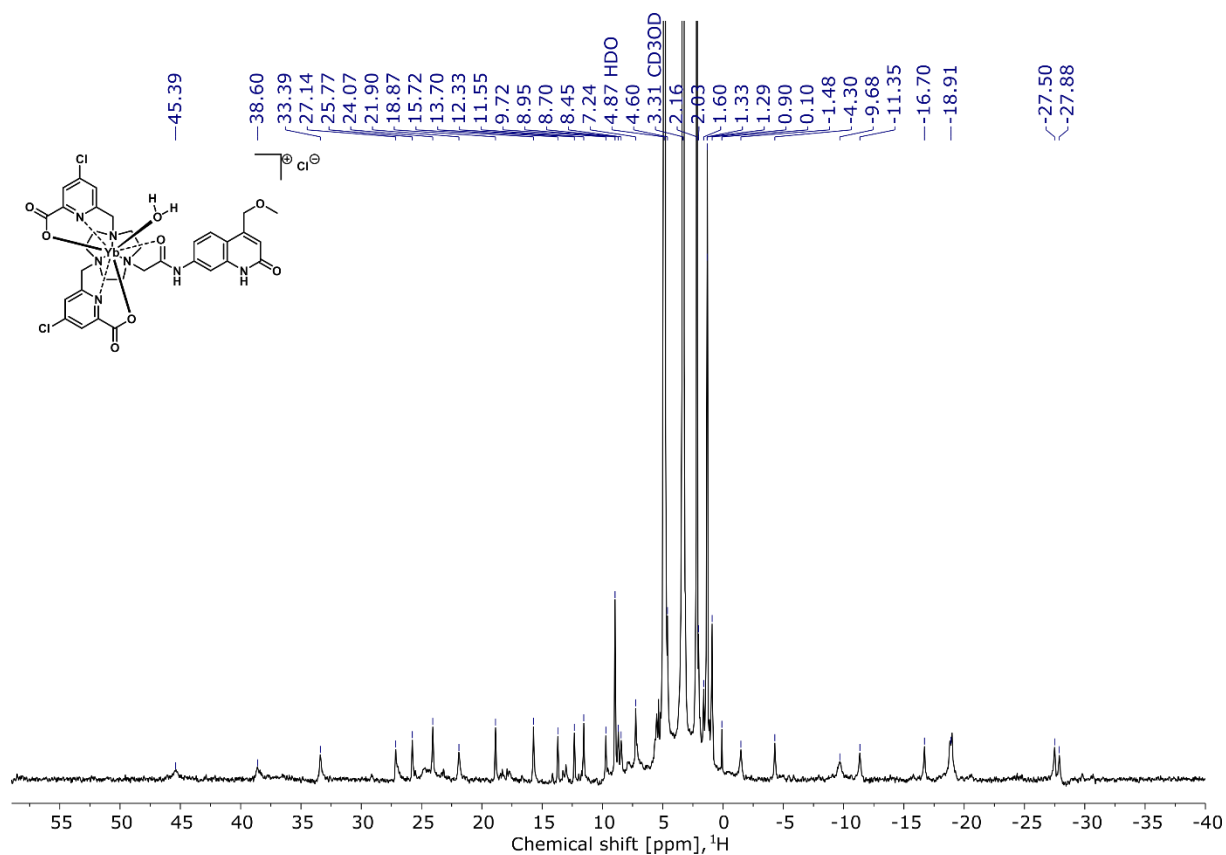


**Figure S3.**  $^1\text{H}$  NMR spectrum (400 MHz) of  $\text{YbL}^{\text{Cl}}$  measured in  $\text{CD}_3\text{OD}$  at 298 K.

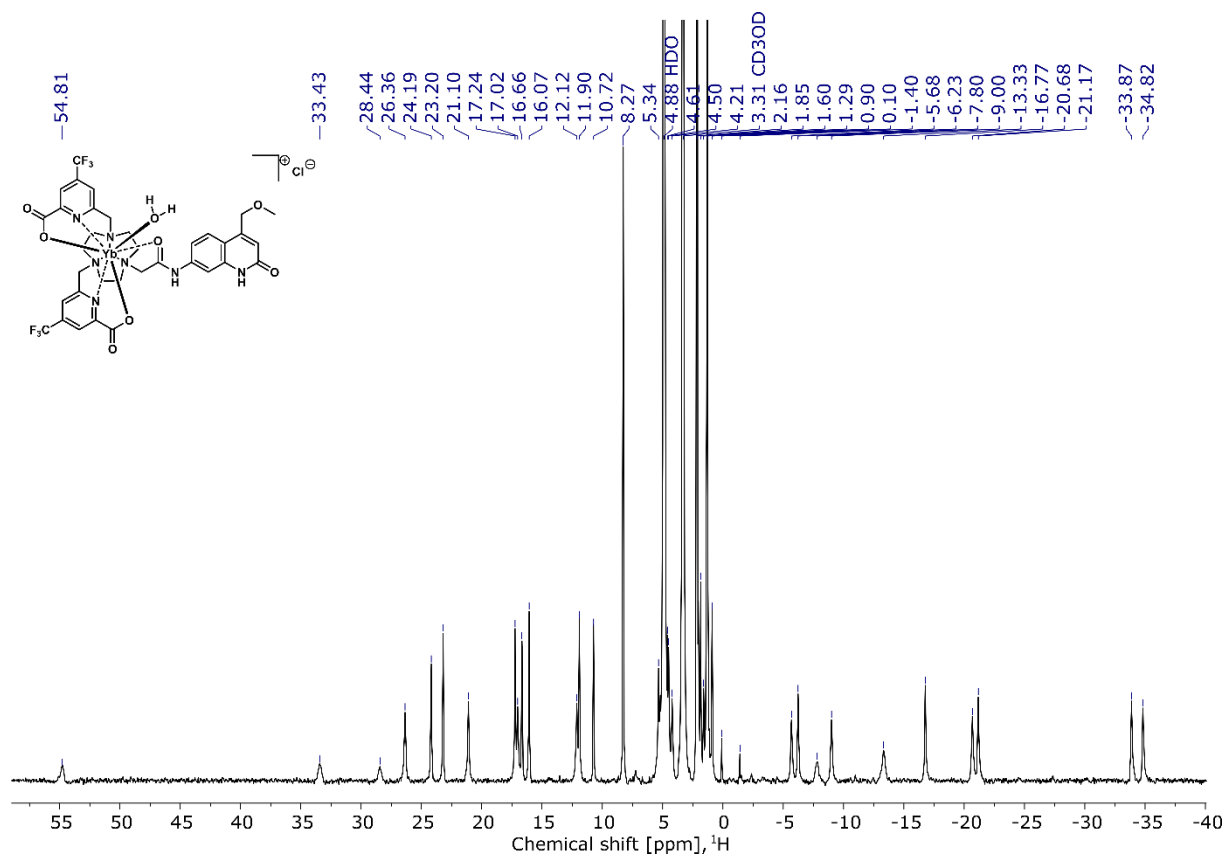


**Figure S4.**  $^1\text{H}$  NMR spectrum (400 MHz) of  $\text{YbL}^{\text{CF}_3}$  measured in  $\text{CD}_3\text{OD}$  at 298 K.

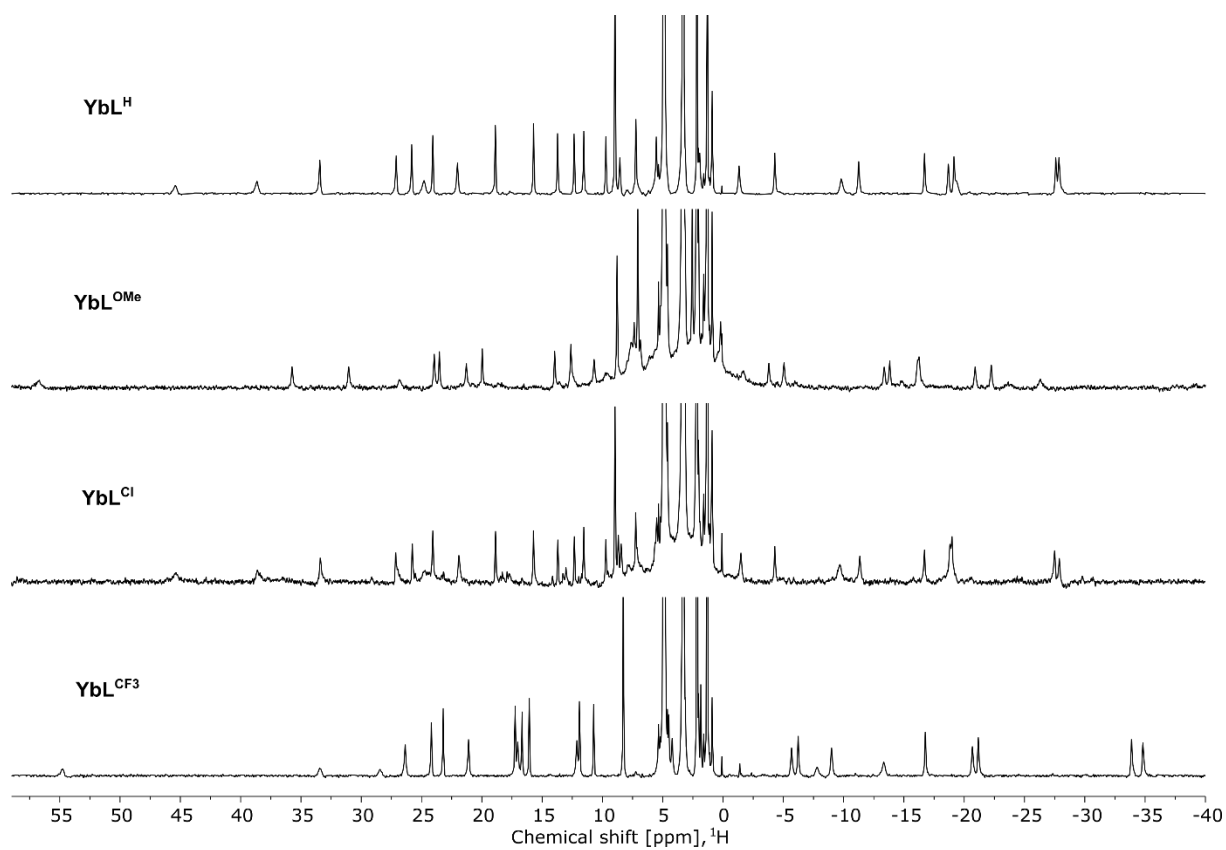


**Figure S5.** Stacked  $^1\text{H}$  NMR spectra (400 MHz) of  $\text{YbL}^{\text{X}}$  measured in  $\text{CD}_3\text{OD}$  at 298 K.

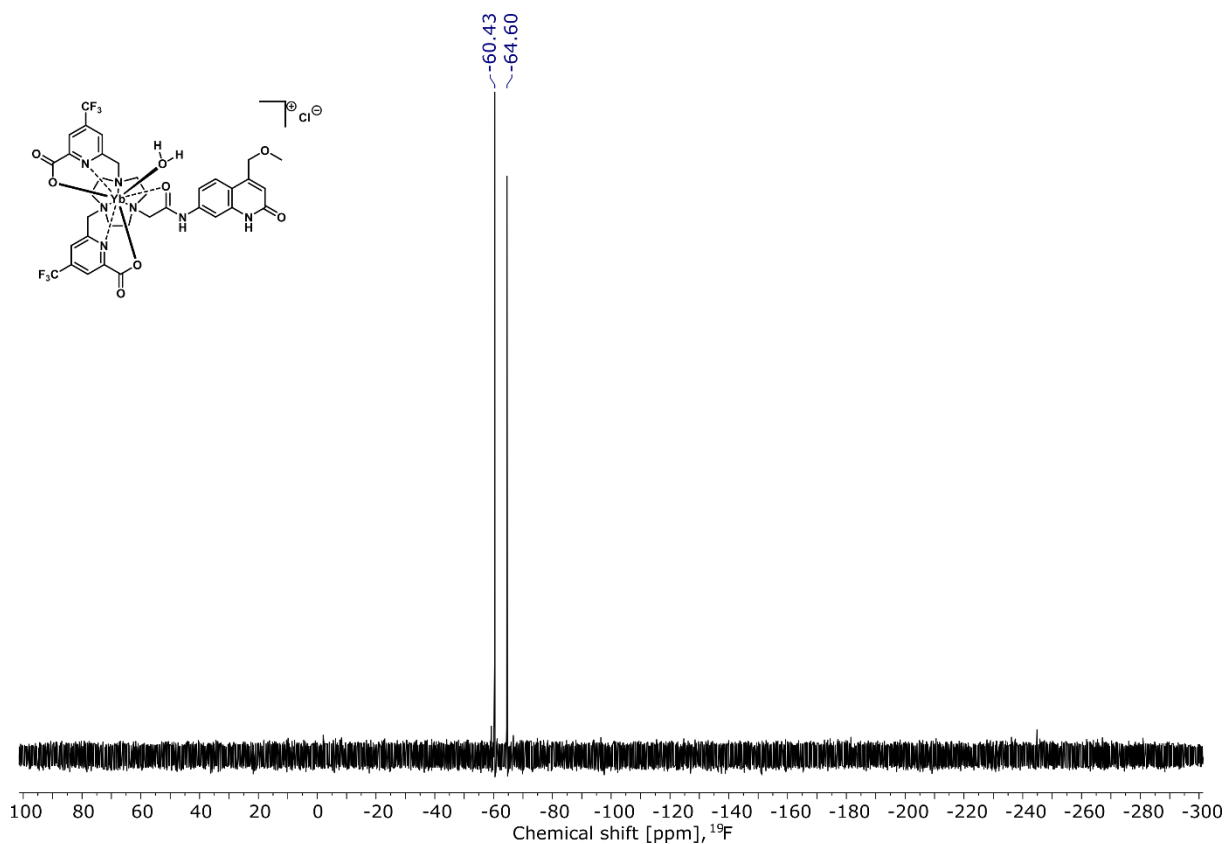


**Figure S6.**  $^{19}\text{F}$  NMR spectrum (376 MHz) of  $\text{YbL}^{\text{CF}_3}$  measured in  $\text{CD}_3\text{OD}$  at 298 K.

## X-RAY CRYSTALLOGRAPHY

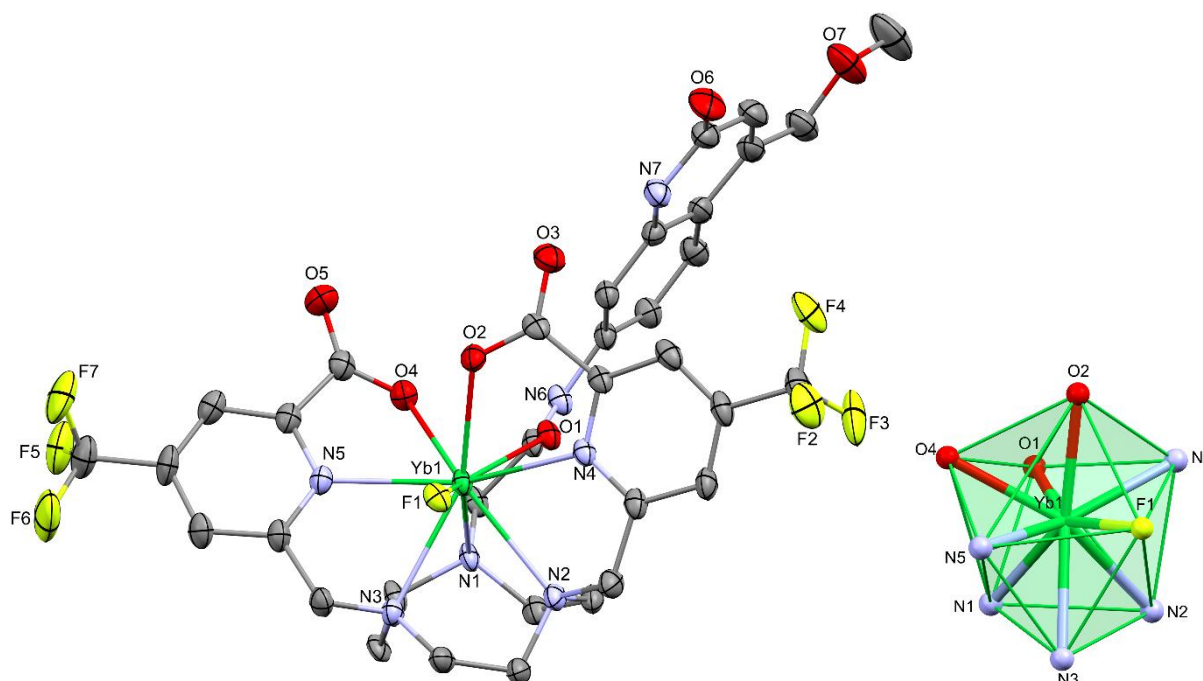


**Figure S7.** Single crystal structure of  $\text{YbL}^{\text{CF}_3\text{-F}}$  (left) and the coordination environment of Yb (right). H atoms and water molecules omitted for clarity. Ellipsoids displayed at 50% probability.

### Crystallographic tables

**Table S1.** NCCN(tacn) and NCCO/NCCN<sub>Py</sub> (°) torsion angles for  $\text{YbL}^{\text{H}}$  and  $\text{YbL}^{\text{CF}_3\text{-F}}$ .

Parameter	$\text{YbL}^{\text{H}}$		$\text{YbL}^{\text{CF}_3\text{-F}}$	
	Yb1	Yb2	Yb1	Yb1
X =	$\text{H}_2\text{O}$	$\text{H}_2\text{O}$	<b>F</b>	<b>F</b>
$\text{N}_1\text{C}_1\text{C}_2\text{N}_2$	$\pm 48.15$	$\pm 48.44^{\text{a}}$	$-50.24$	$50.24$
$\text{N}_2\text{C}_{10}\text{C}_{11}\text{N}_4$	$\pm 48.85$	$\pm 49.91^{\text{b}}$	$-55.29^{\text{g}}$	$55.29^{\text{g}}$
$\text{N}_4\text{C}_{19}\text{C}_{20}\text{N}_1$	$\pm 51.25$	$\pm 50.72^{\text{c}}$	$-47.84^{\text{h}}$	$47.84^{\text{h}}$
<b>Mean NCCN torsion angle</b>	$\pm 49.42$	$\pm 49.69$	$-51.12$	$51.12$
$\text{N}_1\text{C}_{21}\text{C}_{22}\text{O}_1$	$\pm 21.45$	$\pm 24.23^{\text{d}}$	$19.72^{\text{i}}$	$-19.72^{\text{i}}$
$\text{N}_2\text{C}_3\text{C}_4\text{N}_3$	$\pm 24.96$	$\pm 22.07^{\text{e}}$	$-32.61^{\text{j}}$	$32.61^{\text{j}}$
$\text{N}_4\text{C}_{12}\text{C}_{13}\text{N}_5$	$\pm 41.28$	$\pm 43.93^{\text{f}}$	$30.10^{\text{k}}$	$-30.10^{\text{k}}$
<b>Isomer<sup>3</sup></b>	$\Lambda(\delta\delta\delta)$ $\Lambda(\lambda\lambda\lambda)$	$\Lambda(\lambda\lambda\lambda)$ $\Lambda(\delta\delta\delta)$	$\Lambda(\lambda\lambda\lambda)$	$\Lambda(\delta\delta\delta)$

<sup>a</sup> The torsion angle of  $\text{N}_8\text{C}_{34}\text{C}_{35}\text{N}_9$ . <sup>b</sup> The torsion angle of  $\text{N}_9\text{C}_{43}\text{C}_{44}\text{N}_{11}$ . <sup>c</sup> The torsion angle of  $\text{N}_{11}\text{C}_{52}\text{C}_{53}\text{N}_8$ . <sup>d</sup> The torsion angle of  $\text{N}_8\text{C}_{54}\text{C}_{55}\text{O}_9$ . <sup>e</sup> The torsion angle of  $\text{N}_9\text{C}_{36}\text{C}_{37}\text{N}_{10}$ . <sup>f</sup> The torsion angle of  $\text{N}_{11}\text{C}_{45}\text{C}_{46}\text{O}_{12}$ . <sup>g</sup> The torsion angle of  $\text{N}_2\text{C}_{11}\text{C}_{12}\text{N}_3$ . <sup>h</sup> The torsion angle of  $\text{N}_3\text{C}_{21}\text{C}_{22}\text{N}_1$ . <sup>i</sup> The torsion angle of  $\text{N}_1\text{C}_{23}\text{C}_{24}\text{O}_1$ . <sup>j</sup> The torsion angle of  $\text{N}_2\text{C}_3\text{C}_4\text{N}_4$ . <sup>k</sup> The torsion angle of  $\text{N}_3\text{C}_{13}\text{C}_{14}\text{N}_5$ .

Selected Yb–O, Yb–N and Yb–X distances (where X denotes the co-ligand, either fluoride or water) are displayed in Table S2 for tacn complexes and Table S3 for cyclen complexes. The tables follow the conventions outlined in Figure S34. If the solid-state structure contains two Yb centres in the asymmetric unit, the numbering presented in Figure S34 is employed for Yb1, and followed numerically using the convention for Yb2.

**Table S2.** Selected bond lengths (Å) for **YbL<sup>CF3</sup>-F** and **YbL<sup>H</sup>**. The X ligand denotes the ligand which occupies the capping position of the capped square antiprism.

Parameter	<b>YbL<sup>CF3</sup>-F</b>	<b>YbL<sup>H</sup></b>
<b>Yb1–O1</b>	2.400(2)	2.355(2)
<b>Yb1–O2</b>	2.352(2)	2.389(2)
<b>Yb1–O4</b>	2.396(2)	2.306(2)-
<b>Yb2–O8</b>	-	2.361(2)
<b>Yb2–O9</b>	-	2.384(2)
<b>Yb2–O11</b>	-	2.323(2)
<b>Yb1–N1</b>	2.542(2)	2.547(2)
<b>Yb1–N2</b>	2.632(2)	2.599(2)
<b>Yb1–N3</b>	2.640(2)	2.467(2)
<b>Yb1–N4</b>	2.478(2)	2.632(2)
<b>Yb1–N5</b>	2.512(2)	2.456(2)
<b>Yb2–N8</b>	-	2.513(3)
<b>Yb2–N9</b>	-	2.601(3)
<b>Yb2–N10</b>	-	2.477(3)
<b>Yb2–N11</b>	-	2.649(4)
<b>Yb2–N12</b>	-	2.473(3)
<b>Yb1–X1</b>	2.110(2)	2.313(2)
<b>Yb2–X2</b>	-	2.326(2)
<b>NNO<sub>PL</sub>–Yb1–NNN<sub>PL</sub>, °</b>	123.4(2)	125.4(2)
<b>NNO<sub>PL</sub>–Yb1–NNN<sub>PL</sub>, °</b>	-	125.2(2)
<b>Yb1–NNO<sub>PL</sub></b>	0.652(2)	0.660(2)
<b>Yb2–NNO<sub>PL</sub></b>	-	0.656(2)
<b>Yb1–NNN<sub>PL</sub></b>	1.986(2)	1.967(2)
<b>Yb2–NNN<sub>PL</sub></b>	-	1.967(2)
<b>X1 =</b>	F <sup>-</sup>	H <sub>2</sub> O
<b>X2 =</b>	-	H <sub>2</sub> O

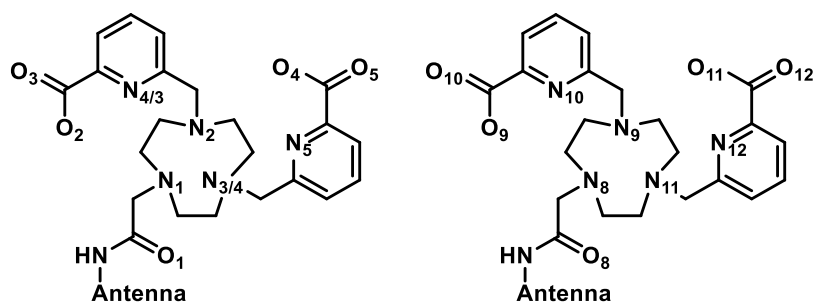


**Figure S8.** Numbering convention for Table S2 for Yb1 (left) and Yb1 and Yb2 (left and right).

CCDC 2095001 and 2095002 contain the supplementary crystallographic data for this paper. The data can be obtained free of charge from The Cambridge Crystallographic Data Centre via [www.ccdc.cam.ac.uk/structures](http://www.ccdc.cam.ac.uk/structures).

**Table S3.** Crystal data and structure refinement.

Compound	<b>YbL<sup>CF3</sup>-F</b>	<b>YbL<sup>H</sup></b>
<b>Chemical formula</b>	C <sub>35</sub> H <sub>33</sub> F <sub>7</sub> N <sub>7</sub> O <sub>7</sub> Yb ·4.2(H <sub>2</sub> O)·0.4(HO)	C <sub>33</sub> H <sub>35</sub> N <sub>7</sub> O <sub>8</sub> Yb· C <sub>33</sub> H <sub>34</sub> N <sub>7</sub> O <sub>8</sub> Yb ·2(Cl)·13(O)
<i>M<sub>r</sub></i>	1052.19	1939.33
<b>Crystal system, space group</b>	Monoclinic <i>P21/c</i>	Triclinic <i>P</i> -1
<b>Temperature (K)</b>	170	170
<i>a, b, c</i> (Å)	13.0200 (14) 22.477 (2) 14.9599 (16)	16.0996 (14) 17.255 (2) 20.7070 (18)
<i>α, β, γ</i> (°)	- 113.294(2) -	87.265 (2) 77.241 (1) 63.270 (1)
<i>V</i> (Å <sup>3</sup> )	4021.2 (7)	5001.9 (9)
<i>Z</i>	4	2
<b>Radiation type</b>	Mo K <sub>α</sub>	Mo K <sub>α</sub>
<i>μ</i> (mm <sup>-1</sup> )	2.43	1.98
<b>Crystal size (mm)</b>	0.52 × 0.18 × 0.08	0.64 × 0.16 × 0.13
<b>Diffractometer</b>	Bruker D8 APEX-II	Bruker D8 APEX-II
<b>Absorption correction</b>	Multi-scan	Multi-scan
<i>T<sub>min</sub>, T<sub>max</sub></i>	0.452, 0.746	0.622, 0.746
<b>No. of measured, independent and observed [<i>I</i> &gt; 2<i>s</i>(<i>I</i>)] reflections</b>	88634 11433	108395 30639
<i>R<sub>int</sub></i>	8768 0.098	25020 0.045
( <i>sin θ/λ</i> ) <sub>max</sub> (Å <sup>-1</sup> )	0.719	0.718
<i>R</i> [ <i>F</i> <sup>2</sup> > 2σ( <i>F</i> <sup>2</sup> )], <i>wR</i> ( <i>F</i> <sup>2</sup> ), <i>S</i>	0.038, 0.082, 1.00	0.032, 0.096, 1.02
<b>No. of parameters</b>	639	1038
<b>No. of restraints</b>	27	-
<b>H-atom treatment</b>	Independent and constrained	Constrained
<i>Δ</i> <sub>max</sub> , <i>Δ</i> <sub>min</sub> (e Å <sup>-3</sup> )	2.14, -1.53	1.82, -1.19
<b>CCDC No.</b>	2095001	2095002

## ELECTROCHEMICAL CHARACTERISATION

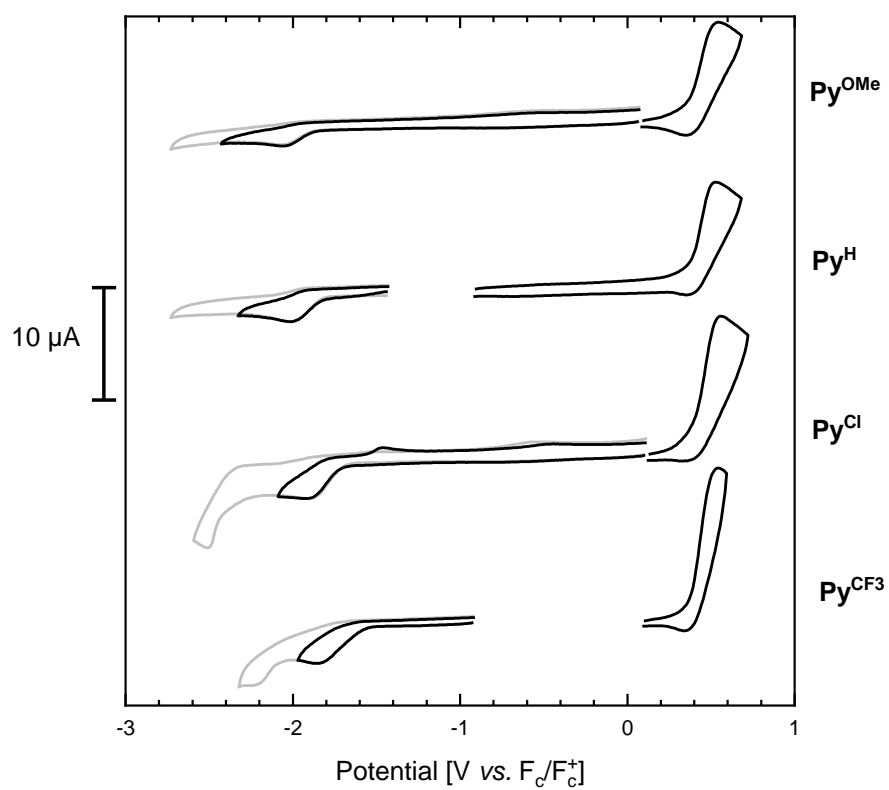


**Figure S9.** Cyclic voltammograms of  $\text{Py}^{\text{X}}$  in DMF (0.1M  $\text{NBu}_4\text{ClO}_4$ ). [ $\text{Py}^{\text{X}}$ ], 0.5 mM; reference electrode,  $\text{Ag}/\text{AgNO}_3$  (10 mM in MeCN); working electrode, GC electrode; counter electrode, Pt wire; scan rate, 0.1 V/s. All measurements were conducted in a glovebox.

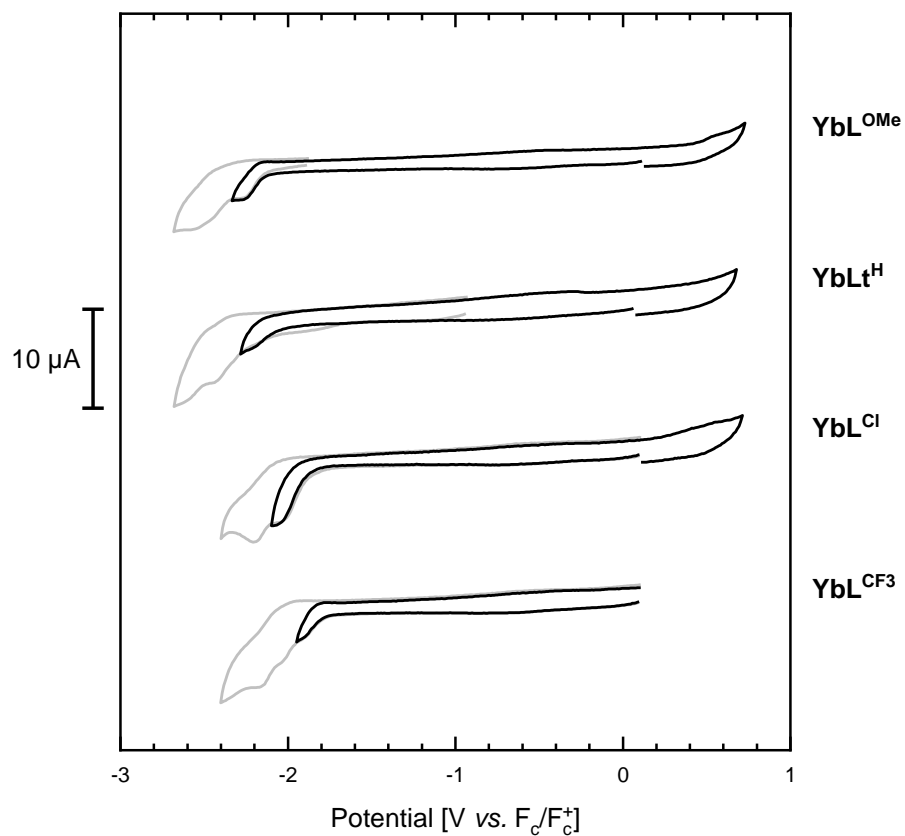


**Figure S10.** Cyclic voltammograms of **YbL<sup>X</sup>** in DMF (0.1M NBu<sub>4</sub>ClO<sub>4</sub>). [**YbL<sup>X</sup>**], 0.5 mM; reference electrode, Ag/AgNO<sub>3</sub> (10 mM in MeCN); working electrode, GC electrode; counter electrode, Pt wire; scan rate, 0.1 V/s. All measurements were conducted in a glovebox.

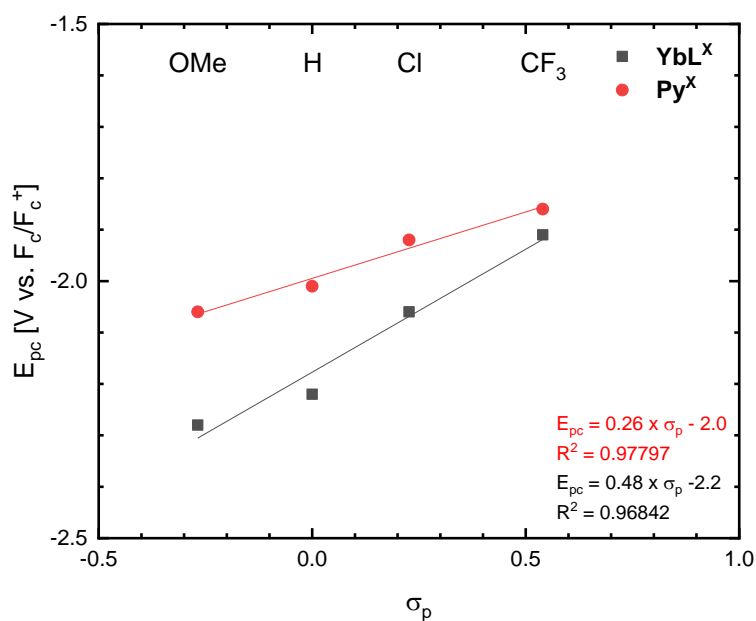


**Figure S11.** Linear fit of cathodic peak potential values ( $E_{pc}$ ) of  $\text{Py}^{\text{X}}$  and  $\text{YbL}^{\text{X}}$  versus Hammett  $\sigma_p$  constants.

**Table S4.** Peak potential ( $E_{pa}$ ,  $E_{pc}$ ) values and Hammett  $\sigma_p$  constants of  $\text{YbL}^{\text{X}}$ , and model compounds  $\text{Py}^{\text{X}}$  in DMF. Electrolyte, 0.1 M  $\text{NBu}_4\text{ClO}_4$ ; scan rate, 0.1 V/s.

	$E_{pa}$ [V vs. $\text{Fc}/\text{Fc}^+$ ]	$E_{pa}$ [V vs. NHE]	$E_{pc}$ [V vs. $\text{Fc}/\text{Fc}^+$ ]	$E_{pc}$ [V vs. NHE]	$\sigma_p$
$\text{YbL}^{\text{OMe}}$	--	--	-2.28	-1.88	-0.268
$\text{YbL}^{\text{H}}$	--	--	-2.22	-1.82	0
$\text{YbL}^{\text{Cl}}$	--	--	-2.06	-1.66	0.227
$\text{YbL}^{\text{CF}_3}$	--	--	-1.91	-1.51	0.54
$\text{Py}^{\text{OMe}}$	0.54	0.94	-2.06	-1.66	-0.268
$\text{Py}^{\text{H}}$	0.53	0.93	-2.01	-1.61	0
$\text{Py}^{\text{Cl}}$	0.56	0.96	-1.92	-1.52	0.227
$\text{Py}^{\text{CF}_3}$	0.54	0.94	-1.86	-1.46	0.54

## PHOTOPHYSICAL CHARACTERISATION

### Absorbance, excitation and emission spectra

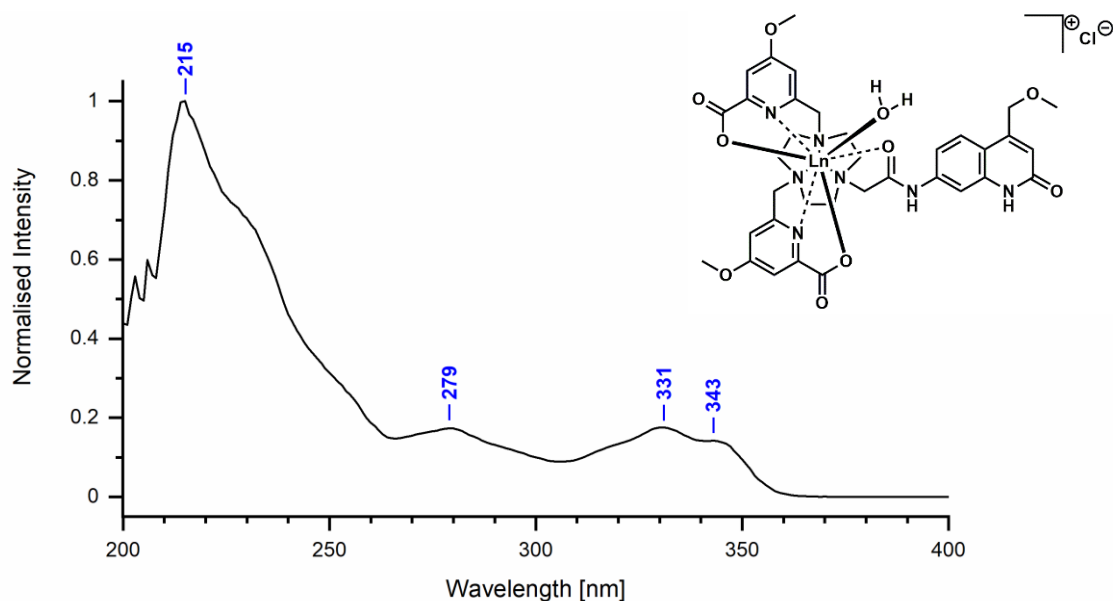


**Figure S12.** Normalised UV absorption spectrum of **YbL<sup>OMe</sup>** ( $A = 0.10$ ) in 10 mM PIPES-buffered aqueous solution, pH = 6.5. Blue numbers indicate the local maxima of the spectrum.

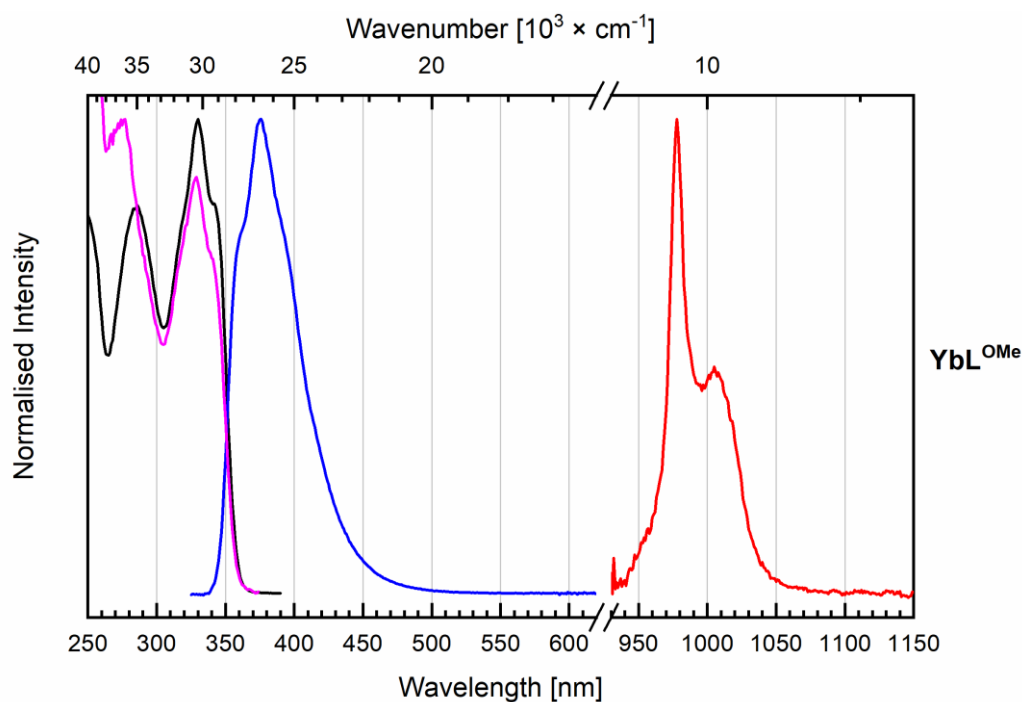


**Figure S13.** The excitation spectra of ligand fluorescence and Yb(III) emission (black and magenta lines, left,  $\lambda_{em} = 405$  and 978 nm, respectively) and steady-state emission spectra of **YbL<sup>OMe</sup>** at r.t. (blue and red lines, right,  $\lambda_{ex} = 329$  and 323 nm, respectively).  $[\text{YbL}^{\text{OMe}}] = 10 \mu\text{M}$ , 10 mM PIPES-buffered aqueous solution, pH = 6.5.

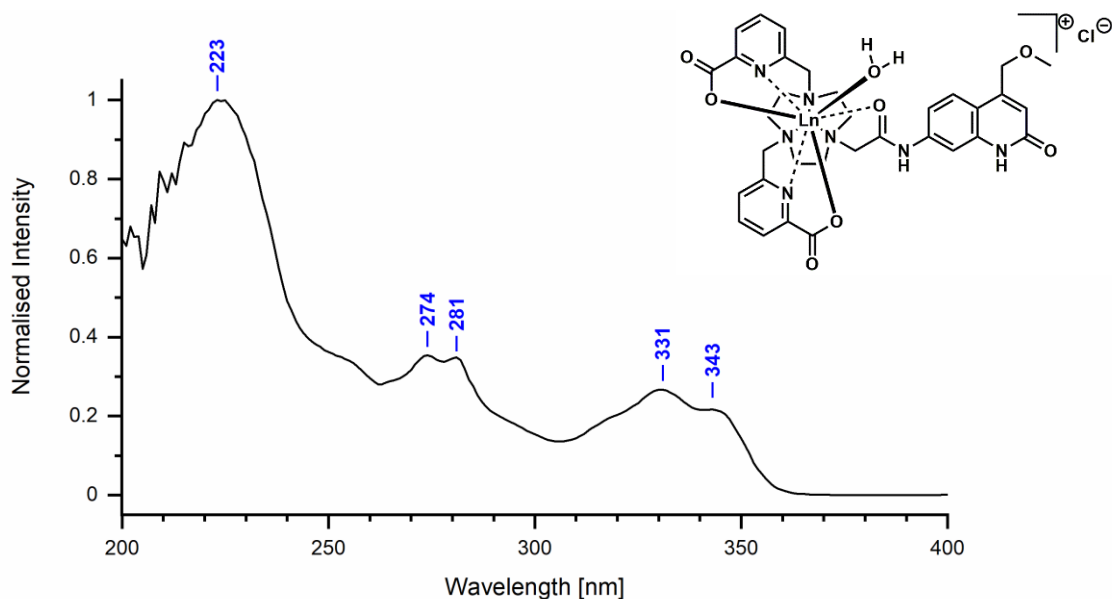


**Figure S14.** Normalised UV absorption spectrum of  $\mathbf{YbL}^{\text{H}}$  ( $A = 0.10$ ) in 10 mM PIPES-buffered aqueous solution, pH = 6.5. Blue numbers indicate the local maxima of the spectrum.

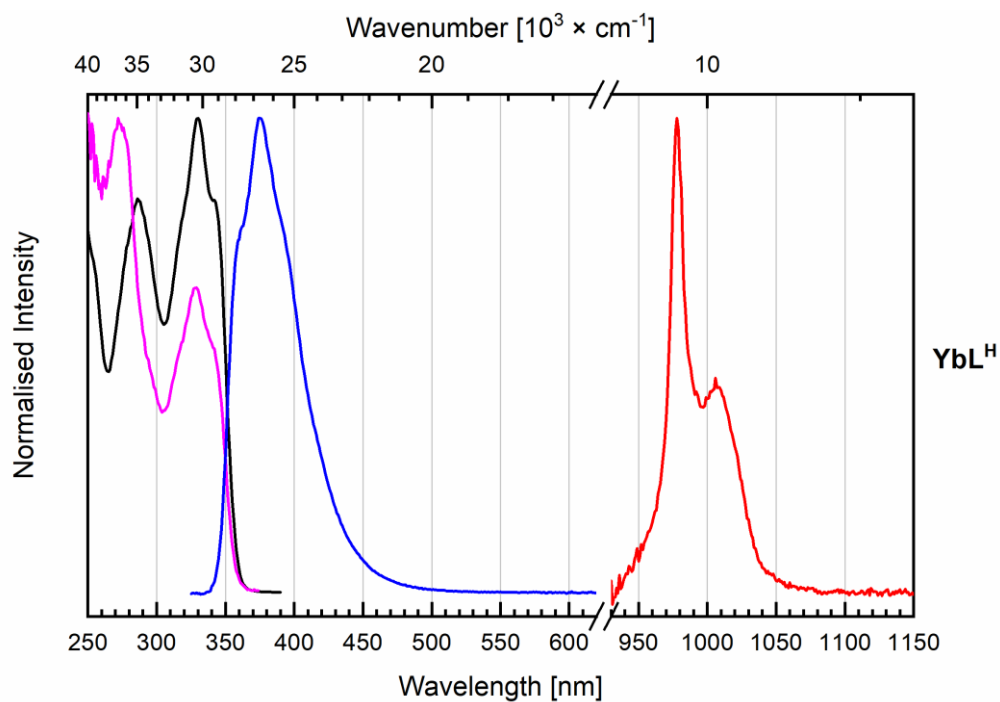


**Figure S15.** The excitation spectra of ligand fluorescence and Yb(III) emission (black and magenta lines, left,  $\lambda_{\text{em}} = 405$  and  $978$  nm, respectively) and steady-state emission spectra of  $\mathbf{YbL}^{\text{H}}$  at r.t. (blue and red lines, right,  $\lambda_{\text{ex}} = 329$  and  $323$  nm, respectively).  $[\mathbf{YbL}^{\text{H}}] = 10 \mu\text{M}$ , 10 mM PIPES-buffered aqueous solution, pH = 6.5.

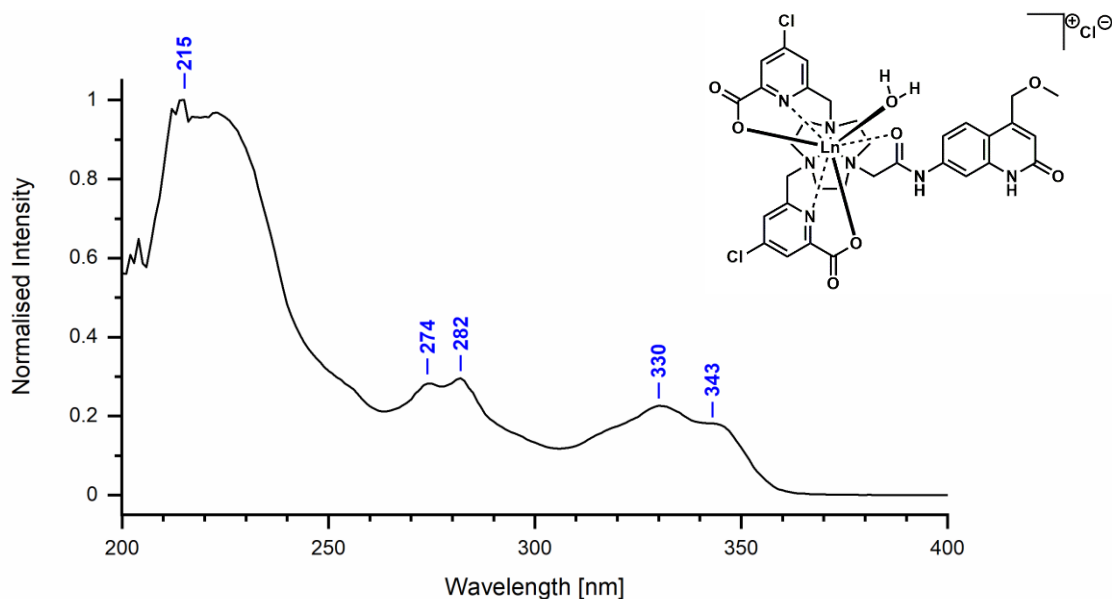


**Figure S16.** Normalised UV absorption spectrum of  $\text{YbL}^{\text{Cl}}$  ( $A = 0.10$ ) in 10 mM PIPES-buffered aqueous solution, pH = 6.5. Blue numbers indicate the local maxima of the spectrum.

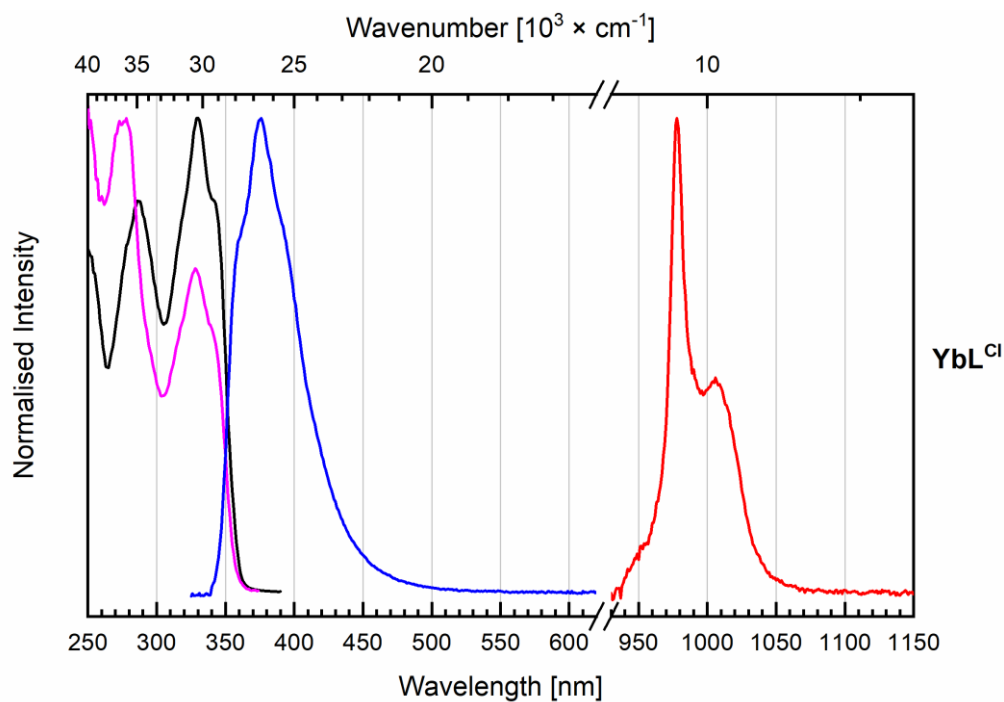


**Figure S17.** The excitation spectra of ligand fluorescence and Yb(III) emission (black and magenta lines, left,  $\lambda_{\text{em}} = 405$  and 978 nm, respectively) and steady-state emission spectra of  $\text{YbL}^{\text{Cl}}$  at r.t. (blue and red lines, right,  $\lambda_{\text{ex}} = 329$  and 323 nm, respectively).  $[\text{YbL}^{\text{Cl}}] = 10 \mu\text{M}$ , 10 mM PIPES-buffered aqueous solution, pH = 6.5.



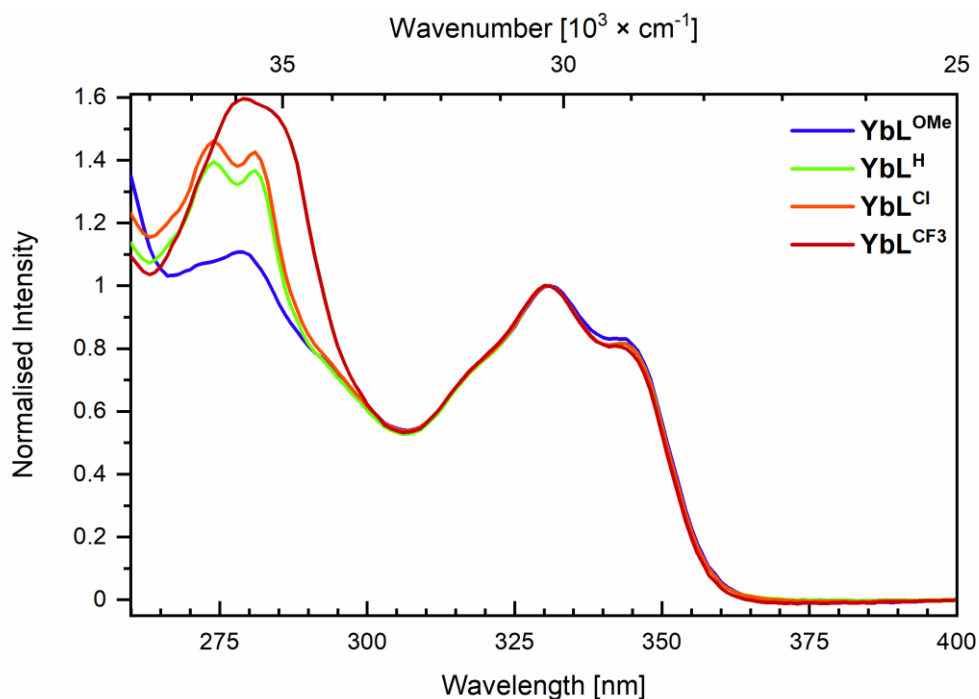


**Figure S20.** Superimposed normalised UV absorption spectra of  $\text{YbL}^{\text{X}}$  in 10 mM PIPES-buffered aqueous solutions at pH = 6.5,  $A = 0.10$ .

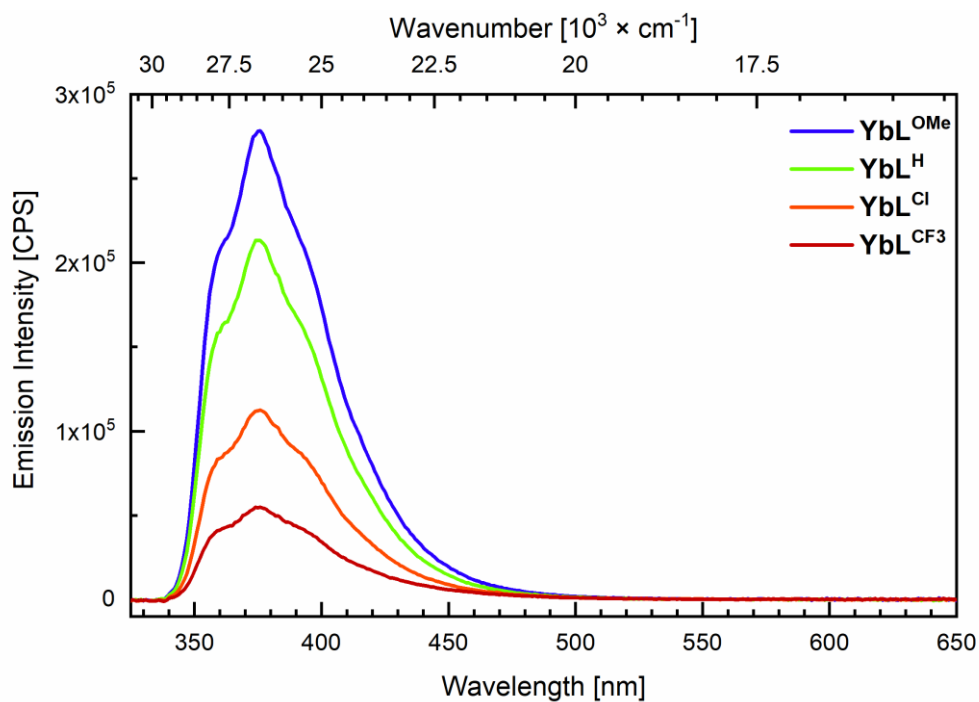


**Figure S21.** Steady-state fluorescence spectra of  $\text{YbL}^{\text{X}}$  indicating relative emission intensities under identical samples absorptions.  $[\text{YbL}^{\text{X}}] = 10 \mu\text{M}$  in 10 mM PIPES-buffered solutions, pH = 6.5,  $\lambda_{\text{ex}} = 329 \text{ nm}$ , front slit: 2 nm, exit slit: 1.5 nm.

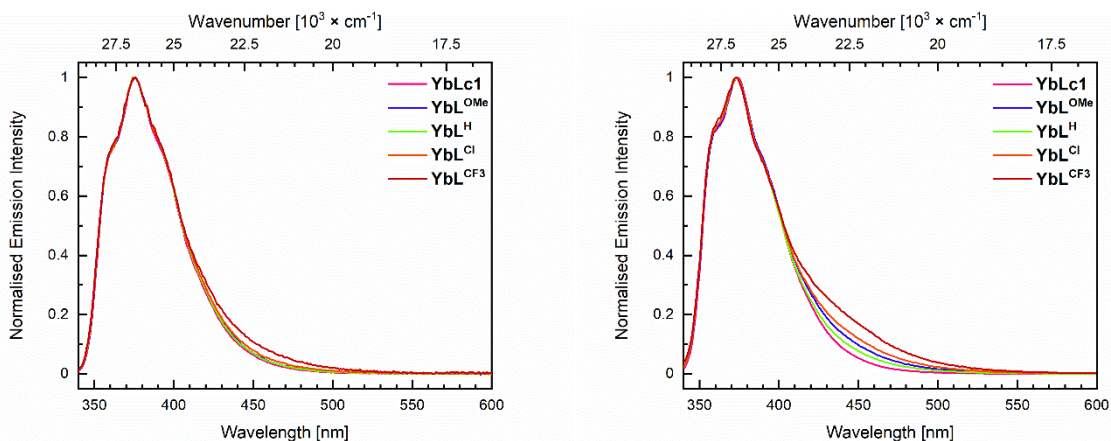


**Figure S22.** Normalised steady-state fluorescence spectra of  $\mathbf{YbL}^X$  under identical samples absorptions from two independent measurements.  $[\mathbf{YbL}^X] = 10 \mu\text{M}$  in 10 mM PIPES-buffered solutions, pH = 6.5; left:  $\lambda_{\text{ex}} = 329 \text{ nm}$ , front slit: 2 nm, exit slit: 1.5 nm; right:  $\lambda_{\text{ex}} = 323 \text{ nm}$ , front slit: 14–14.7 nm, exit slit: 1 nm.

**Table S5.** Residual ligand fluorescence quantum yields of  $\mathbf{YbL}^X$  from several independent experiments.  $[\mathbf{YbL}^X] = 10 \mu\text{M}$  in 10 mM PIPES-buffered  $\text{H}_2\text{O}$ , pH = 6.5.

Complex	$\Phi_L^a$ [%]	$\Phi_{L,\text{av}}^b$ [%]	St. Dev. [%]
$\mathbf{YbL}^{\text{OMe}}$	4.86	4.62	0.167
	4.51		
	4.50		
$\mathbf{YbL}^{\text{H}}$	3.71	3.66	0.033
	3.64		
	3.64		
$\mathbf{YbL}^{\text{Cl}}$	1.99	2.01	0.017
	2.03		
	2.02		
$\mathbf{YbL}^{\text{CF}_3}$	1.03	0.977	0.038
	0.954		
	0.947		

<sup>a</sup> Determined relative to QS ( $\Phi = 0.59^1$ ) in  $\text{H}_2\text{SO}_4$  (0.05 M). <sup>b</sup> Average quantum yield from two or three independent measurements.

## 77 K measurements

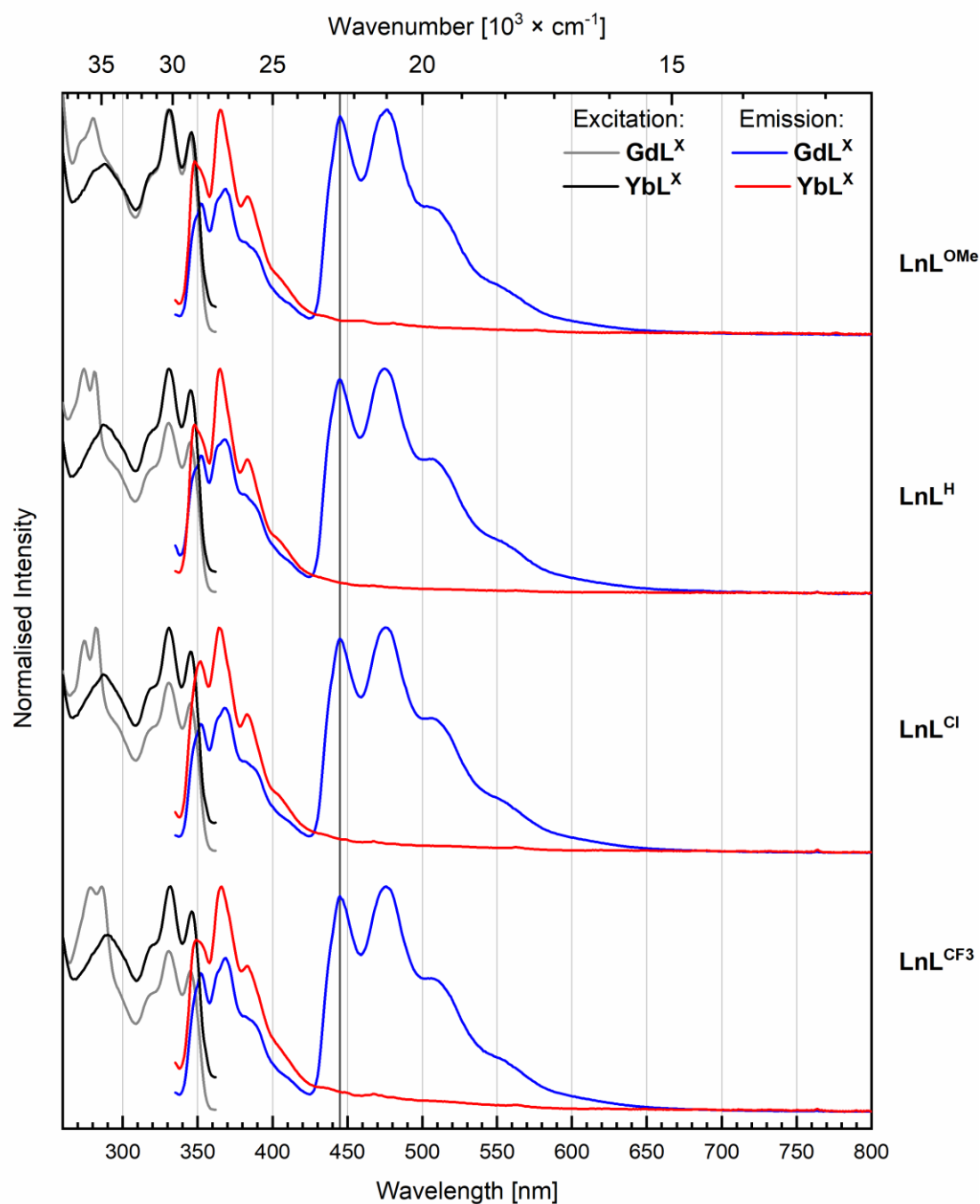


**Figure S23.** Ligand phosphorescence excitation and steady-state emission spectra of  $\text{LnL}^{\text{X}}$  (Ln = Gd, Yb) complexes at 77 K with 10% glycerol added to 10 mM PIPES-buffered aqueous solutions (pH 6.5).  $[\text{LnL}^{\text{X}}] = 10 \mu\text{M}$ ,  $\lambda_{\text{ex}} = 344$  (Ln = Gd), 329 (Ln = Yb);  $\lambda_{\text{em}} = 445$  (Ln = Gd), 385 (Ln = Yb). The dark grey lines are at the maxima of the first visible vibronic component of the phosphorescence spectra ( $\lambda_{\text{em}} = 445$  nm for  $\text{GdL}^{\text{X}}$ ).

**Table S6.** Integration of S<sub>1</sub> and T<sub>1</sub> emission band of LnL<sup>X</sup> (Ln = Gd, Yb) from the normalised emission spectra recorded at 77 K (Figure S23), and ratios S<sub>1</sub>/T<sub>1</sub>. Ligand steady-state emission spectra of LnL<sup>X</sup> (Ln = Gd, Yb) were recorded at 77 K with 10% glycerol added to 10 mM PIPES-buffered aqueous solutions (pH 6.5, A = 0.10). Integration range for S<sub>1</sub>: 335–425 nm; for T<sub>1</sub>: 425–800 nm.

	<b>Yb</b>			<b>Gd</b>		
	I <sub>S1</sub>	I <sub>T1</sub>	I <sub>S1</sub> /I <sub>T1</sub>	I <sub>S1</sub>	I <sub>T1</sub>	I <sub>S1</sub> /I <sub>T1</sub>
<b>L<sup>OMe</sup></b>	42.78	8.49	5.04	30.09	83.36	0.36
<b>L<sup>H</sup></b>	40.62	5.66	7.18	32.91	86.60	0.38
<b>L<sup>Cl</sup></b>	44.04	7.59	5.80	29.69	85.72	0.35
<b>L<sup>CF3</sup></b>	45.70	10.56	4.33	31.22	85.99	0.36

## Fluorescence decay fits and residuals

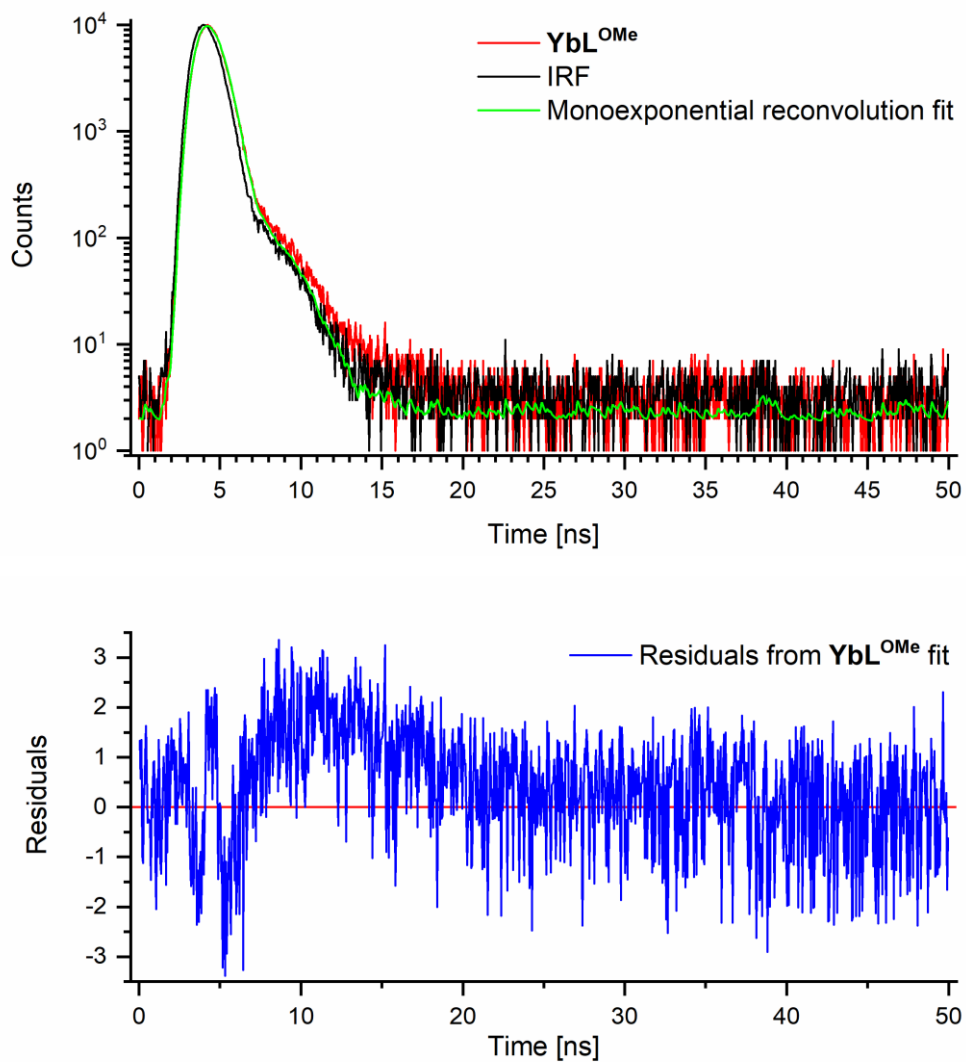


**Figure S24.** The fluorescence decay and reconvolution fit of  $\text{YbL}^{\text{OMe}}$  in 10 mM PIPES  $\text{H}_2\text{O}$ , pH 6.5,  $A = 0.10$  (top) and residuals of the fit (bottom).

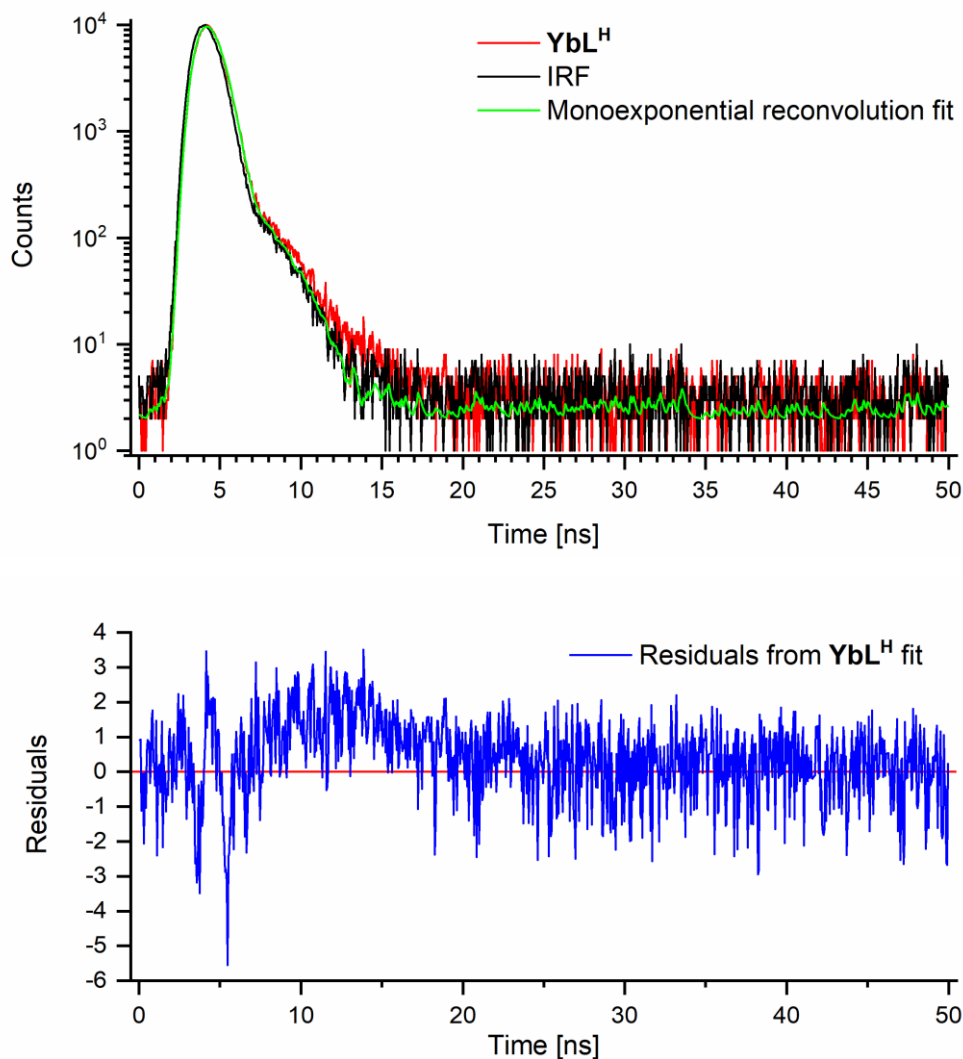


**Figure S25.** The fluorescence decay and reconvolution fit of  $\text{YbL}^{\text{H}}$  in 10 mM PIPES  $\text{H}_2\text{O}$ , pH 6.5,  $A = 0.10$  (top) and residuals of the fit (bottom).

**Table S7.** Measured lifetimes ( $\tau_{\text{f,L}}$ ) of  $\text{YbL}^{\text{X}}$  ( $X = \text{OMe}, \text{H}$ ) antenna fluorescence in  $\text{H}_2\text{O}$  ( $\lambda_{\text{ex}} = 341.5 \text{ nm}$ ,  $\lambda_{\text{em}} = 377 \text{ nm}$ , monoexponential reconvolution fit), and calculated  $\tau_{\text{rad,L}}$ ,  $k_{\text{rad,L}}$ ,  $k_{\text{f,L}}$  ( $\text{s}^{-1}$ ),  $k_{\text{nr,L}}$ .

Compound	$\tau_{\text{f,L}}$ [ns]	$\tau_{\text{rad,L}}$ [ns]	$k_{\text{f,L}}$ [ $\text{ns}^{-1}$ ]	$k_{\text{rad,L}}$ [ $\text{ns}^{-1}$ ]	$k_{\text{nr,L}}$ [ $\text{ns}^{-1}$ ]
$\text{YbL}^{\text{OMe}}$	0.26	5.55	0.180	3.90	3.72
$\text{YbL}^{\text{H}}$	0.20	5.32	0.188	5.13	4.95

Measurements were performed in 10 mM aqueous PIPES buffer solutions at pH 6.5,  $A = 0.10$ .  $k_{\text{f,L}}$ ,  $\tau_{\text{rad,L}}$ ,  $k_{\text{rad,L}}$ ,  $k_{\text{nr,L}}$ , and  $k_{\text{PeT}}$  were calculated as follows:  $k_{\text{f,L}} = 1/\tau_{\text{f,L}}$ ,  $\tau_{\text{rad,L}} = \tau_{\text{f,L}}/\Phi_{\text{L}}$ ,  $k_{\text{rad,L}} = 1/\tau_{\text{rad,L}}$ ,  $k_{\text{nr,L}} = k_{\text{f,L}} - k_{\text{rad,L}}$ .

## Photostability experiments

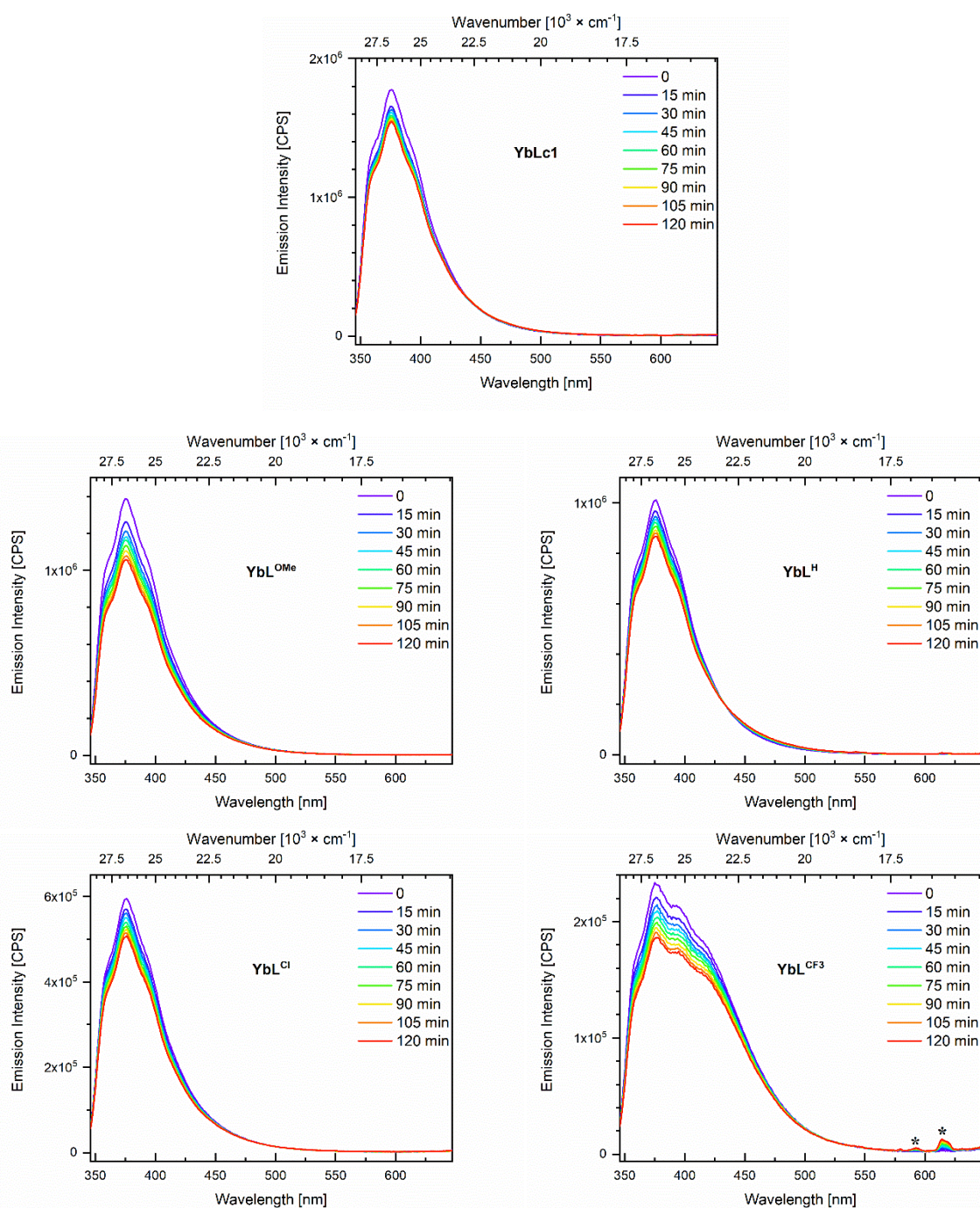


**Figure S26.** Steady-state fluorescence spectra of **YbLc1** and **YbL<sup>X</sup>** upon continuous light irradiation under identical samples absorptions ( $A = 0.10$ ).  $[\text{YbLc1}, \text{YbL}^X] = 10 \mu\text{M}$  in 10 mM PIPES-buffered solutions,  $\text{pH} = 6.5$ ;  $\lambda_{\text{ex}} = 331 \text{ nm}$ , front slit: 3 nm, exit slit: 2.5 nm. Peaks marked with an asterisk indicate traces of Eu(III) contamination from the cuvette.

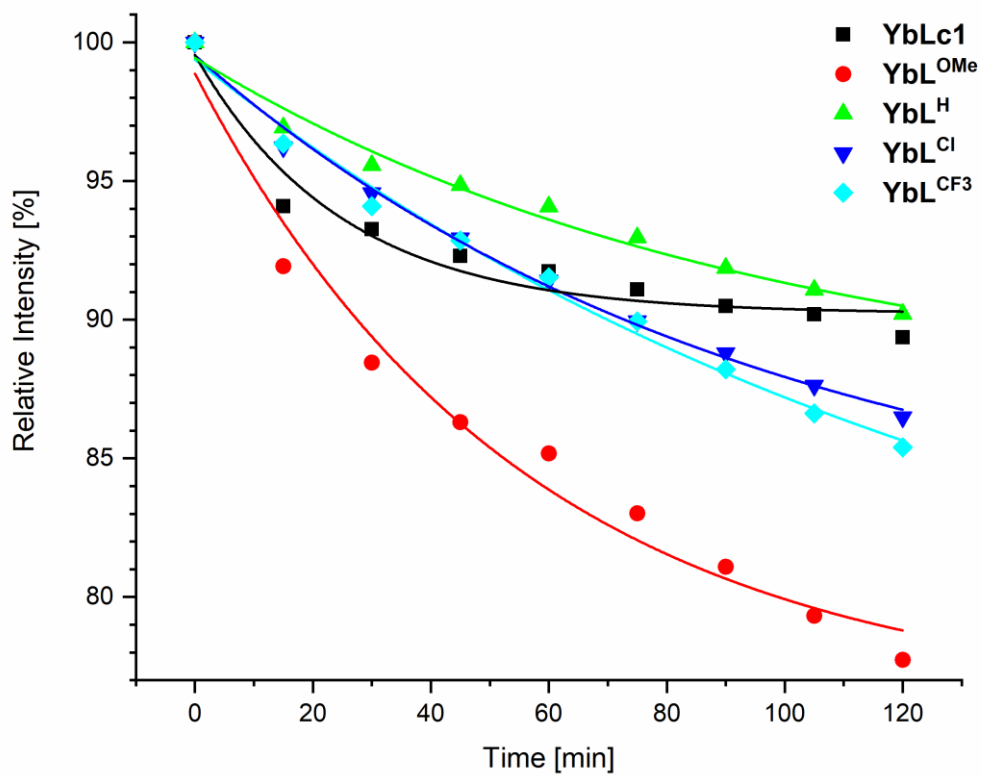


**Figure S27.** Relative emission intensity of **YbLc1** and **YbL<sup>X</sup>** upon continuous light irradiation under identical samples absorptions (see Figure S26). After blank signal subtraction, each spectrum was integrated (346–647 nm), and the integrated intensity was divided by that at  $t_0$  and multiplied by 100%. The lines next to the data values are for the eye guidance only.

## DRIVING FORCE FOR PHOTOINDUCED ELECTRON TRANSFER

The driving force for photoinduced electron transfer from the excited carbostyryl (MOM) was calculated according to Equation (4):

$$\Delta G(eT) = (E_{ox}^{MOM} - E_{red}) - E_s^{MOM} - \frac{e_0^2}{\varepsilon} \quad (4)$$

$$E(\text{Pic}^{\cdot-} - \text{Ant}^{\cdot+}) = E_{ox}^{MOM} - E_{red}^{Py} \quad (5)$$

$$E(\text{Yb(II)} - \text{Ant}^{\cdot+}) = E_{ox}^{MOM} - E_{red}^{Yb} \quad (6)$$

with  $\Delta G(eT)$  the free energy of electron transfer,  $E_{ox}^{MOM}$  the oxidation potential of the ground state of the acetylated carbostyryl antenna (approximated with  $E_{ox}^{MOM} = 1.76$  V vs. NHE measured with 0.1 M  $\text{NBu}_4\text{PF}_6$  as a supporting electrolyte in MeCN under Ar at 0.1 V/s scan rate),<sup>4</sup>  $E_{red}$  is the reduction potential of the electron acceptor. The two analysed cases below are for  $E_{red}^{Py}$ , which is the pyridine-based reduction potential of  $\text{YbL}^X$  (Table S8), and  $E_{red}^{Yb}$ , which is the estimated Yb(III)-based reduction potential of  $\text{YbL}^X$  (Table S9).  $E_s^{MOM}$  the excited state of oxidation potential of the antenna estimated from its singlet excited state (3.53 eV),<sup>1</sup> and  $\frac{e_0^2}{\varepsilon}$  the attraction between the radical ion pair ( $\sim 0.15$  eV for an exciplex).<sup>7</sup>  $E(\text{Pic}^{\cdot-} - \text{Ant}^{\cdot+})$  was obtained

**Table S8.** Picolinate reduction potential of  $\text{YbL}^X$  and driving force for intraligand PeT from the excited carbostyryl (MOM) to the picolinate.

Compound	$E_{red}^{Py}$ [V vs NHE]	$\Delta G(eT)$ [eV]	$E(\text{Pic}^{\cdot-} - \text{Ant}^{\cdot+})$ [eV]
$\text{Py}^{\text{OMe}}$	-1.66	-0.26	3.42
$\text{Py}^{\text{H}}$	-1.61	-0.31	3.37
$\text{Py}^{\text{Cl}}$	-1.52	-0.40	3.28
$\text{Py}^{\text{CF}_3}$	-1.46	-0.46	3.22
$\text{YbL}^{\text{OMe}}$	-1.88	-0.04	3.64
$\text{YbL}^{\text{H}}$	-1.82	-0.10	3.58
$\text{YbL}^{\text{Cl}}$	-1.66	-0.26	3.42
$\text{YbL}^{\text{CF}_3}$	-1.51	-0.41	3.27

**Table S9.** Yb(III)/Yb(II) reduction potential of  $\text{YbL}^X$  ( $E_{red}^{Yb}(\text{YbL}^X) \approx E_{red}^{Yb}(\text{YbLc1})$ ) and driving force for SteT from the excited carbostyryl (MOM) to Yb(III) calculated using Eq. (4).

	$E_{red}^{Yb}$ [V vs NHE]	$\Delta G(eT)$ [eV]	$E(\text{Yb(II)} - \text{Ant}^{\cdot+})$ [eV]
$\text{YbL}^X$	-1.92 <sup>a</sup>	0	3.68

## CALCULATION OF FRANCK-CONDON FACTORS

The Franck-Condon factors were calculated for  $T_1 \rightarrow {}^2F_{5/2}$  and  $T_1 \rightarrow S_0$  processes via Equation 7:

$$FC_{(T=0)} = |\langle \chi_{a,p} | \chi_{b,0} \rangle| = \frac{e^{-S} S^p}{p!} \quad (7)$$

$$E_{Stokes} = (2S - 1) \cdot \hbar\omega_Q \quad (8)$$

where  $S$  is the Huang-Rhys factor related to Stokes shift (either taken as  $S = 2$  for  $4f-4f$  transitions,<sup>5</sup> or calculated as  $S = 2.2-2.4$  using Ref<sup>6</sup> and rounded to  $\sim 2$ ),  $p$  is the reduced energy gap (estimated in units of  $\hbar\omega_Q$  between |a) and |b)  $v=0$  levels).

**Table S10.** Huang-Rhys factor calculated for **YbL<sup>X</sup>**.

Complex	Absorption max [cm <sup>-1</sup> ]	Emission max [cm <sup>-1</sup> ]	$E_{Stokes}$ [cm <sup>-1</sup> ]	$\hbar\omega_Q$ [cm <sup>-1</sup> ] <sup>a</sup>	$S$ <sup>b</sup>
<b>YbL<sup>OMe</sup></b>	30213	26596	3617	979	2
<b>YbL<sup>H</sup></b>	30213	26667	3546	1059	2
<b>YbL<sup>Cl</sup></b>	30213	26596	3617	1059	2
<b>YbL<sup>CF3</sup></b>	30299	26596	3703	1065	2

<sup>a</sup> Calculated as difference between the local maxima of antenna  $\pi \rightarrow \pi^*$  absorption bands (343/344 nm vs 330/331 nm, from Figures S12, S14, S16, S18). <sup>b</sup> Calculated by using Eq. 8.

**Table S11.** Franck-Condon factors and other parameters calculated for **YbL<sup>X</sup>**.

Complex	$T_1$ [cm <sup>-1</sup> ] <sup>a</sup>	$p(T_1)$ <sup>b</sup>	$\Delta(T_1 - {}^2F_{5/2})$ [cm <sup>-1</sup> ] <sup>c</sup>	$p(\Delta(T_1 - {}^2F_{5/2}))$ <sup>d</sup>	FC ( $T_1 \rightarrow {}^2F_{5/2}$ ) <sup>e</sup>	FC ( $T_1 \rightarrow S_0$ ) <sup>e</sup>	$\frac{FC(T_1 \rightarrow {}^2F_{5/2})}{FC(T_1 \rightarrow S_0)}$
<b>YbL<sup>OMe</sup></b>	22472	23	12212	13	$1.8 \cdot 10^{-7}$	$4.4 \cdot 10^{-17}$	$4.1 \cdot 10^9$
<b>YbL<sup>H</sup></b>	22472	21	12212	12	$1.2 \cdot 10^{-6}$	$5.6 \cdot 10^{-15}$	$2.1 \cdot 10^8$
<b>YbL<sup>Cl</sup></b>	22472	21	12212	12	$1.2 \cdot 10^{-6}$	$5.6 \cdot 10^{-15}$	$2.1 \cdot 10^8$
<b>YbL<sup>CF3</sup></b>	22472	21	12212	12	$1.2 \cdot 10^{-6}$	$5.6 \cdot 10^{-15}$	$2.1 \cdot 10^8$

<sup>a</sup> Taken from the 77 K spectra of **GdL<sup>MOM</sup>**, see figure S23. <sup>b</sup> Calculated as  $T_1/\hbar\omega_Q$ . <sup>c</sup> Calculated as the difference between  $T_1$  and  ${}^2F_{5/2}$  (10260 cm<sup>-1</sup>). <sup>d</sup> Calculated as  $(T_1 - {}^2F_{5/2})/\hbar\omega_Q$ . <sup>e</sup> Calculated by using Eq. 7.

# <sup>1</sup>H, <sup>13</sup>C, AND <sup>19</sup>F NMR SPECTRA

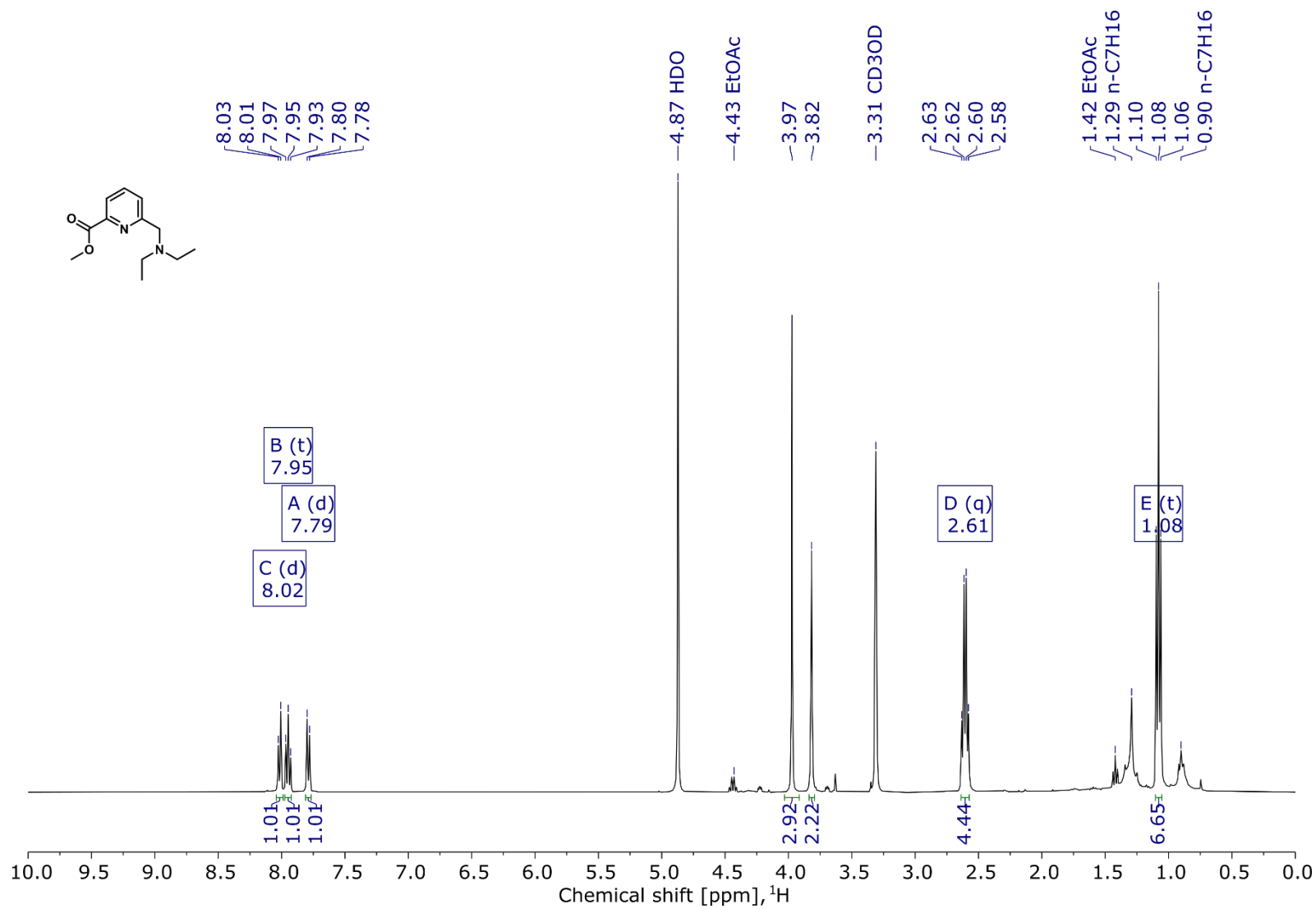


Figure S28. <sup>1</sup>H NMR spectrum of S2<sup>H</sup> (400 MHz, CD<sub>3</sub>OD).

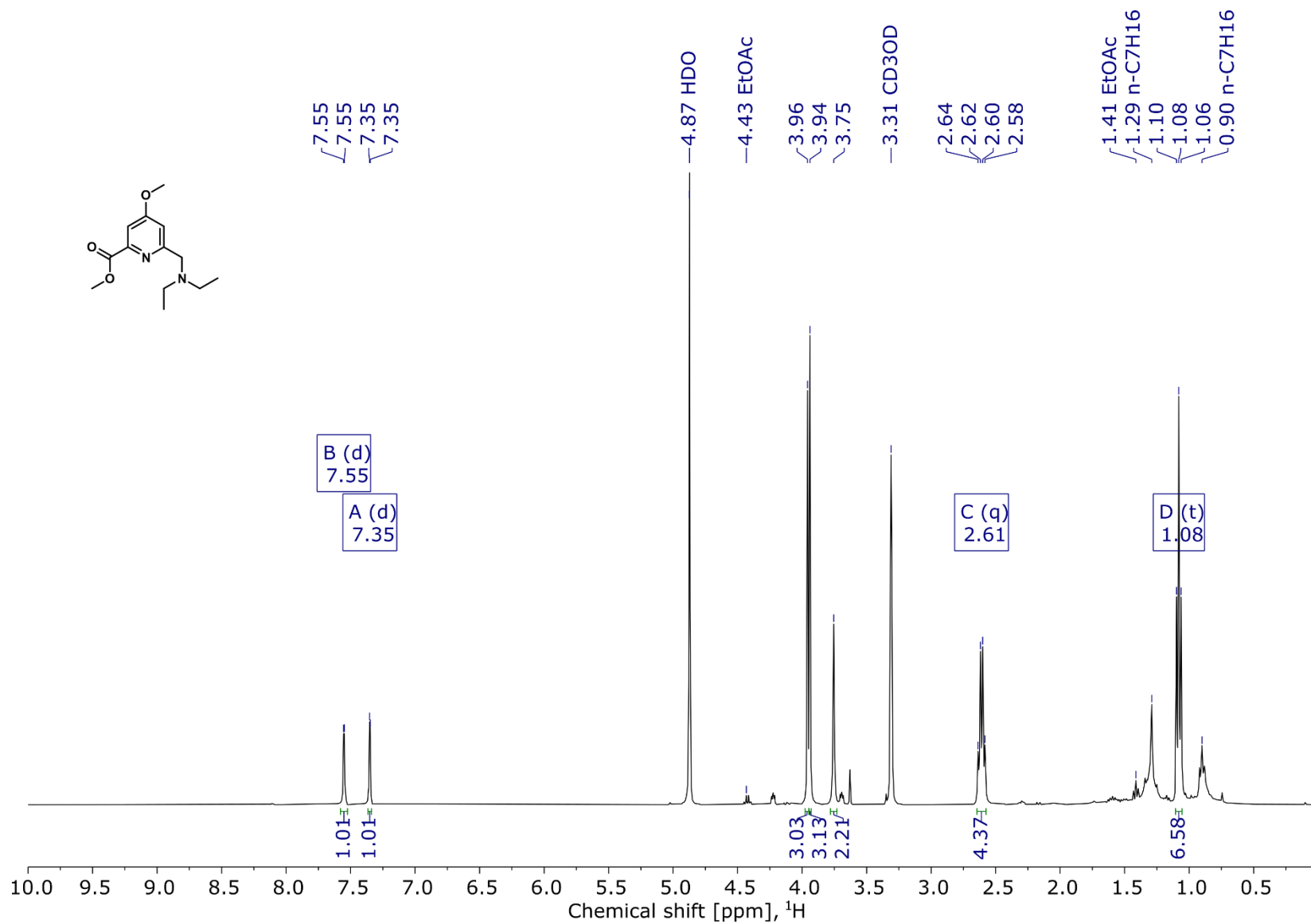


Figure S29. <sup>1</sup>H NMR spectrum of S2<sup>OMe</sup> (400 MHz, CD<sub>3</sub>OD).

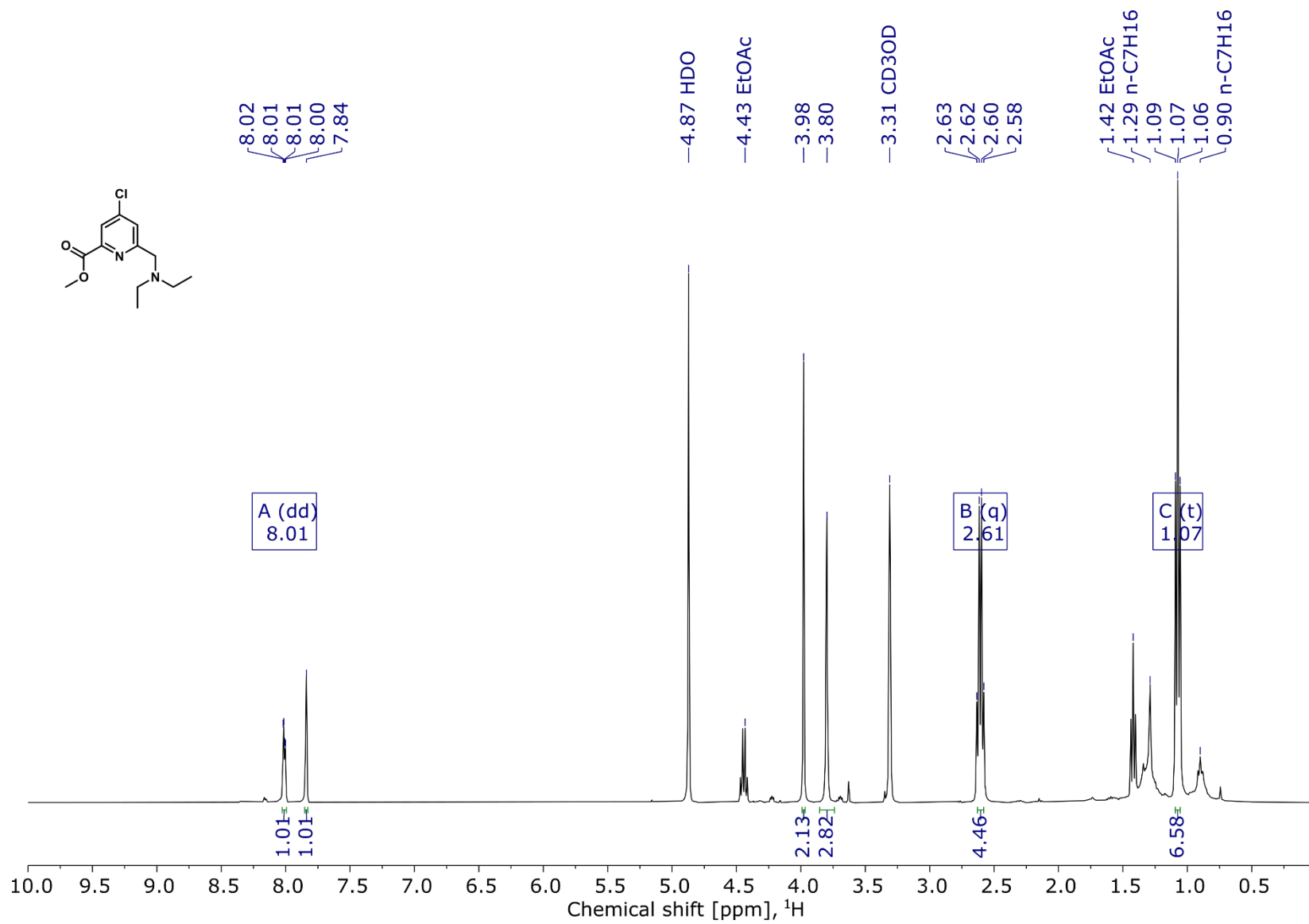
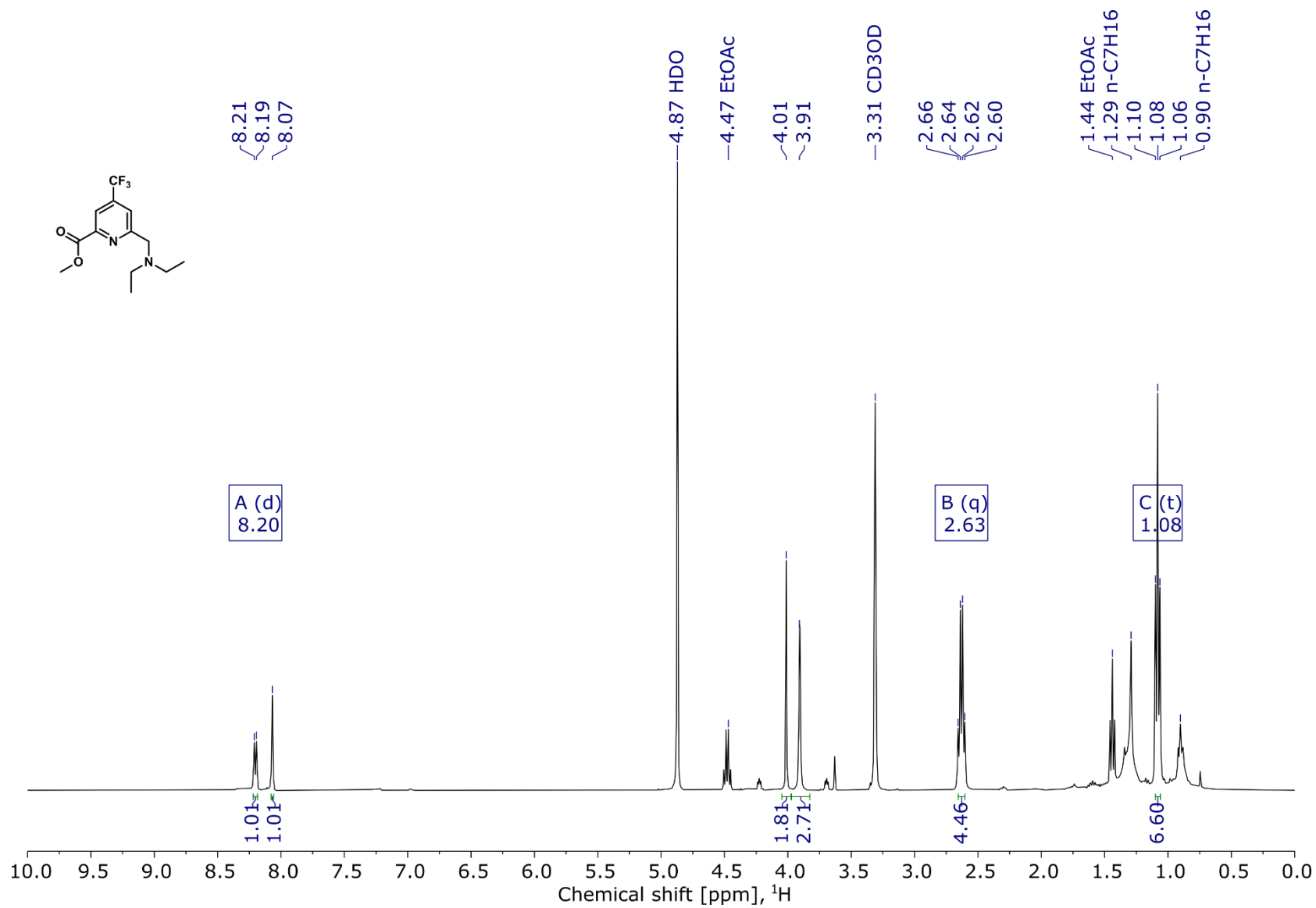
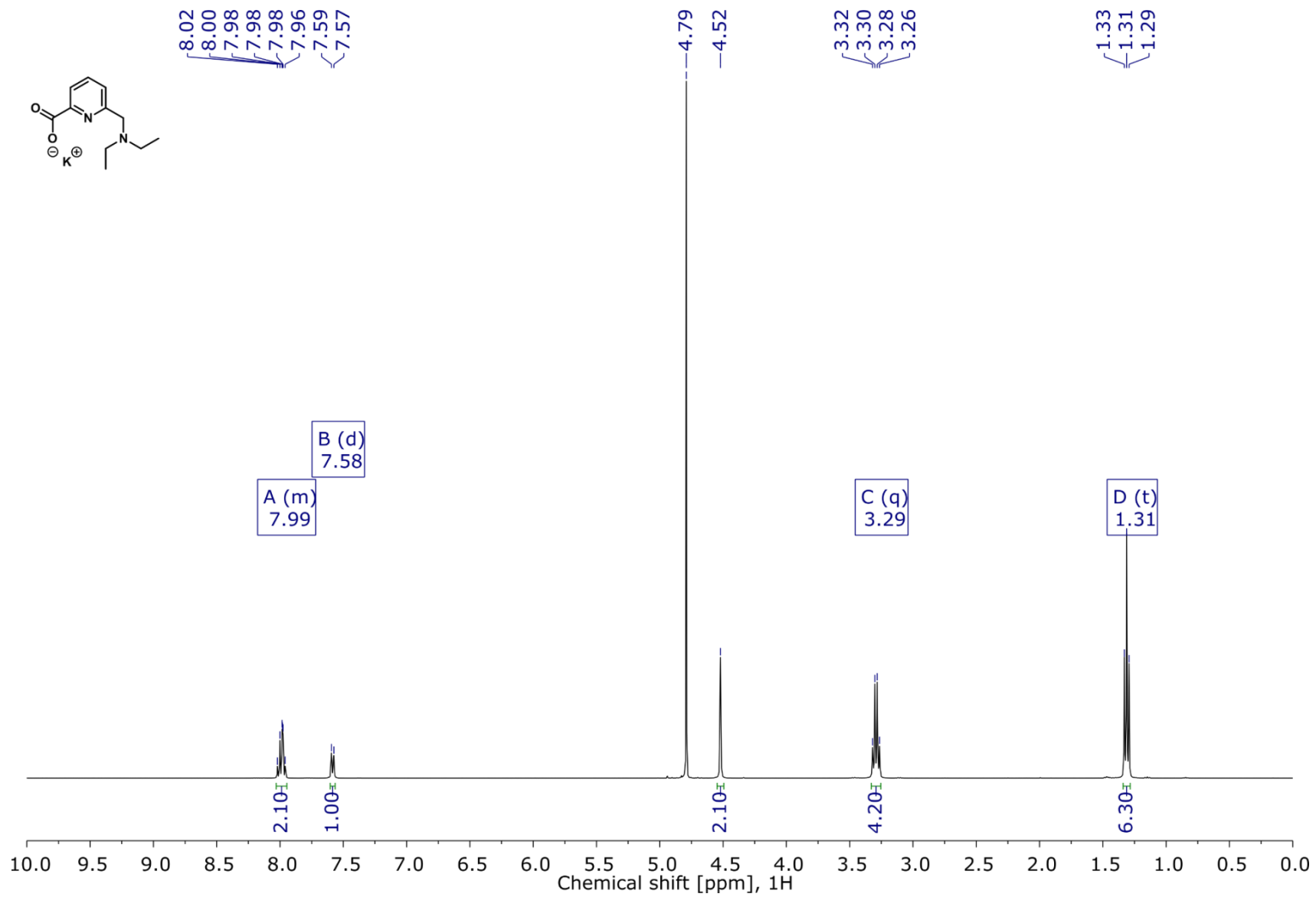


Figure S30.  $^1H$  NMR spectrum of  $S2^{Cl}$  (400 MHz,  $CD_3OD$ ).



**Figure S31.** <sup>1</sup>H NMR spectrum of **S2**<sup>CF<sub>3</sub></sup> (400 MHz, CD<sub>3</sub>OD).



**Figure S32.** <sup>1</sup>H NMR spectrum of Py<sup>H</sup> (400 MHz, D<sub>2</sub>O).

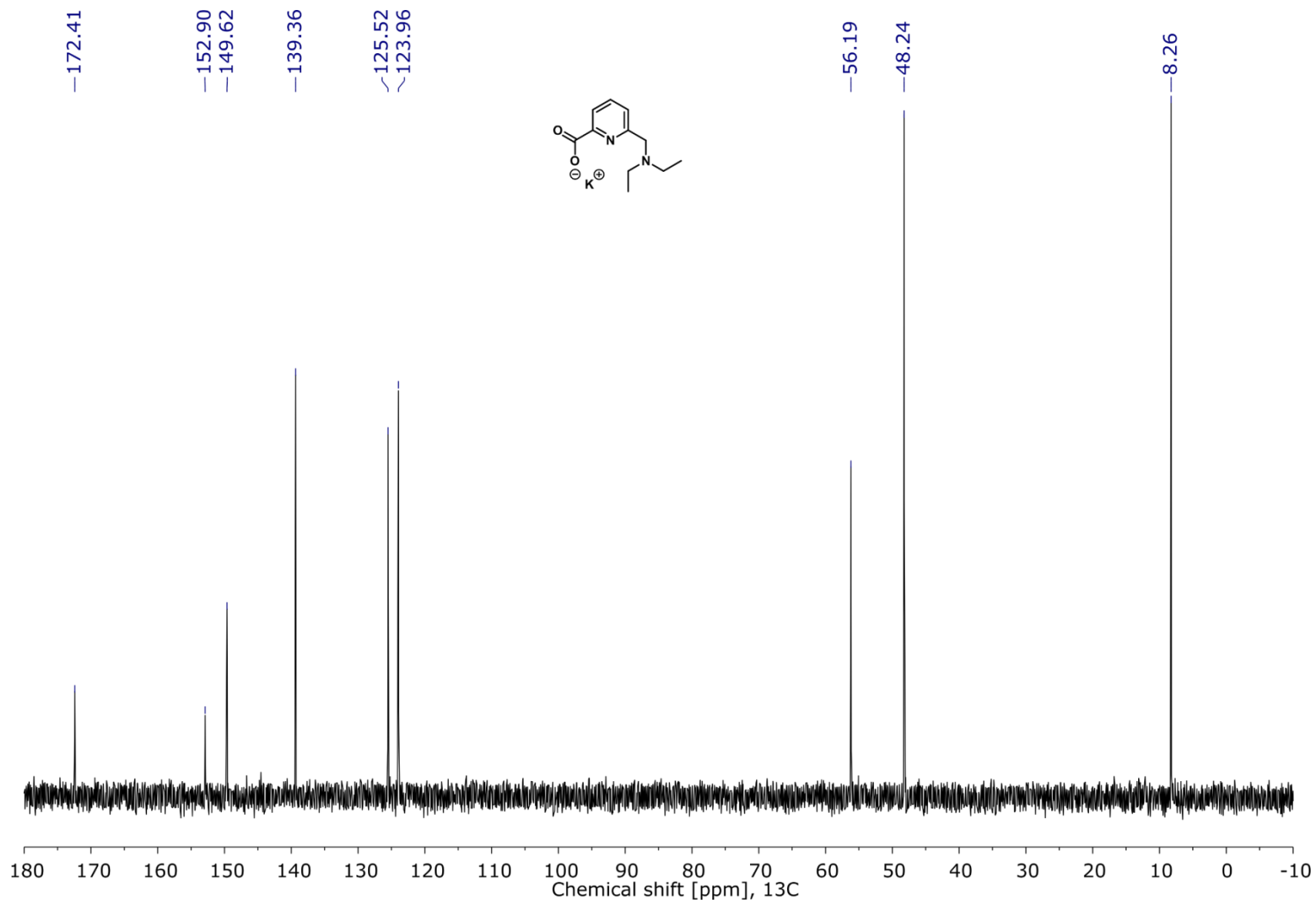


**Figure S33.** <sup>13</sup>C NMR spectrum of Py<sup>H</sup> (101 MHz, D<sub>2</sub>O).

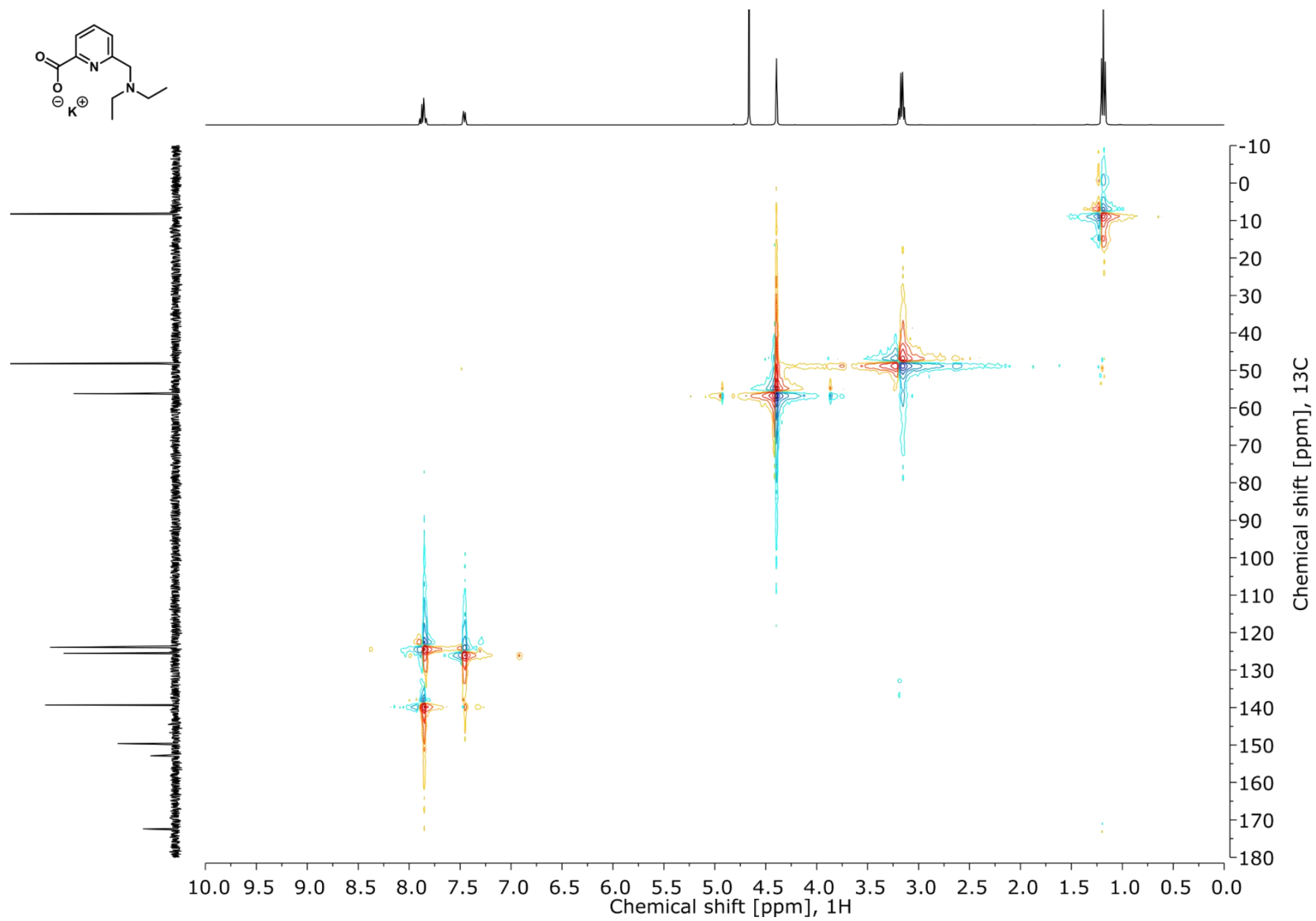
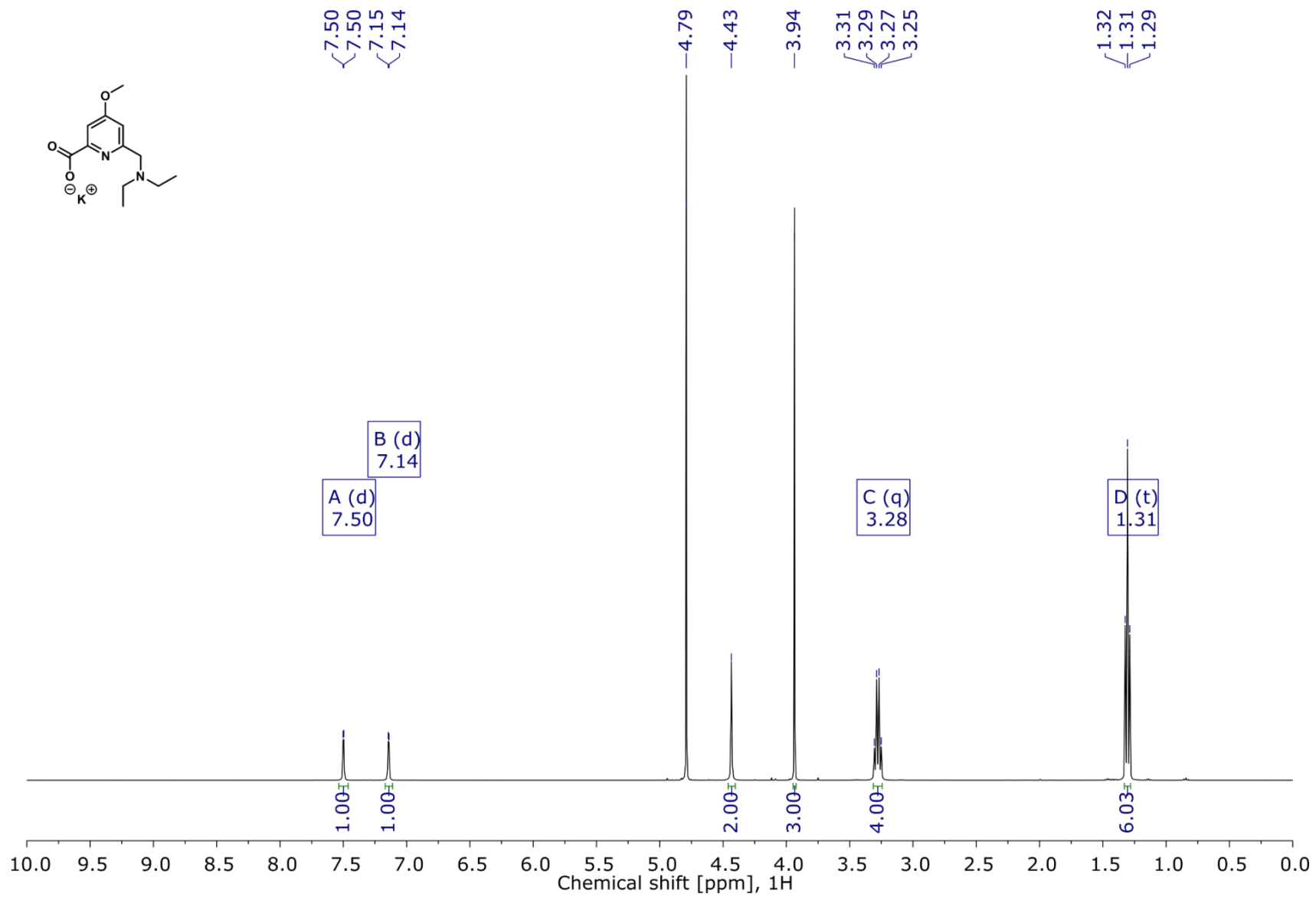
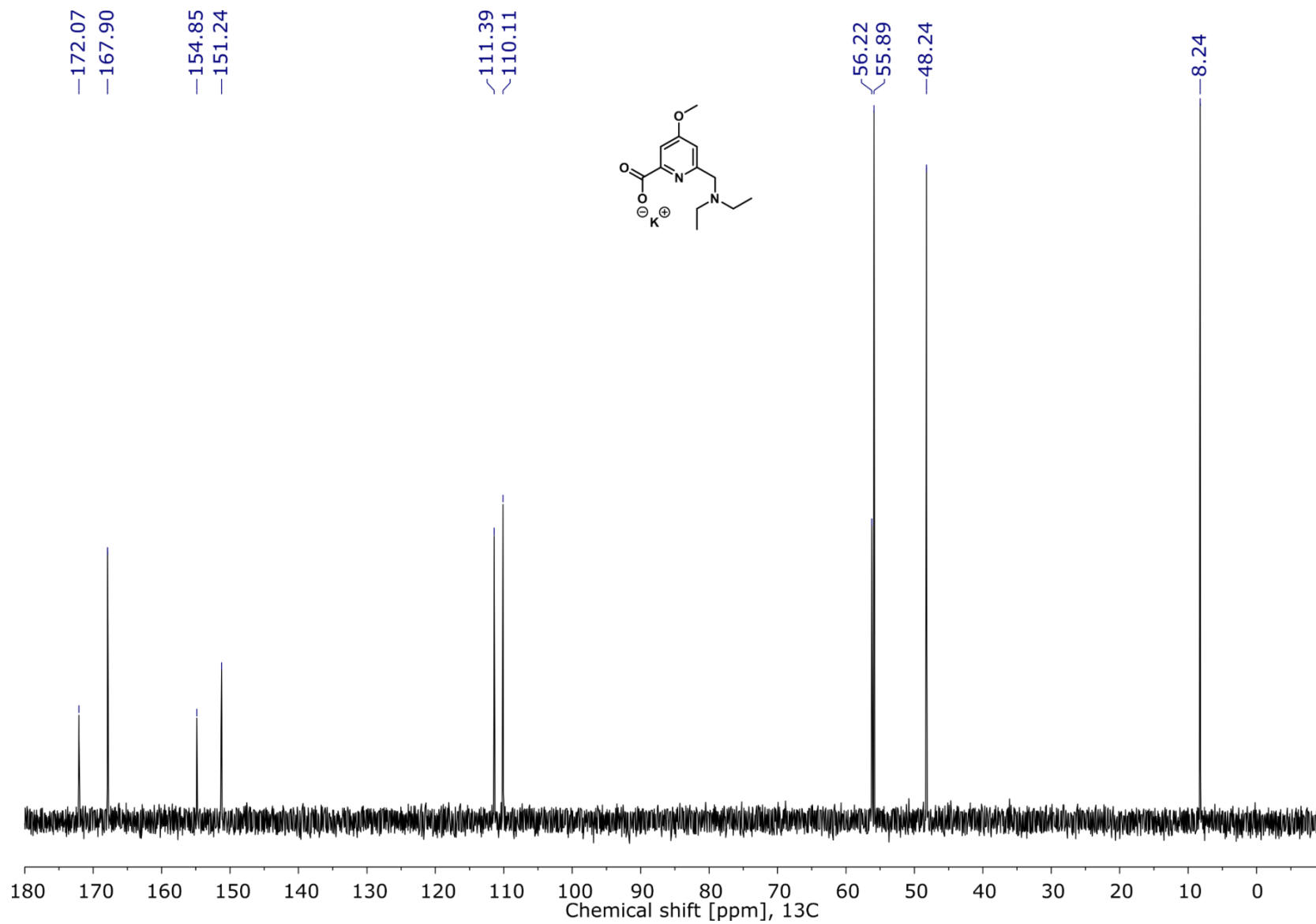


Figure S34. HSQC spectrum of Py<sup>H</sup> (400 MHz, D<sub>2</sub>O).



**Figure S35.** <sup>1</sup>H NMR spectrum of **Py<sup>OMe</sup>** (400 MHz, D<sub>2</sub>O).



**Figure S36.** <sup>13</sup>C NMR spectrum of Py<sup>OMe</sup> (101 MHz, D<sub>2</sub>O).

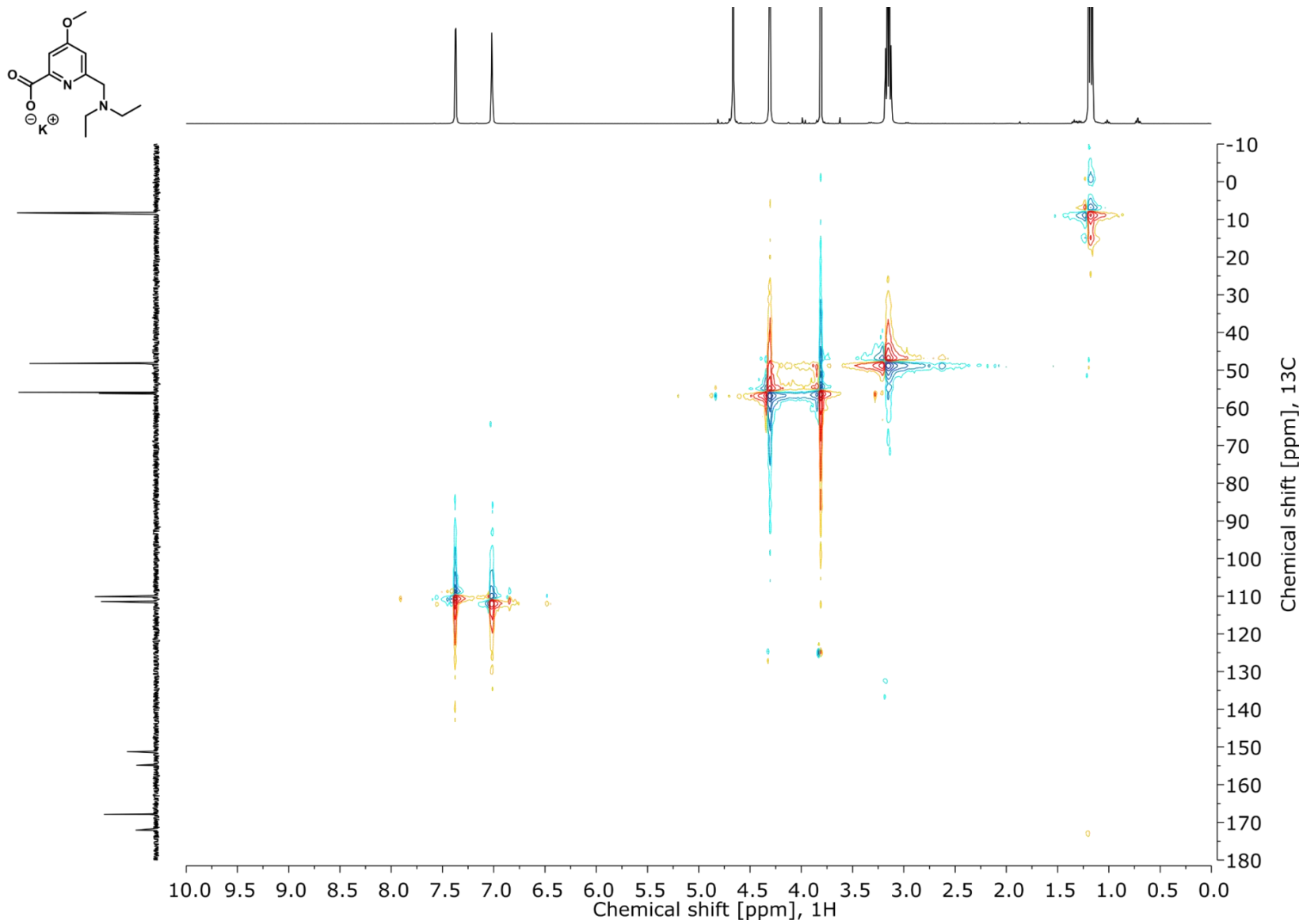


Figure S37. HSQC spectrum of Py<sup>OMe</sup> (400 MHz, D<sub>2</sub>O).

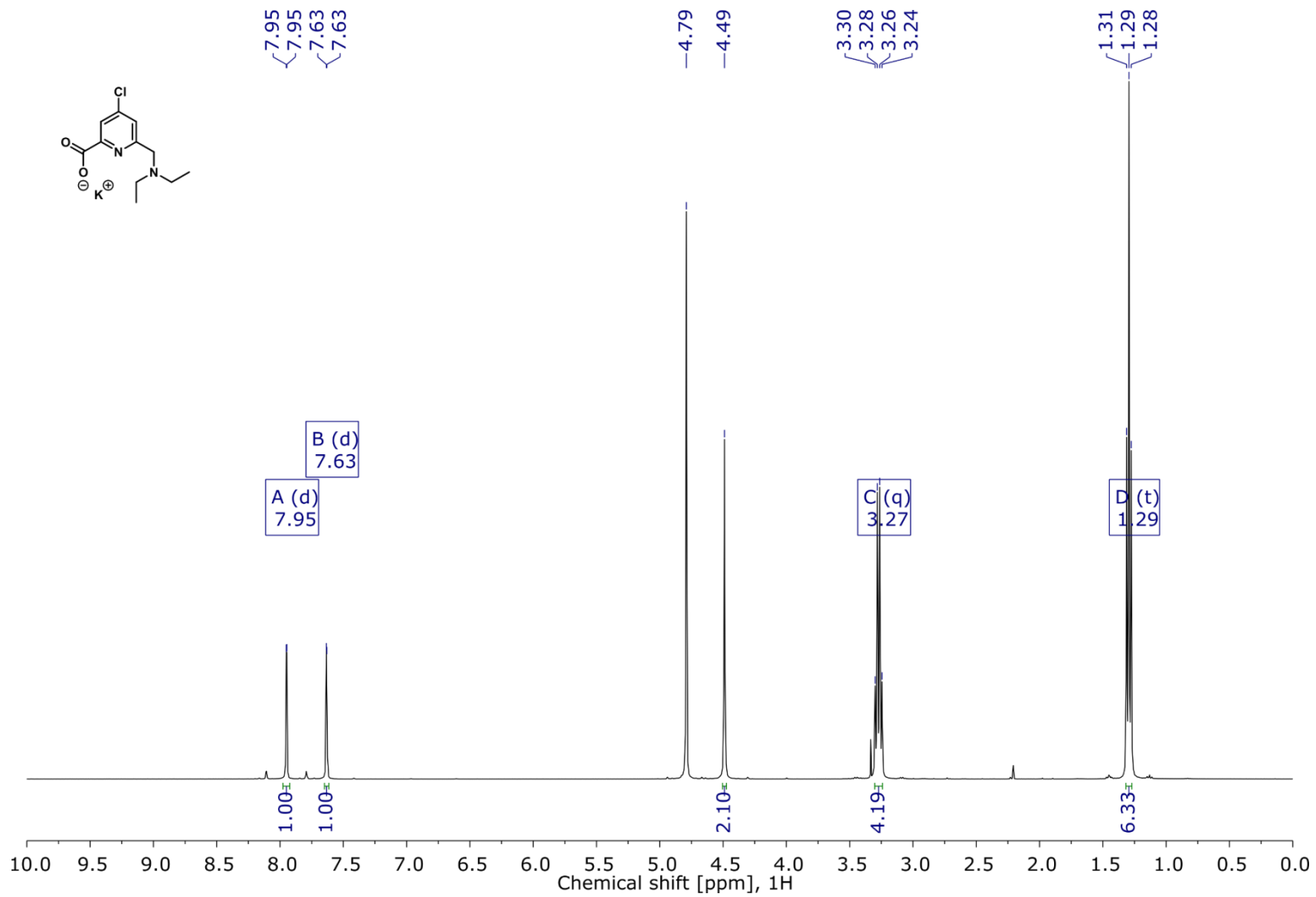
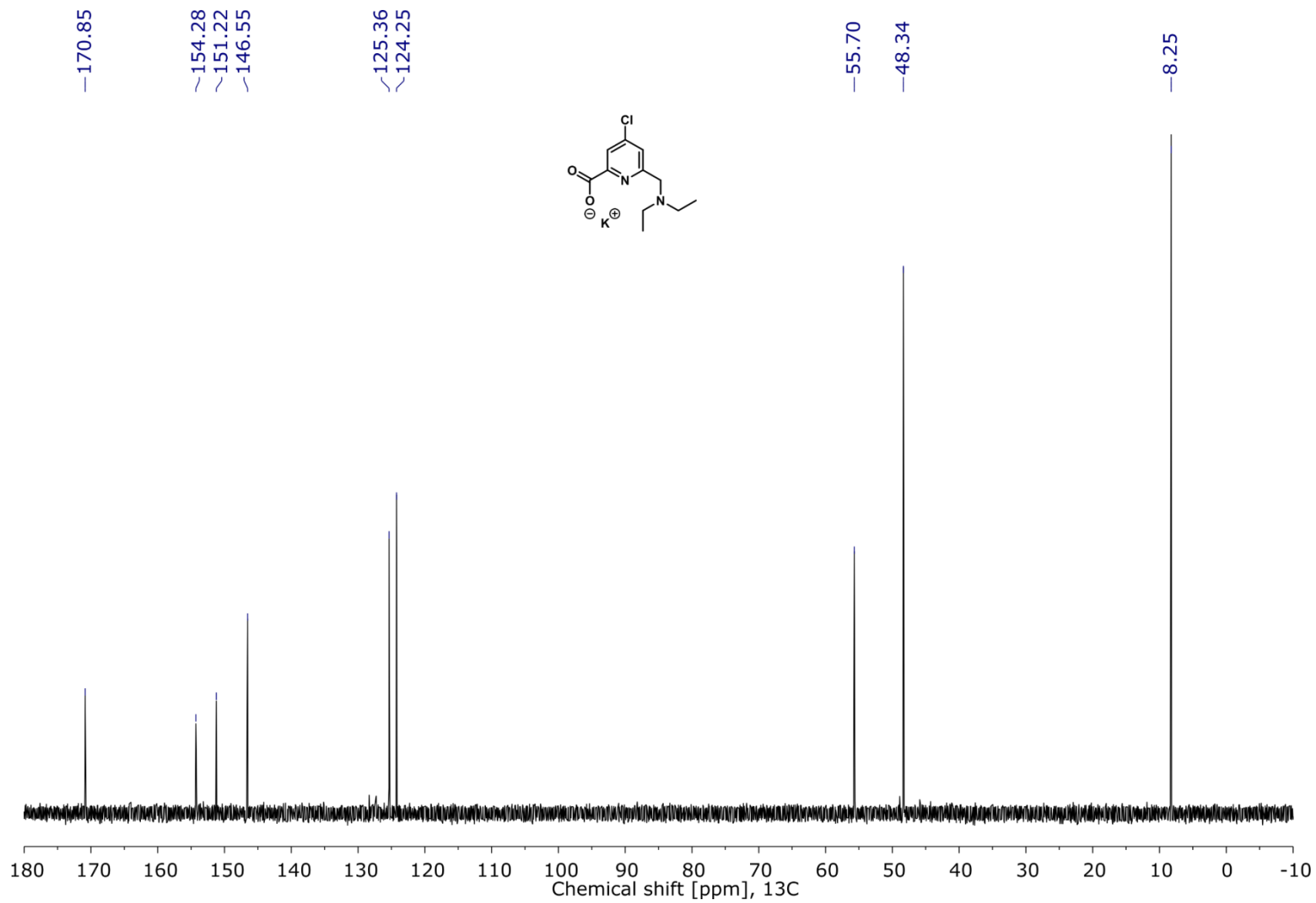
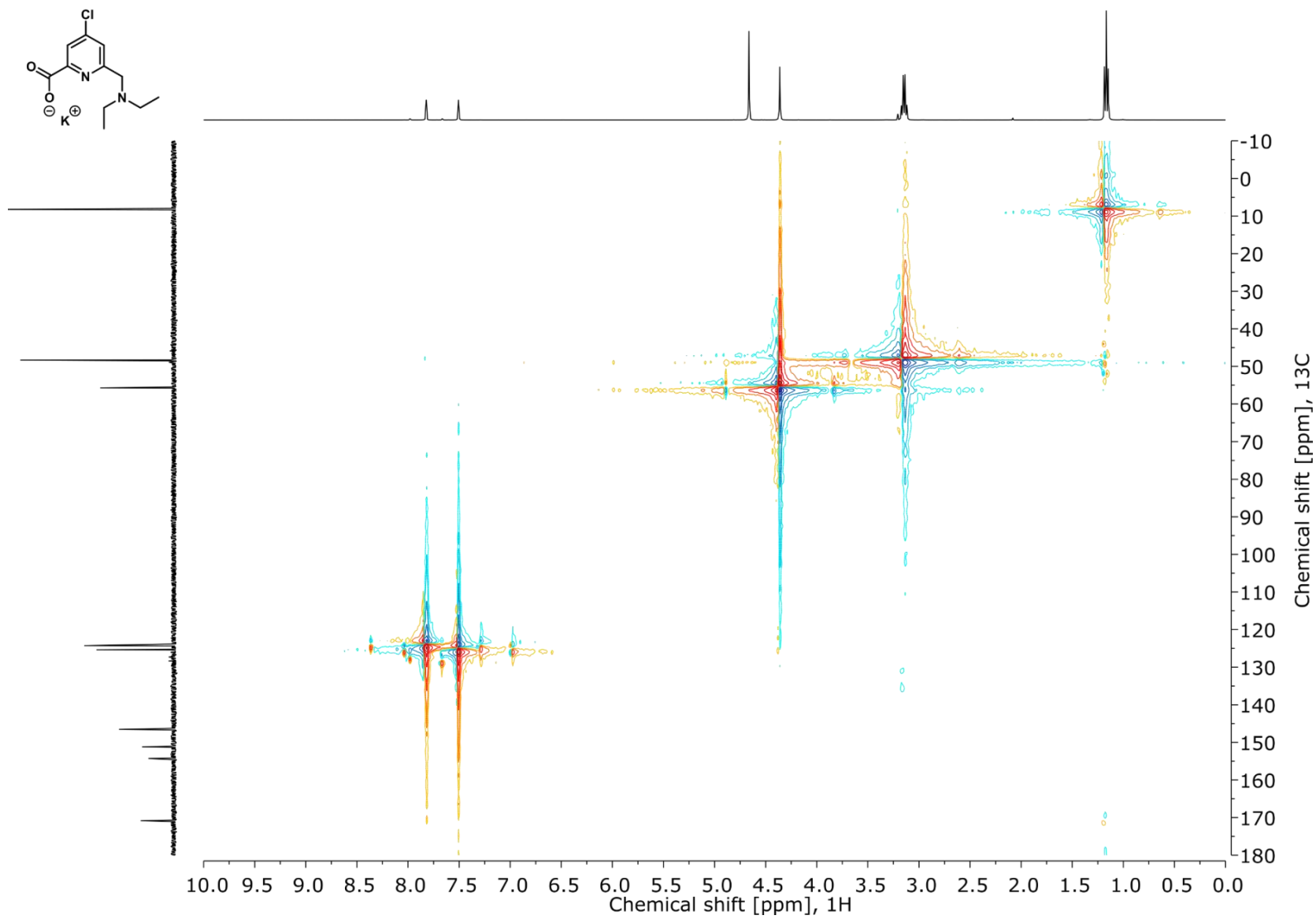


Figure S38. <sup>1</sup>H NMR spectrum of Py<sup>Cl</sup> (400 MHz, D<sub>2</sub>O).



**Figure S39.**  $^{13}\text{C}$  NMR spectrum of  $\text{Py}^{\text{Cl}}$  (101 MHz,  $\text{D}_2\text{O}$ ).



**Figure S40.** HSQC spectrum of **Py<sup>Cl</sup>** (400 MHz, D<sub>2</sub>O).

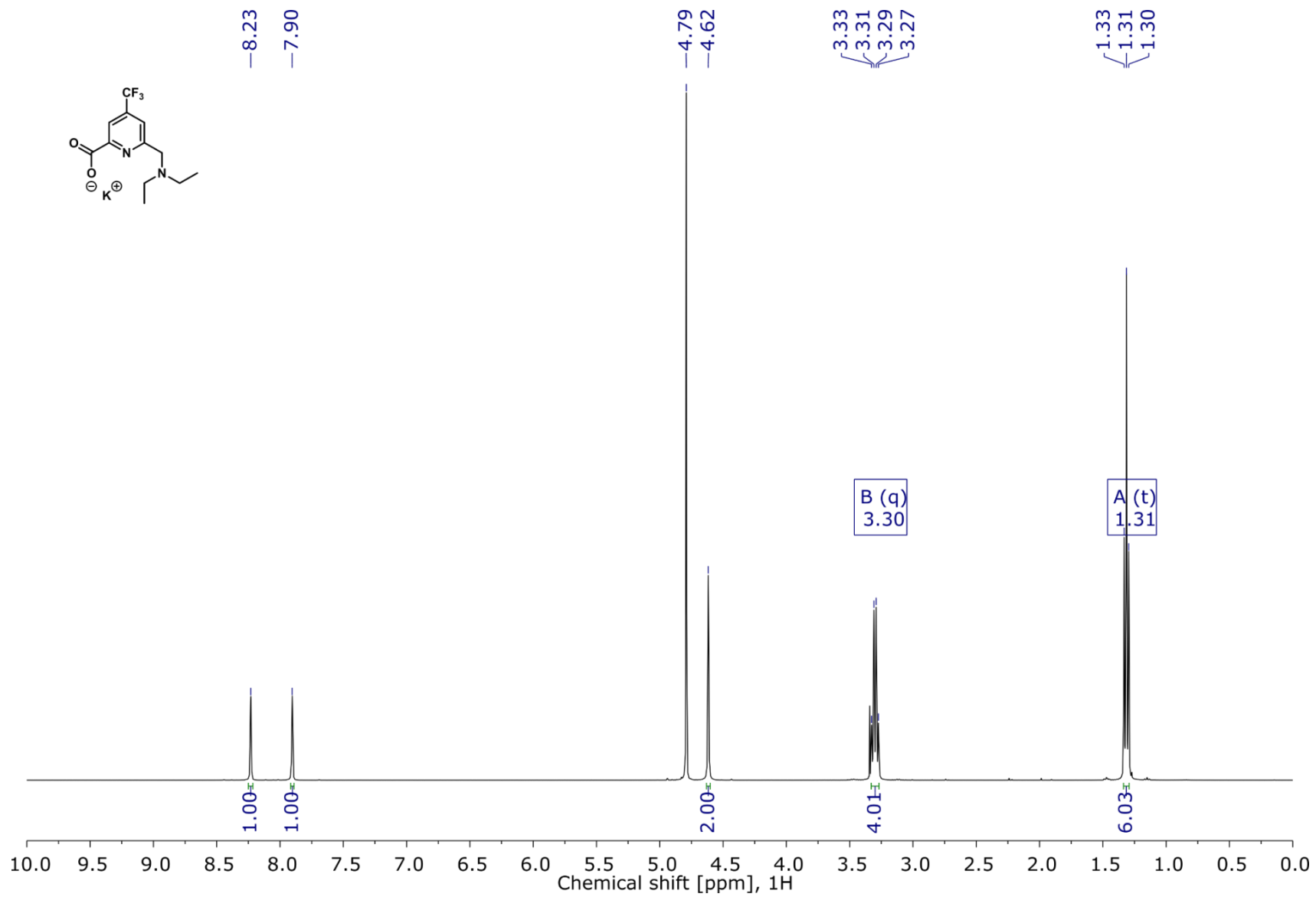


**Figure S41.** <sup>1</sup>H NMR spectrum of Py<sup>CF3</sup> (400 MHz, D<sub>2</sub>O).

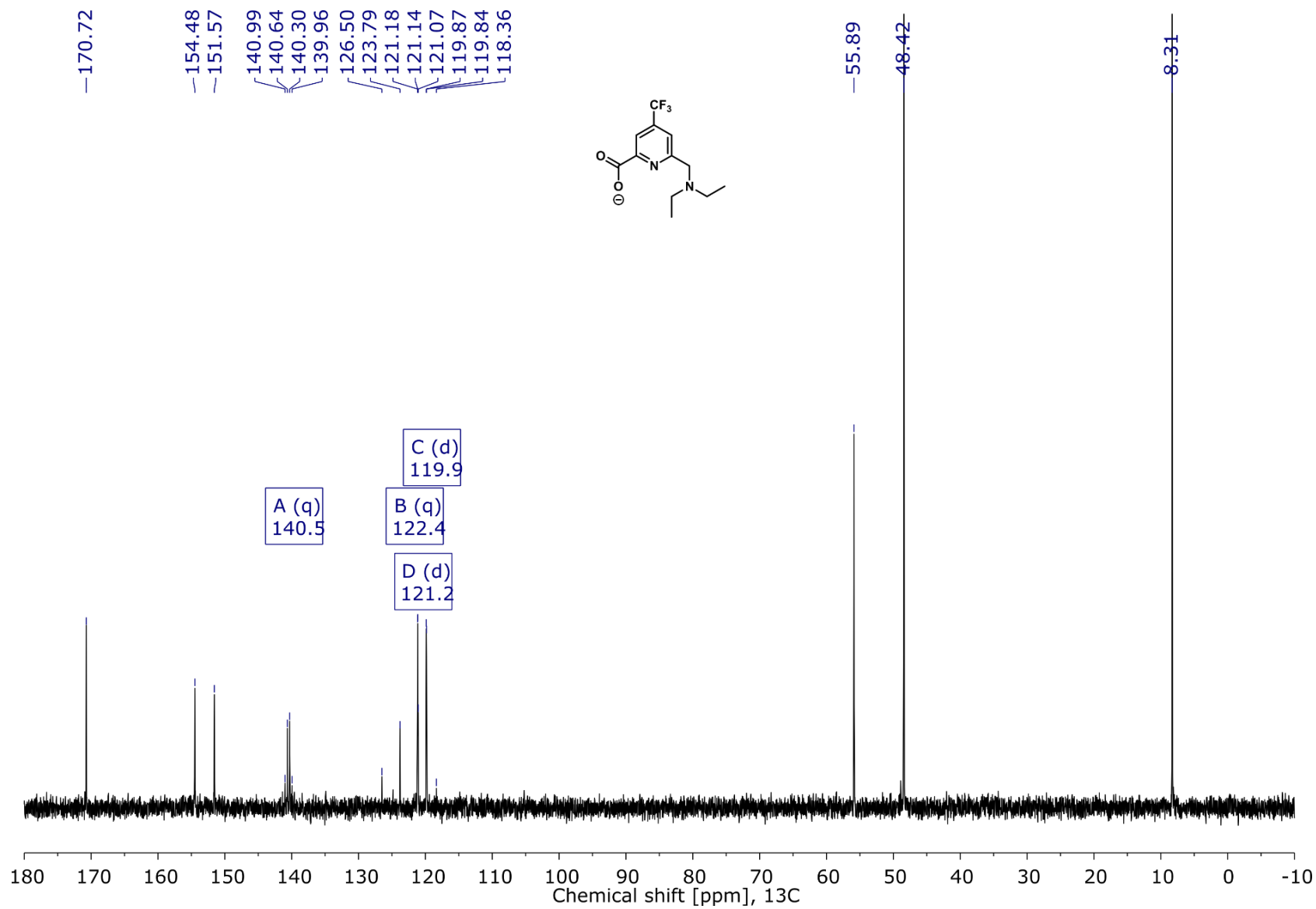


**Figure S42.**  $^{13}\text{C}$  NMR spectrum of  $\text{Py}^{\text{CF}_3}$  (101 MHz,  $\text{D}_2\text{O}$ ).

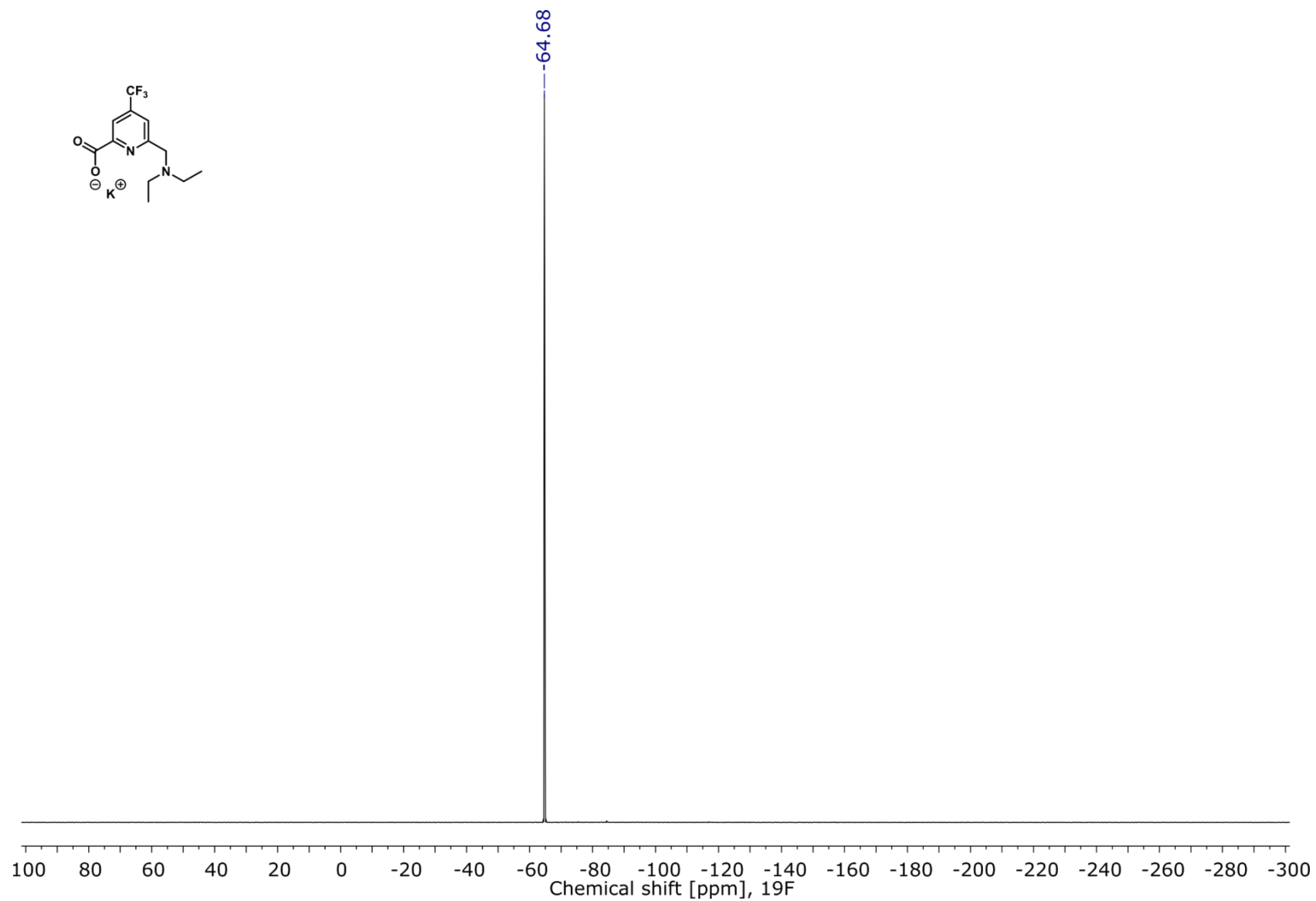


**Figure S43.**  $^{19}\text{F}$  NMR spectrum of  $\text{Py}^{\text{CF}_3}$  (376 MHz,  $\text{D}_2\text{O}$ ).

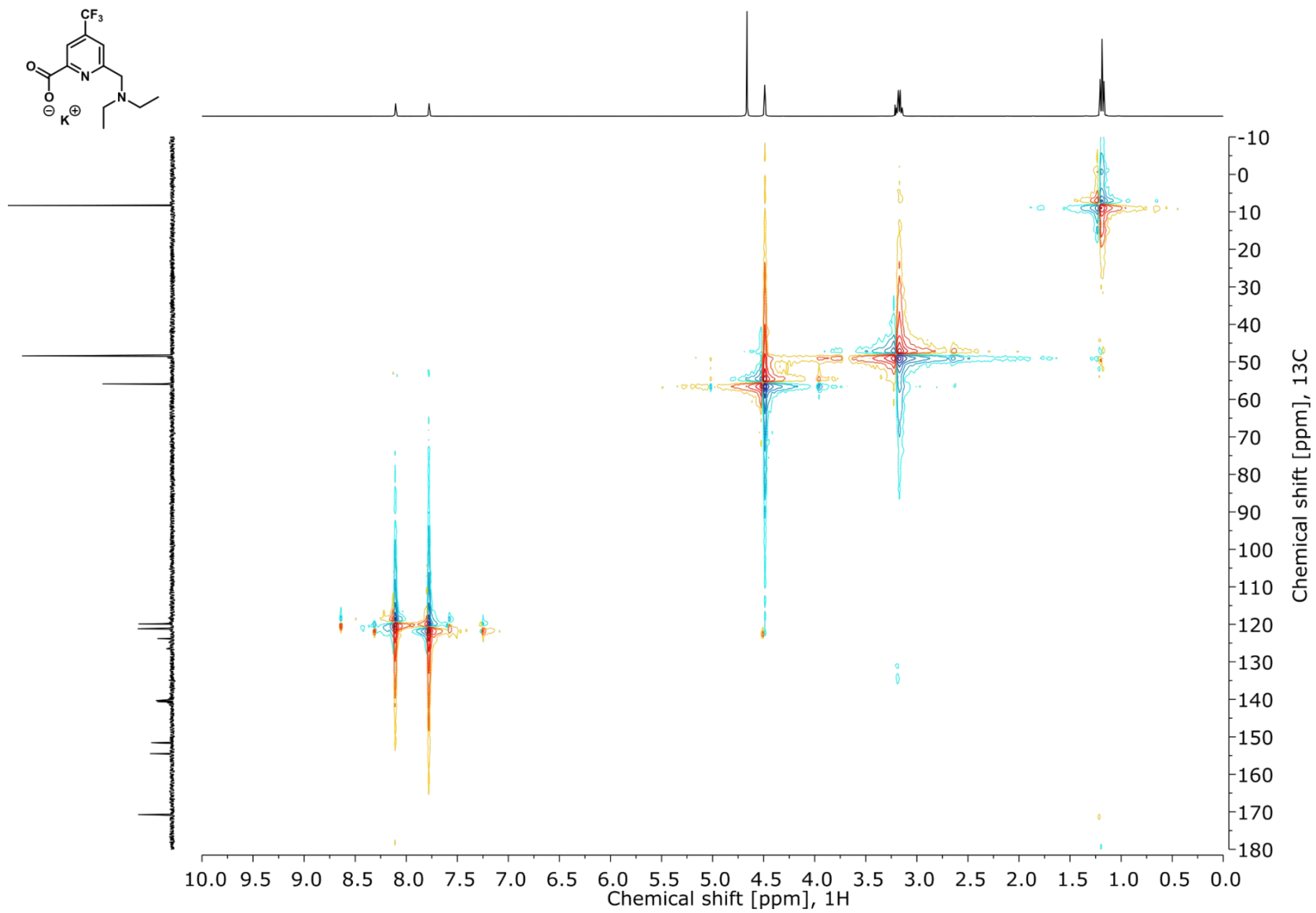


Figure S44. HSQC spectrum of  $\text{Py}^{\text{CF}_3}$  (400 MHz,  $\text{D}_2\text{O}$ ).

## HPLC-MS TRACES

C:\CaliburA...Yb\DKS65\_086Yb\_5um\_10iso

2/28/2019 3:47:38 PM

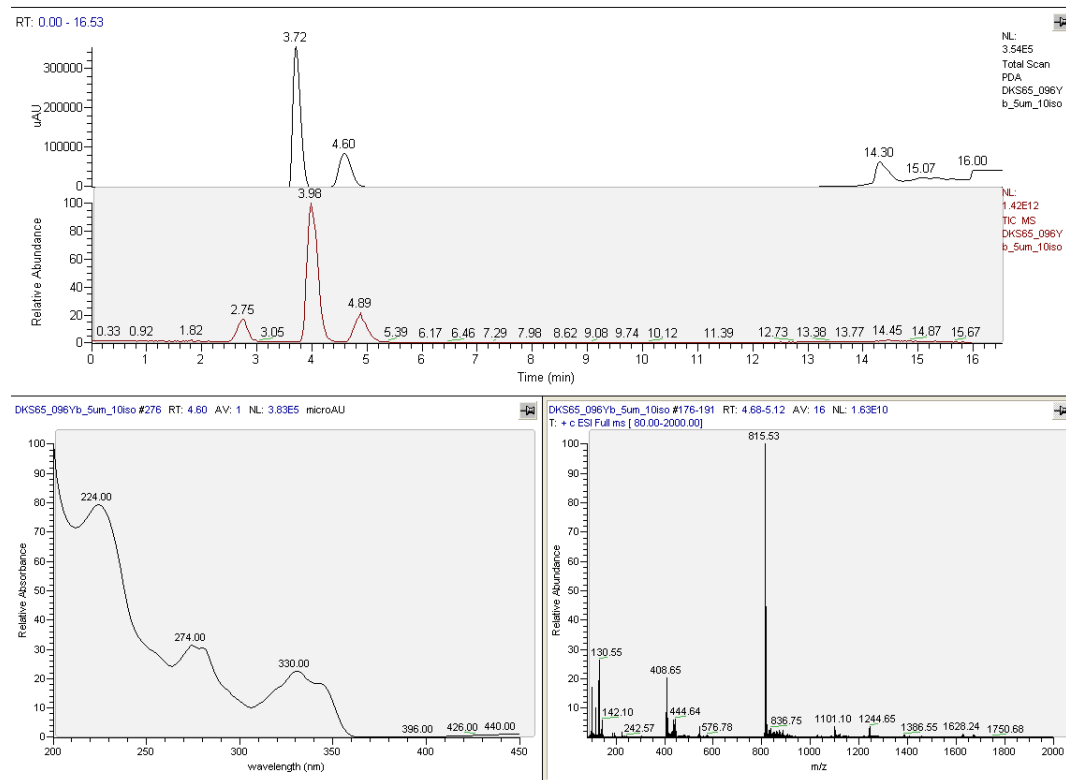


Figure S45. HPLC-MS analysis of YbL<sup>H</sup>.

C:\CaliburA...DKS65\_097Yb2\_5um\_10-20

3/1/2019 12:54:57 AM

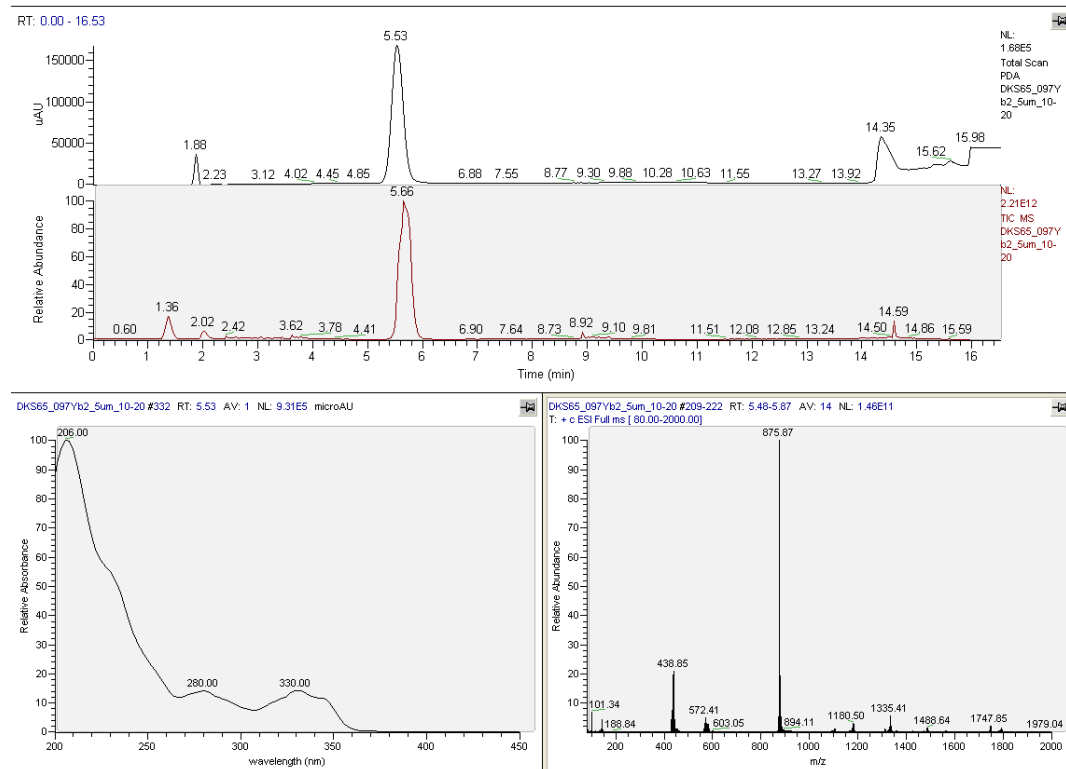
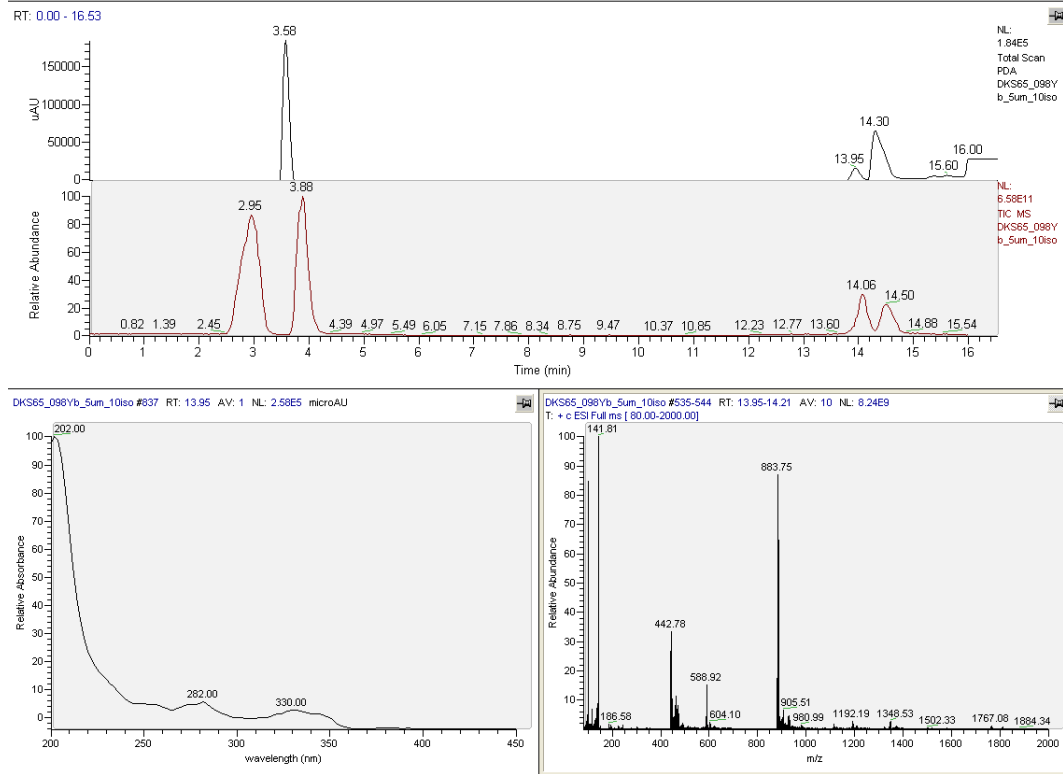
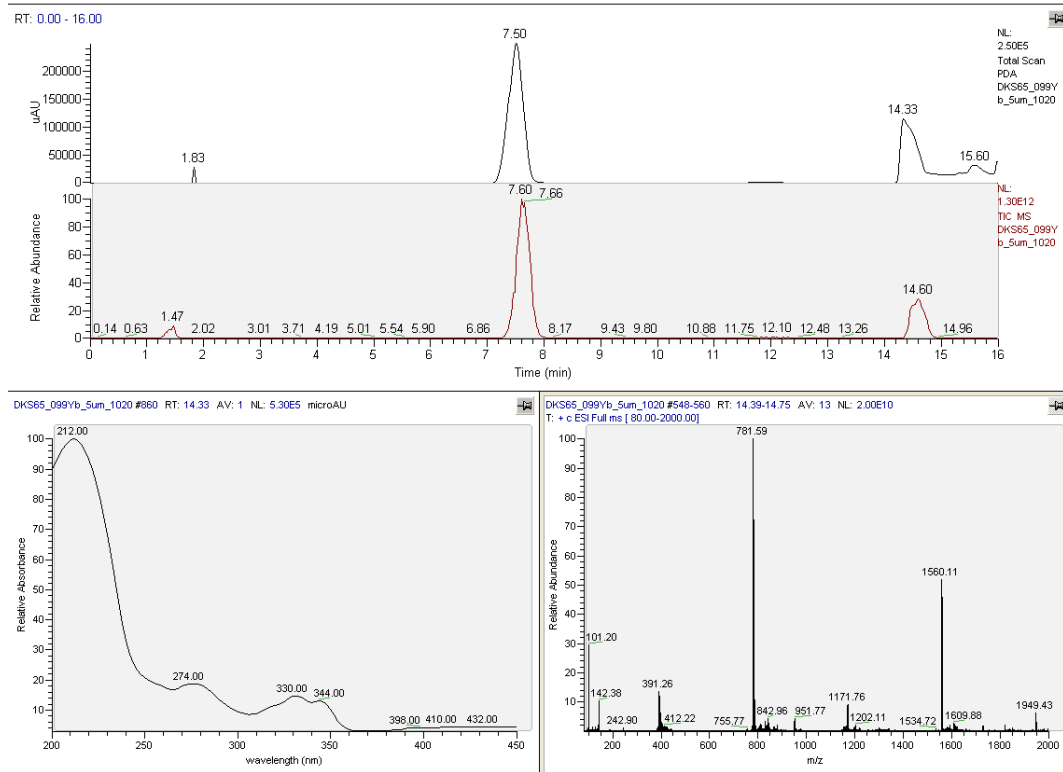


Figure S46. HPLC-MS analysis of YbL<sup>OMe</sup>.



**Figure S47.** HPLC-MS analysis of YbL<sup>Cl</sup>.



**Figure S48.** HPLC-MS analysis of YbL<sup>CF3</sup>.

## FT-IR SPECTRA OF YbL

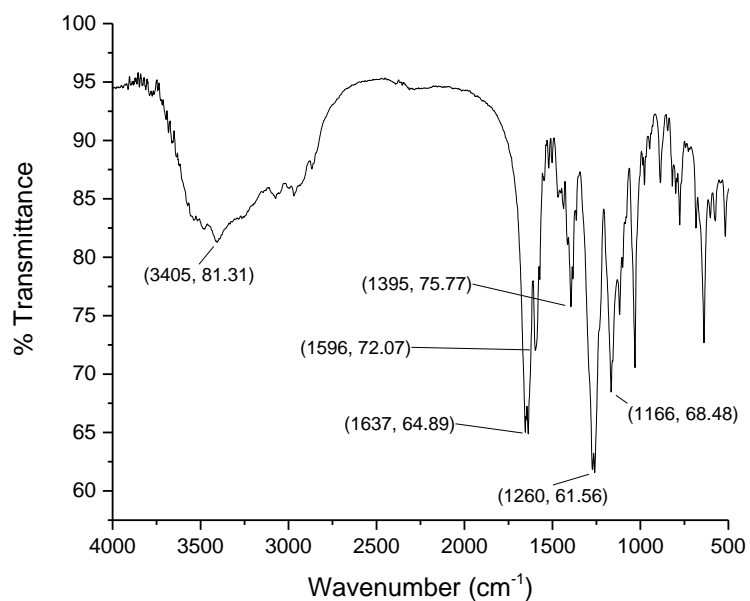


**Figure S49.** FT-IR spectrum of YbL<sup>H</sup>.

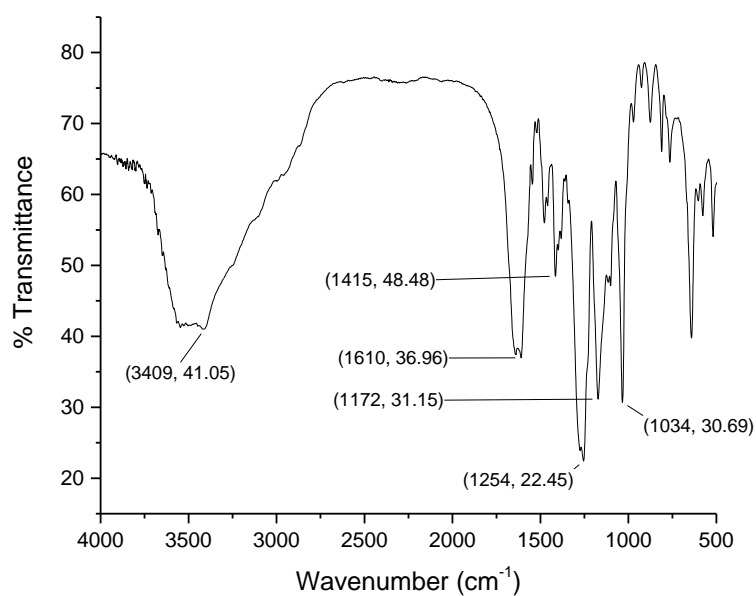


**Figure S50.** FT-IR spectrum of YbL<sup>OMe</sup>.

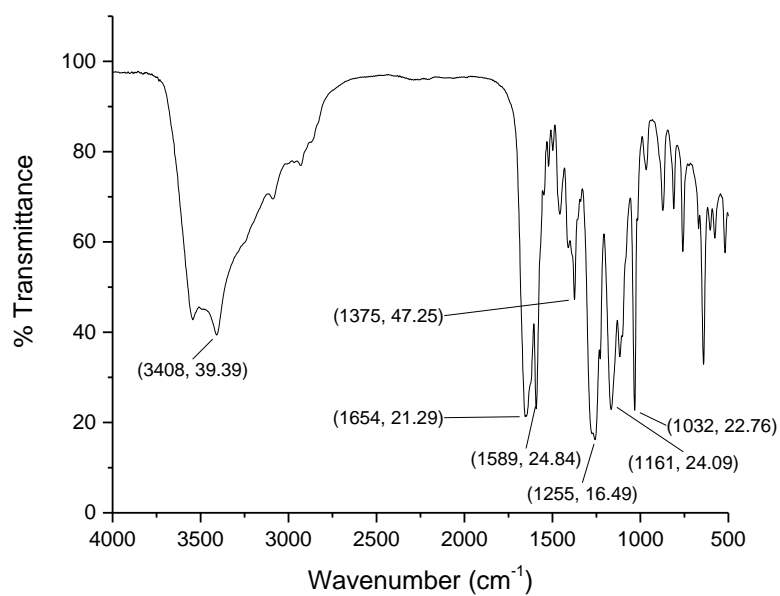


**Figure S51.** FT-IR spectrum of  $\text{YbL}^{\text{Cl}}$ .

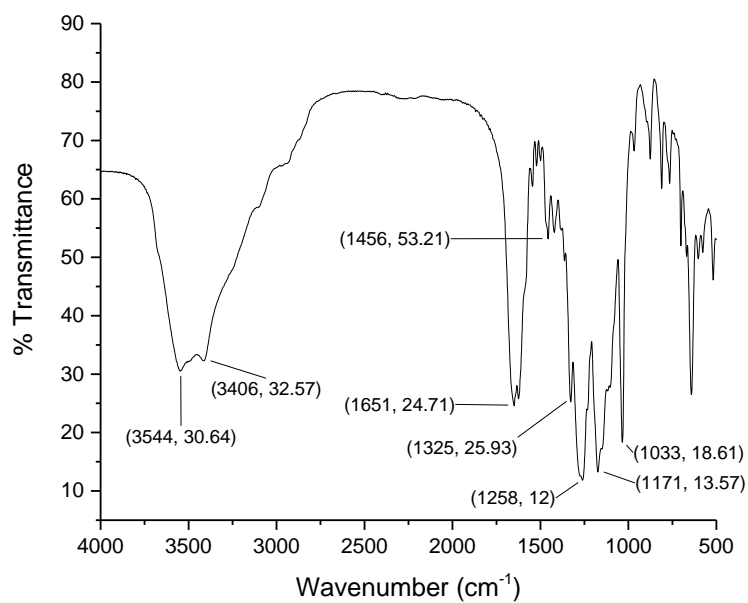


**Figure S52.** FT-IR spectrum of  $\text{YbL}^{\text{CF}_3}$ .

## **REFERENCES**

- (1) Suzuki, K.; Kobayashi, A.; Kaneko, S.; Takehira, K.; Yoshihara, T.; Ishida, H.; Shiina, Y.; Oishi, S.; Tobita, S. *Phys. Chem. Chem. Phys.* **2009**, *11*, 9850.
- (2) Kovacs, D.; Mathieu, E.; Kiraev, S. R.; Wells, J. A. L.; Demeyere, E.; Sipos, A.; Borbas, K. E. *J. Am. Chem. Soc.* **2020**, *142*, 13190.
- (3) Walton, J. W.; Carr, R.; Evans, N. H.; Funk, A. M.; Kenwright, A. M.; Parker, D.; Yufit, D. S.; Botta, M.; De Pinto, S.; Wong, K.-L. *Inorg. Chem.* **2012**, *51*, 8042.
- (4) Kovacs, D.; Kocsi, D.; Wells, J. A. L.; Kiraev, S. R.; Borbas, K. E. *Dalton Transactions* **2021**, *50*, 4244.
- (5) Dijk, J. M. F. v.; Schuurmans, M. F. H. *J. Chem. Phys.* **1983**, *78*, 5317.
- (6) de Jong, M.; Seijo, L.; Meijerink, A.; Rabouw, F. T. *Phys. Chem. Chem. Phys.* **2015**, *17*, 16959.